Auto-Ignition of Liquid *n*-Paraffin Fuels Mixtures as Single Droplets using Continuous Thermodynamics

Shaun Sabourin

A thesis submitted to the Faculty of Graduate and Postdoctoral Studies
in partial fulfillment of the requirements for the degree of

MASTER OF APPLIED SCIENCE

in Mechanical Engineering

Ottawa-Carleton Institute for Mechanical and Aerospace Engineering
University of Ottawa
Ottawa, Canada

April 2011-04-30

Abstract

This thesis reports a model to predict the auto-ignition time of single droplets of *n*-paraffin fuel mixtures using the method of continuous thermodynamics. The model uses experimental data for pure fuels to fit rate parameters for a single-step global chemical reaction equation; from this, correlations for rate parameters as a function of species molecular mass are derived, which are integrated to produce a continuous thermodynamics expression for mixture reaction rate. Experiments were carried out using the suspended droplet-moving furnace technique. The model was then tested and compared to experimental data for three continuous mixtures with known compositions: one ranging from *n*-octane to *n*-hexadecane, the second ranging from *n*-dodecane to *n*-eicosane, and the third being a combination of the first two mixtures to produce a "dumbbell" mixture. Discrete and continuous mixture models of the ASTM standard distillation test were compared to design the experimental mixtures and provide the distribution parameters of the continuous mixtures intended to simulate them. The results of calculations were found to agree very well with measured ignition times for the mixtures.

Acknowledgements

I am grateful for the financial support, guidance and mentorship of my supervisor Dr. William L.H. Hallett.

I owe my deepest gratitude to the support of my family; wife Jena Montgomery, parents William and Joanne Sabourin and in-laws Kenneth and Bonnie Whyte, as they have been very supportive in my pursuit to achieve my master's degree and finish my thesis.

I would also like to thank the lab technicians, John Perrins, Léo Denner and James MacDermid for their expertise, the use of the engineering machine shop and assistance with the experimental apparatus.

Lastly, I would like to thank NSERC for financial support of this work.

Table of Contents

List of Figures

List of Tables

Nomenclature

A	pre-exponential coefficient
c	molar density, [kmol/m^3]
$\bar{C}_P$	mixture specific hear, [kJ/kmol K]
D	diffusion coefficient, [m^2/s]
D_{im}	effective diffusivity of component *i* in the mixture, [m^2/s]
$\bar{D}, \widetilde{D}$	average diffusivities weighted with respect to the mol fraction and the variance of the distribution, [m^2/s]
E	activation Energy, [kJ/gmol]
f(I)	probability density function, distribution function, [kmol/kg]
Δh	enthalpy of reaction, [kJ/kg]
I	molecular mass, distribution variable, [kg/kmol]
J_i^*	molar flux, [kmol/m^{2}s]
K	pre-exponential coefficient
k_{ov}	reaction rate, [kg/m^3 s]
M	molecular weight, [kg/kmol]
Q	vapour molar density, [kmol/m^3]
r	radial position, [m]
R	droplet radius, [m]
$\bar{R}$	universal gas constant, [8.314 kJ/kmol K]
$\dot{R}$	=dR/dt
t	time, [s]
Δt	difference in time, [s]
T	Temperature, [K]
v	velocity, [m/s]
v^*	molar average velocity, [m/s]
W	reaction rate, [kg/m^3 s]
w	velocity relative to ξ coordinate, [m/s]
X	mass fraction
Y	mole fraction

Greek Letters:

α, β	parameters of the gamma distribution
γ	origin of the distribution
Γ	gamma function
θ	mean molecular mass [kg/kmol]
λ	thermal conductivity, [W/m K]
ξ	=r/R, dimensionless coordinate
ρ	mass density, [kg/m3]
σ	standard deviation
Ψ	second moment about the origin of the density function

Subscripts:

1, 2	component or mixture 1 or 2 respectively
∞	ambient conditions
A, F	refers to air and fuel respectively
avg	average
e, w	eastern and western control volume faces
E, W	eastern and western grid point respectively
i	index for chemical species
j	index for mixture *j*
N	number of grid points in the vapour phase
O	refers to oxygen or ambient gas
P	grip point

Superscripts:

^{0}	previous time step
m,n	fuel and oxygen exponents, concentration exponents

Linearization Coefficients:

a_c, b_c	linear variation coefficients in the equation for Cp(I)
a_E, b_E	linear variation coefficient in the equation for E(I)
a_K, b_K	linear variation coefficient in the equation for K(I)

Chapter 1 Introduction

1.1 Motivation

The motivation of this thesis is to work toward modelling fuel sprays of complex liquid mixtures during evaporation and ignition. In most liquid fuelled combustion systems, fuels burn in sprays. Before sprays can be modelled, however, a full understanding of the process along with an accurate model must be developed for fuels as single droplets. This thesis studies the ignition of mixtures of single droplets of liquid mixtures, using the technique of continuous thermodynamics to model the mixture. The ignition of pure components has already been studied to a significant amount, but the fuels used in practical combustion systems are mixtures containing hundreds of constituents, and very little work has been done on the ignition of liquid mixtures. The main purpose is to produce a model, using continuous thermodynamics rather than discrete components, based on data from experiments on pure fuels, and to test the model using experiments on mixtures. Continuous thermodynamics is much more practical and efficient than discrete components when modelling mixtures with more two components, as continuous thermodynamics can sufficiently represent mixtures with many components with the use of three variables, while the discrete method requires new equations for each component within the mixture. The mixtures studied for this thesis consist of five to seven components, while most of the research on ignition has been done for pure compounds or two-component mixtures.

1.2 Ignition of a fuel droplet

Previous work on the ignition of single droplets dealt mostly with one or two component mixtures, although for evaporation, up to seven component mixtures has been studied. Very few researchers, including Hallett and Ricard (1991) and Abdel-Qader and Hallett (2004), have studied more complex mixtures, or the combination of two separate multi-component mixtures. In particular, the modelling of chemical reaction using continuous thermodynamics for complex mixtures has yet to be researched and developed for these or other types of combustion problems.

For ignition to occur, fuel and air must be well mixed and in an environment with a sufficiently high temperature. . A fuel spray is used in most systems for fuel combustion, such as Diesel engines, gas turbines and industrial furnaces. Spray injection is used as it is a way of increasing the rate of evaporation of the fuel and therefore the efficiency of the combustion process. A spray is formed with an atomizing nozzle which injects the fuel into the combustion region. Atomization is the process by which a liquid fuel is reduced to fine droplets. Producing small droplets increases the surface area along with the evaporation rate of the droplets, in turn producing more vapour.

The processes for ignition are the injection of fuel as fine droplets, heat transfer to the droplets, evaporation to produce fuel vapour, mixing with air, and heating of the mixture until chemical reaction becomes rapid, followed by full-fledged combustion of the remaining vapour. From this process the performance is dependent mostly on the vaporization and heating of the droplets. Due to the complexity of spray evaporation and combustion processes, a good

understanding of single liquid droplet evaporation and combustion is required. This is why much liquid combustion research is done with single fuel droplets. (Tamim, 1996)

The processes and profiles involved in the evaporation of a liquid fuel droplet are the following and can be seen below in Figure 1-1. A hot surrounding atmosphere which is sufficiently higher than the temperature of the droplet surface produces a temperature gradient. This temperature gradient transfers heat towards the droplet by conduction and heats up the droplet, vaporizing the liquid at the surface. The vapour produced diffuses outwards from the droplet surface. The droplet heats up towards its boiling point; however, the boiling point is never reached since, as the temperature rises, the rate at which vapour is produced increases and the rate at which heat is removed from the surface by evaporation therefore also increases. The droplet tends towards a temperature at which this heat removal due to vapour diffusion from the surface balances out the heat conduction towards the surface. This balance occurs as the temperature of the droplet approaches the boiling point and prevents it from actually reaching or exceeding the boiling point. The diffusion of fuel vapour from the droplet surface occurs because of the concentration gradient: vapour concentrations are highest at the surface and lowest in the ambient far from the surface. The removal of fuel vapour from the surface allows for additional vapour to be formed at the surface. As fuel vapour diffuses away from the droplet surface, oxygen from the surrounding air diffuses towards the surface. This diffusion of ambient gas towards the droplet occurs because the ambient concentration is large relative to the amount present near the surface of the droplet. The processes which control the vaporization of a fuel droplet are heat and mass transfer.

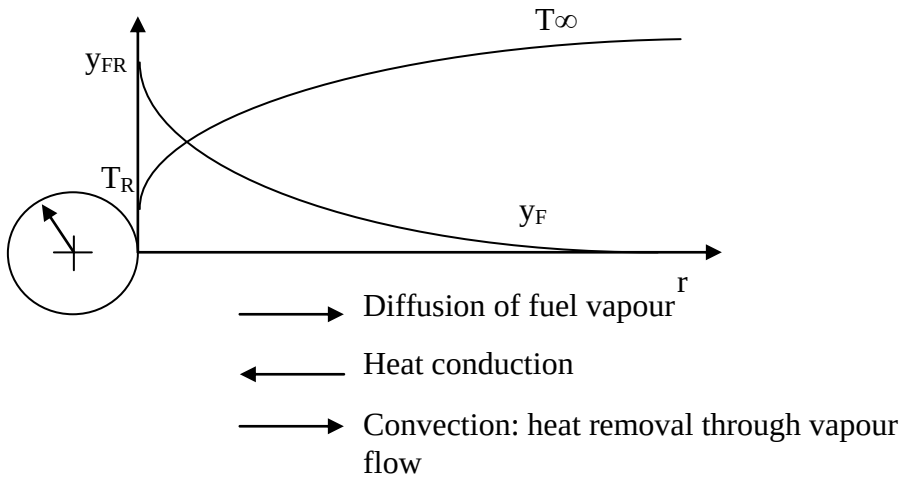

Figure 1-1 Temperature and fuel concentrations around a vaporizing droplet

The previous processes describe evaporation of a single fuel droplet. Droplet ignition has the same initial processes, requiring the droplet to be exposed to high temperatures and produce vapour. The vapour diffuses out while oxygen diffuses toward the droplet, producing a mixture of roughly stoichiometric proportions at some distance from the surface. Chemical reaction begins in this mixture, causing the temperature to rise. This accelerates the reaction further, until the temperature rises to a point where very rapid chemical reaction ("thermal runaway") occurs. This is the moment of ignition, which occurs fairly close to the droplet surface, where the ratio of oxygen to fuel is close to stoichiometric conditions.

1.3 Continuous Thermodynamics

Most fuels used in engineering applications consist of very complex mixtures containing hundreds or even thousands of components. It is not practical to model all the hundreds of

components of a commercial fuel mixture, and instead one can use probability density functions - continuous thermodynamics. Continuous thermodynamics replaces the mole fractions of individual species with a continuous distribution function *f*(I), where I is the characterizing variable defined as molecular mass, carbon number, boiling point or others. The continuous distribution function *f*(I) can be described using three distribution parameters: the mean θ, standard deviation σ, and origin γ (higher moments may be added, if desired). These three variables can describe any continuous mixture with any number of individual components rather than describing the mixture with the fraction or properties of each individual component separately. Continuous thermodynamics is valid for fuel mixtures that contain enough components that the concentrations can be assumed to vary continuously (Abdel-Qader and Hallett, 2004).

1.4 Objectives

The purpose of this thesis work is to study the ignition behaviour of complex multi-component mixtures using continuous thermodynamics to model the mixtures. Continuous thermodynamics has been widely used to model droplet evaporation and chemical processes (Tamim and Hallett 1995, Hallett 2000, Abdel-Qader and Halett 2004, Hallett and Beauchamp-Kiss 2010), but it has not been extensively applied to chemical reactions in mixtures, and this work will therefore help improve the understanding of ignition delay time with complex mixtures. An existing continuous thermodynamics model for droplet evaporation developed by Tamim (1996) will be modified by the addition of a reaction model and applied to droplet ignition. It will then be tested with experiments that can be carried out fairly easily on controlled

mixtures and the data used to assist in developing appropriate relationships for the rate parameters of the mixture components to be used in the Arrhenius rate equation.

Since most commercial fuels are complex mixtures, this will improve the level of realism of models of combustion systems. This thesis has then two main objectives: to create a simple reaction model (one-step Arrhenius rate equation) using continuous thermodynamics to describe the combustion of a mixture with a large number of different components, and to apply it to droplet ignition; and to create sample mixtures of controlled composition and perform droplet ignition delay time tests over a variety of temperatures using the suspended droplet / moving furnace technique. The theoretical model will be compared to the experimental tests to test and improve the model. To determine the distribution function parameters for the continuous thermodynamics models of the experimental mixtures, models of the ASTM standard distillation test for liquid fuels for both discrete component mixtures and continuous mixtures were required.

The following Chapter will discuss the previous research on droplet evaporation, continuous thermodynamics and droplet ignition. These topics will focus more on single droplets as mixtures, what models were developed and what conclusions arose. The experimental setup and method will be discussed in Chapter 3. In Section 4.1 the mathematical model that applies continuous thermodynamics to reaction and its application to droplet ignition will be outlined. The numerical solution used will be discussed in Section 4.2. The results and discussion will be presented in Chapter 5 and the conclusion and recommendations will be presented in Chapter 6.

Chapter 2 Literature Survey

2.1 Introduction

Single liquid fuel droplets undergoing droplet evaporation are frequently encountered in various applications and have an important role in the ignition properties of liquid fuels. These applications include mostly spray injection applications such as diesel engines and gas turbines. In fuel sprays, a vapour cloud is produced surrounding the droplets and mixes with surrounding air. The auto-ignition of the fuel will occur when a few key elements are fulfilled: a sufficiently high temperature must be present in the surroundings, and mixing between the fuel and the air is required. The same processes occur when a single droplet ignites and burns, so that it serves as a simple model system for the spray. There has been considerable research on single liquid fuel droplet vaporization and ignition. However, this research has been done mostly for single or two-component mixtures. For more complex mixtures the technique of continuous thermodynamics is a useful tool for mixture modelling, although it has not yet been applied to droplet ignition. This chapter will briefly discuss the literature on the work and models that this thesis further develops and extends, in particular the topics of droplet evaporation, continuous thermodynamics and ignition.

2.2 Droplet Evaporation

2.2.1 Basic Process

Droplet evaporation is initiated when a fuel droplet is exposed to surroundings at a temperature much higher than the droplet surface temperature. This creates a temperature gradient, which causes heat conduction towards the droplet, causing it to heat and vaporize. The droplet continues to produce vapour as the vapour at the surface of the droplet diffuses outward in the radial direction to areas of lower fuel concentration. The model most often used for droplet evaporation is the classical quasi-steady model (Tamin 1996); however, it can not be used for ignition, as ignition is by its nature not a quasi-steady process. "Quasi steady" assumes that all properties in the vapour phase are at a nearly steady state at any time. Other assumptions for this simple model include a spherically symmetrical geometry, and the neglect of forced and natural convection. For a pure fuel, the square of the diameter varies linearly with time. This is referred to as the "d^2 law". Thermal expansion occurs during the early lifetime of an evaporating droplet; this behaviour no longer follows a d^2 law, but it can be added to the model. This thesis does not assume quasi-steady conditions; rather it uses a full transient solution.

2.2.2 Multi-Component Droplets

Almost all research on droplets of mixtures has used two component mixtures (Law, Prakash and Sirignano 1976, Tong and Sirignano 1986, Talley and Yao 1986, Aggarwal 1988, Hallett and Beauchamp-Kiss 2010), as it was first required to understand the fundamentals of

evaporation and ignition of pure fuels. A multi-component droplet experiences the same evaporation process as a single component droplet; however, with the addition of other components the droplet temperature no longer tends to a fixed quasi-steady value. As the lighter components evaporate, the boiling temperature of the liquid increases and so does the liquid droplet temperature.

The exact rate at which the components evaporate from the surface depends on the state of mixing in the liquid phase. The two limiting cases are referred to as diffusion-limited or well-mixed. Well-mixed refers to the concentration of species being uniform throughout the droplet, while diffusion-limited means that mixing is restricted to molecular diffusion in the radial direction. The easier of the two to model is the well-mixed case; it also requires much less computational effort, making it more practical when modelling single droplets or droplets in sprays. In reality the state of mixing in the liquid lies somewhere between the two cases, and there may be internal flow within the droplet to accelerate mixing.

Law, Prakash and Sirignano (1976) modelled vortex flow within the liquid droplet, concluding that internal circulation increases with decreasing vaporization rates and liquid viscosities. They also concluded that diffusion of components of different volatilities occurs in the radial direction and the relative rates of mass, heat and momentum transfer would significantly influence droplet behaviour. Tong and Sirignano (1986) compared diffusion-limited, well-mixed, and vortex diffusion and recommended the diffusion-limited model for droplets in stagnated situations (no relative gas-droplet motion). Talley and Yao (1986) also compared diffusion-limited, well-mixed and vortex mixing and found more extensive mixing in experiments than the Tong and Sirignano (1986) model had predicted. Aggarwal (1988) demonstrated that liquid motion has less effect on evaporation rates of multi-component mixtures

(*i.e.* mixtures with more than two components) and illustrated that the differences between the diffusion-limited and well-mixed cases at the surface of a liquid droplet are minor for these mixtures. Bergeron and Hallett (1989b) had looked at these two limiting states for two-component mixtures and concluded that the diffusion-limited and well-mixed cases can influence the conditions at the droplet surface; however, the effects are less than 5% of the ignition delay. Hallett (2009) states that the rate at which the vapour is produced is determined by the liquid phase transport process and that liquid phase diffusion is very slow; however, most droplets experience some form of internal circulation, from shear from the spray atomizer or from adjacent gas streams in convection for example, increasing the rate of internal mixing and approaching the well-mixed case more closely.

Another aspect of mixtures is the classical quasi-steady evaporation behaviour of multi-component mixtures. Ghassemi et al (2006) studied the evaporation of kerosene droplets at elevated pressures and temperatures and concluded that kerosene droplets (a mixture) followed the d^2-law after an initial heating period and that the evaporation rate increased linearly with increasing ambient temperatures.

For a two-component mixture, the lighter component produces most of the vapour at the start of the droplet lifetime. Since the vapour pressure increases roughly exponentially with temperature, this will greatly affect the vapour concentrations if the two component boiling points differ by more than a few 10's of degrees. Also, the initial part of the droplet lifetime can be said to be dominated by the lighter component, followed by vapour being composed mostly of the heavier component.

2.2.3 Continuous Thermodynamics

Until recently, the modelling of the evaporation of single fuel droplets has been done with a small number of discrete components. As mentioned in Section 1.3, continuous thermodynamics is more practical for modelling fuel mixtures with more than two components and describes a mixture using a probability density function, which can be described using a few distribution parameters (mean, standard deviation and origin), instead of the large number of components of the original mixture. The following authors have developed the basic theory of continuous thermodynamics and applied it to chemical processes, in particular petroleum distillation: Cotterman et al. (1985), Willman and Teja (1987) and Rätzsch et al (1988).

Tamim and Hallett (1995) developed the first continuous thermodynamics model for droplet evaporation, applying the approach to the mixture composition, properties, vapour phase transport equations and the liquid phase balances. The liquid phase was approximated as well-mixed. The temperature throughout the droplet was also assumed constant in space but varying in time. It was shown that by choosing appropriate distribution parameters one could successfully model the evaporation of complex mixtures such as gasoline and Diesel fuel. This model and method will be extended in this thesis to include chemical reaction.

Hallett (2000) simplified the model with little loss in accuracy, from full transient calculations, which made it difficult to apply to spray combustion, to quasi-steady calculations by assuming quasi-steadiness, producing a result for droplet evaporation very similar to the "classical" theory for pure fuel droplets. This simpler model was applied to two limiting cases of liquid phase mixing, the well-mixed and the diffusion-limited liquid phase. Both limiting cases were shown to fit a d^2 law. This model fit the experimental results well, illustrating that this is a good model to simulate the evaporation of complex mixtures.

The role of liquid mixing in a continuous thermodynamics droplet model was studied by Abdel-Qader and Hallett (2004). They determined that the well-mixed droplet is a reliable assumption for mixtures that have a large enough number of components that their properties can be said to vary continuously. The largest departures from well-mixed behaviour occur when there are two discrete components with widely varying boiling points or molecular weight; this was also experienced, to a much lesser degree; with two continuous distributions which form a "dumbbell" mixture as shown in Figure 2-1. This is a blend of two separate mixtures with broad distributions that are separated by a distance such that the two distributions are distinguishable from one another. The effect of liquid mixing is reduced as the difference in volatility and molecular weight is reduced between components or distributions, and it has the smallest effect when a mixture is described by one continuous distribution function. The authors illustrated that a well-mixed model is sufficient for a single continuous distribution function to represent a mixture, but may become less accurate for "dumbbell" mixtures. The following authors, among others, have also modelled mixtures by applying continuous thermodynamic droplet theory to various problems: Arias-Zugasti and Rosner (2003), Harstad and Bellan (2004), Zhang and Kong (2009), and Rivard and Brüggemann (2010).

Distribution parameters for continuous thermodynamics models can be fitted from distillation curve data using computational models of the ASTM standard distillation test for liquid fuels. An ASTM distillation test for a liquid fuel consists of evaporating a mixture and recording the vapour temperature versus the volume percent evaporated (Annual Book of ASTM Standards, issued annually). A computational model of the ASTM distillation test for a continuous mixture is described by Hallett and Beauchamp-Kiss (2010). It predicts the progress of distillation as the volume of distillate recovered versus the boiling temperature of the liquid

sample, assuming well-mixed vapour and liquid phases. As a mixture evaporates, the lighter components are evaporated out initially, and the continuous distribution function becomes narrower and shifts in mean molecular mass towards the heavier components, as illustrated in Figure 2-2. Hallett and Beauchamp-Kiss (2010) applied this model to ethanol-fuel oil mixtures, with the two fractions treated as separate continuous distributions, and showed that this model, with an appropriate phase equilibrium model and fitting of distribution variables, was successful in matching experimental data. This verified the model developed by Tamim and Hallett (1995) and illustrated that it can be applied to other mixtures.

The quasi-steady model using continuous thermodynamics for evaporating droplets along with experimental techniques was used successfully by Hallett and Legault (2011) and Hallett and Beauchamp-Kiss (2010), thus justifying the quasi-steady assumption.

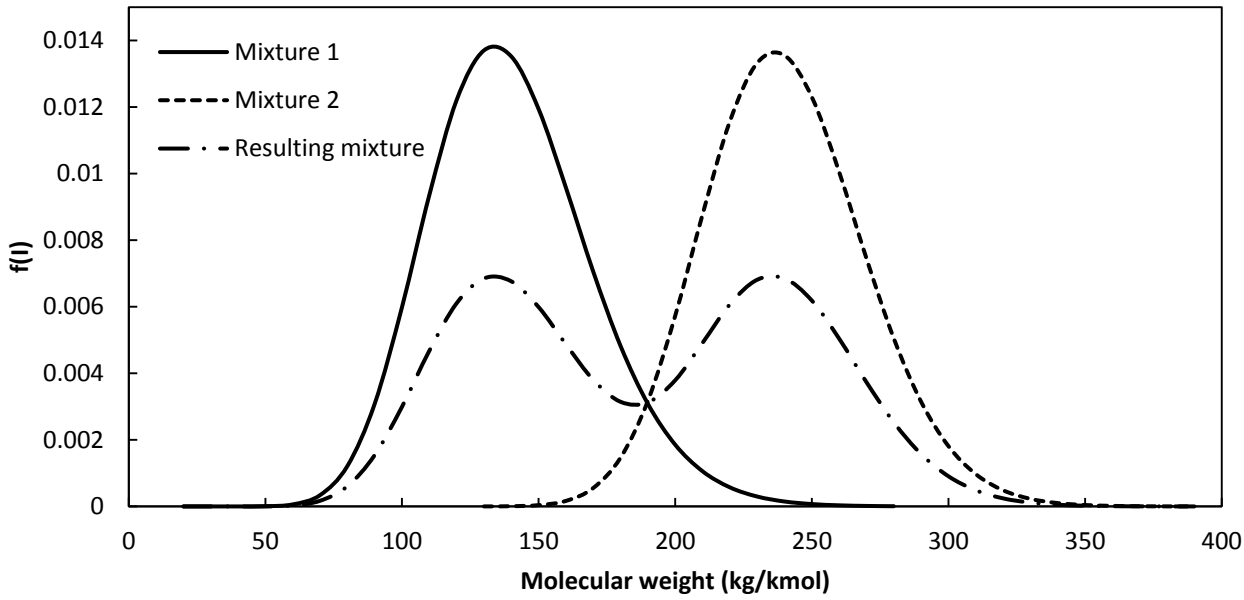

Figure 2-1 Example of a "dumbbell" distribution by mixing mixture 1 and mixture 2 in the proportion 50%/50% by mole

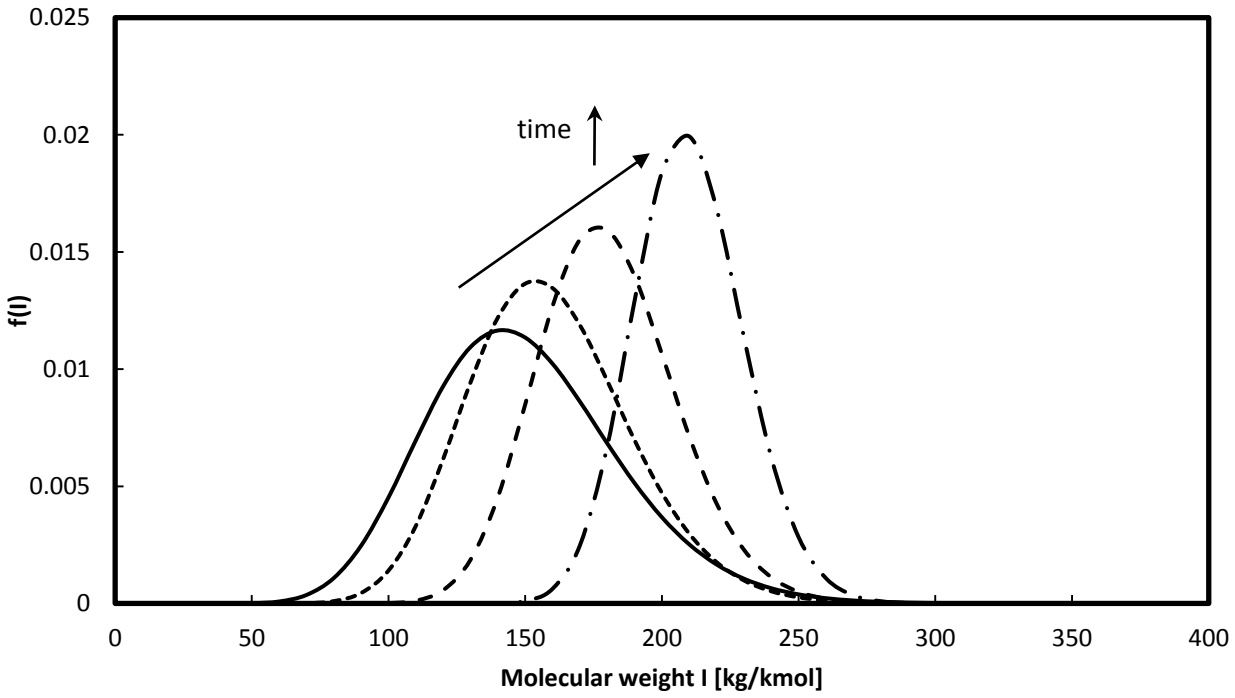

Figure 2-2 Changes in the distribution function of a liquid as evaporation proceeds

2.3 Ignition of fuel droplets

2.3.1 Pure Fuels

The initial process of ignition is similar to that of an evaporating droplet, but with the addition of chemical reaction when mixture forms at a sufficiently high temperature. One of the earliest papers for ignition of pure fuels was that of Faeth and Olson (1968), who used the suspended droplet technique in generating results to compare to their numerical model. Faeth and Olson (1968) had looked at how droplet diameter and ambient temperature affected ignition delay and the ignitable limits. Their paper considered well-mixed versus diffusion-limited cases

for the droplet temperature field and concluded that the prediction for uniform droplet temperature was closer to the experimental results than the case of non-uniform temperature.

Saitoh et al. (1982) studied the ignitable limits of hydrocarbon droplets, comparing and verifying the results with the model of Faeth and Olson (1968), and also examined the effect of initial droplet temperature. A slight increase in ignition time was observed compared to Faeth and Olson (1968), due to a smaller droplet supporting fibre being used in the suspended droplet technique, and the smaller support was concluded to provide less heat to the droplet. A lower initial droplet temperature caused a slight increase in ignition time, since more heating was required to increase the droplet temperature. A larger effect of initial temperature was observed for droplets of larger diameters and negligible effects occurred for small droplet diameters.

Present study of the ignition delay time of fuel mixtures as single droplets extends previous work done at the University of Ottawa by Bergeron and Hallett (1989a), who looked at the ignition characteristics of pure liquid hydrocarbon fuels as single droplets at atmospheric pressure. Experiments, using the suspended droplet technique, were performed and a computational model was developed to determine reaction rate constants from the fuels for use in a one-step Arrhenius rate equation. The computational model developed by Bergeron and Hallett (1989a) for ignition using pure fuels, determines the time which it takes the fuel droplet to ignite when exposed to hot surroundings. Ignition was deemed to occur when the local temperature in the gas phase was high enough to assure rapid reaction (thermal runaway). The model was developed by solving the continuity, energy and diffusion equations over time in the vapour phase using a finite volume method. To simplify the complexity of the problem the following reasonable assumptions were made:

(a) Spherical symmetry was assumed and both forms of convection were neglected. However, the actual droplet was slightly elongated in the vertical direction relative to the horizontal width due to gravity, and this was allowed for using a volume-equivalent spherical diameter. Neglecting convection affects where ignition occurs around the droplet with little effect on the delay time.

(b) The consumption of reactants and the generation of products were neglected. The only effect of the reaction in the model was heat release.

The temperature within the droplet was assumed uniform throughout, it being argued that thermal radiation absorption in droplets of up to 2mm diameter will assist in maintaining a uniform temperature within the droplet (Hottel et al., 1955). While drops up to 2mm will show some temperature difference due to transient heat conduction, this has little affect on ignition delay time (Faeth and Olson, 1968).

The following fuels were used: *n*-heptane, *n*-decane, *n*-dodecane, *n*-hexadecane, *iso*-octane, cyclohexane, methylcyclohexane, decalin, benzene, toluene and 1-methylnaphthalene. The dependence of ignition delay time on droplet diameter was noticed to be small for a few fuels; therefore, more care was taken to measure the effect of temperature on ignition time delay for roughly the same droplet diameter, as temperature had by far the largest effect. All model results agreed well with the experiments.

The chemical kinetics of the fuels was coupled with the physical heating and vaporization of the droplet which created enough vapour for reaction to occur. When comparing fuels of similar boiling point, the reaction rates were the determining factor on delay time. When comparing fuels with similar reaction rates, the lower boiling point fuel had the lower delay time.

Other similar successful models were developed by Aggarwal (1984) and Li and Renksizbulut (1990).

2.3.2 Ignition of Multi-component mixtures

At this point there has been very little research on droplet ignition of mixtures; most studies have been with droplets of single-component and occasionally two-component fuels (Bergeron and Hallett 1989a, b); however, Hallett and Ricard (1991) have modelled ignition of up to seven component fuels using discrete components. Some work has been done on gasoline and other commercial fuels, but without knowing or taking notice of the chemical composition. It is important to study ignition behaviour with mixtures containing large numbers of components, as this better represents the composition of fuels used for real combustion systems. The papers that have studied droplet mixture ignition have created models using discrete components; however, as mentioned previously, this is not as practical or efficient as continuous thermodynamics when modelling more complex mixtures. Additionally, most work on mixtures has been for pure evaporation or quasi-steady combustion rather than ignition.

The following outlines the research of Bergeron and Hallett (1989b), who performed ignition experiments using the suspended droplet technique on a variety of two-component mixtures of controlled composition, and extended the computational model of Bergeron and Hallett (1989a) to two components with similar assumptions. Finite volume techniques were used to solve the model. There had been suggestions of the possibility of micro-explosions caused by vapour nucleation at the bead of the supporting fibre using the suspended droplet technique; however, this was not experienced with any of the mixtures prior to ignition.

They looked at the two limiting cases of mixing inside the droplet, well-mixed and diffusion-limited. The easier of the two is the well-mixed case: it refers to concentrations of species being uniform throughout the droplet. The diffusion-limited model restricts mixing to molecular diffusion in the radial direction. In reality, the state of mixing in the liquid lies somewhere between the two cases, and this was also modelled by using a diffusion-limited model with the liquid diffusivity increased by a factor after the fashion of Talley and Yao (1986).

The reaction rate of a two-component mixture was modelled using a one-step global reaction model and combining pure component rate data to create an expression for mixtures. Three combining rules were used for the rate equation. Model 1 was a linear combination by mol fraction of the individual rates obtained assuming that all fuel was one or the other pure component. The reaction rate for fuel component 1 is,

$$W_1 = -M_1 K_1 \rho^{m_1+n_1} \left[\frac{X_1 + X_2}{M_1}\right]^{m_1} \left[\frac{X_0}{M_0}\right]^{n_1} \exp\left(\frac{-E_1}{RT}\right) \quad \textbf{(2-1)}$$

and similarly for component 2. The overall rate is then

$$W_F = Y_1 W_1 + Y_2 W_2 \quad \textbf{(2-2)}$$

Model 2 was a linear combination by mol fraction of component rate constants, giving

$$K = Y_1 K_1 + Y_2 K_2 \quad \textbf{(2-3)}$$

$$E = Y_1 E_1 + Y_2 E_2 \quad \textbf{(2-4)}$$

$$m = Y_1 m_1 + Y_2 m_2 \quad \textbf{(2-5)}$$

$$n = Y_1 n_1 + Y_2 n_2 \quad \textbf{(2-6)}$$

with the overall rate as

$$W_1 = -M K_1 \rho^{m+n} \left[\frac{X_1 + X_2}{M_1}\right]^{m} \left[\frac{X_0}{M_0}\right]^{n} \exp\left(\frac{-E}{RT}\right) \quad \textbf{(2-7)}$$

where M is the fuel mixture molecular weight,

$$M = Y_1 M_1 + Y_2 M_2 \quad \textbf{(2-8)}$$

Model 3 was a sum of the individual reaction rates for each individual component. The individual rates are calculated the same as model 1 except that the mass fraction is that for that component only instead of the sum of all; however, the overall rate is

$$W_F = W_1 + W_2 \quad \textbf{(2-9)}$$

Model 1 and 2 gave good agreement with the data; Model 3 was less successful.

Introduction of small amounts of volatile fuels decreases the ignition delay time significantly due to the increase of vapour formed early in droplet lifetime, but droplet size and fuel composition have a much smaller effect on ignition delay time than does temperature. The results are more scattered in mixtures than in pure fuels, as noted by Braide et al. (1979) and Bergeron and Hallett (1989b). The latter noticed some substantial discrepancies between measured and computed ignition times for mixtures with small concentrations of a highly volatile component, which was attributed to two-dimensional phenomena not reproduced by the one-dimensional model. These effects were dubbed “aging” because the ignition time depended on the length of time that the droplet sat on the fibre prior to the experiment. This indicates a potential problem with the suspended droplet technique with a more volatile component than *n*-nonane in small concentrations. The different reaction models used generated relatively similar results compared to the scatter for the experimental results, as the scatter was greater than this difference.

Hallett and Ricard (1991) generated a model for auto-ignition of single droplets of multi-component (more than two components) hydrocarbon mixtures; however, it was not tested experimentally. This model predicted the dependence of ignition on the mixture composition, and on the distillation curve of the fuel. The assumptions for the model used are the same as

Bergeron and Hallett (1989b) with the liquid assumed well-mixed. The model tested blends of two types of mixtures, one being of light components and the other with components with higher boiling points. It was shown that the more volatile component tended to control ignition: even at small concentrations: the ignition time dropped sharply initially and then remained almost constant as more light fraction was added. There was no concrete evidence that the distillation curve directly affected ignition delay. A comparison between mixtures that had similar boiling curves but different chemical compositions showed different ignition behaviours. This is due to the most volatile component dominating the production of vapour early in the ignition process.

Stauch and Maas (2007) developed a model, again not tested experimentally, for the auto-ignition of a two-component mixture to test the dependence of ambient temperature and initial droplet temperature. It was shown that for temperatures above 1000K the ignition time starts to become more independent of mixture composition. Also, it was shown that an increasing initial droplet temperature decreases the influence of initial droplet temperature on ignition delay; at lower ambient gas temperatures the initial droplet temperature effect is much smaller.

2.3.3 Reaction rates

There has been some work on reaction rates in continuous mixtures, but it has not been widely applied. The earliest paper was that of Aris and Gavalas (1966), who developed a mathematical theory and applied it to a simple decomposition reaction ($A \rightarrow B$). Astarita and Ocone (1992) likewise only dealt with a simple decomposition. Chou and Ho (1989) also developed a theory of reaction rates; however, an essential element of their theory was that the rate constant was itself the distribution variable, an idea that is difficult to apply to a problem which includes convection and diffusion. These papers are not directly applicable to this thesis,

but are cited as they give an insight into the earlier work on reaction rates for continuous mixtures.

Although multi-step reaction kinetic mechanisms are widely used, application of continuous thermodynamics requires the use of a simple rate model. The most widely used of this type is that of Westbrook and Dryer (1981), who gave one and two-step rate models for a wide variety of hydrocarbons, the latter being more accurate in predicting the product temperature and composition but requiring significantly more computer time. The single-step global reaction represents reaction of a hydrocarbon with oxygen, and in its simplest form the chemical reaction is

$$Fuel + n_1 O_2 \rightarrow n_2 CO_2 + n_3 H_2 O \qquad \textbf{(2-10)}$$

where the n_i are determined by the fuel used. The single-step global reaction rate is usually expressed as,

$$W_F = -KT^{\alpha}\left[Fuel\right]^m \left[Oxidizer\right]^n \exp\left(\frac{-E}{\overline{R}T}\right) \qquad \textbf{(2-11)}$$

where A is the pre-exponential coefficient, m and n are the concentration exponents, E is the activation energy, T is the temperature, and $\overline{R}$ is the universal gas constant. Westbrook and Dryer (1981) set the temperature exponent α to zero. The variables of interest for this thesis are the pre-exponential coefficient, the activation energy and the concentration exponents. For most hydrocarbons Westbrook and Dryer (1981) determined that the concentration exponents m and n should be 0.25 and 1.50 respectively and the values for the pre-exponential coefficient and activation energy were set to match experimental data for laminar flame propagation. It should be noted that activation energies determined by matching flame properties are not appropriate for ignition studies, as noted by Bergeron and Hallett (1989a) in applying this model to droplet ignition.

Little research has gone into the reaction rates model for fuels suitable for ignition alone. Bergeron and Hallett (1989a) and Bergeron and Hallett (1989b) used Westbrook and Dryer's (1981) one-step reaction model, but it required considerable modifications to E and K to match experimental droplet ignition data.

2.4 Conclusion

The conclusions that are drawn from the review of the literature performed here are:

- There are no models currently available to describe the ignition of droplets of complex liquid mixtures
- The technique of continuous thermodynamics has been proven to be successful in modeling complex mixtures for evaporation of single fuel droplets and could be extended to ignition by incorporating a continuous model for mixture reaction rate.
- A sufficient amount of pure component data are available for the selection of reaction rate variables, and rate parameters are available for oxidation of a wide number of hydrocarbons
- The assumption of a well-mixed liquid phase appears to be valid for ignition. Again, however, mixtures with a large difference in component boiling points may show some effects of liquid mixing processes
- The suspended droplet technique is a widely-used technique for carrying out ignition delay tests and appears to give data which are in good agreement with one-dimensional computational models. It may however be subject to some error in dealing with mixtures

containing a very volatile component with a large difference in boiling point between components

It has been identified that there is a lack of ignition models for droplets of complex mixtures in the literature. This thesis will help fill this gap by presenting the model and results illustrating the ignition delay time of single multi-component fuel droplets using the method of continuous thermodynamics.

Chapter 3 Experimental Setup

3.1 Current Techniques

There are a few different experimental techniques used to study the evaporation and combustion of a single droplet. Current experimental approaches include the following:

- the suspended droplet / moving furnace technique, in which a droplet is suspended from a fibre and a hot furnace is moved over the fibre.
- the suspended droplet / hot air jet technique, which also uses a droplet suspended on a fibre, but heats it with a hot air jet flowing by instead of a hot furnace.
- the drop tube furnace, in which a droplet is allowed to fall down a tubular furnace containing a slow flow of hot gases.

The experimental setup used for the tests described in this thesis is the suspended droplet/moving furnace technique, in which a horizontally sliding electric furnace moves to cover a suspended droplet and have subjected it to a step increase in temperature. Recent applications of the suspended droplet technique for ignition of fuel droplets were done by Shaw and Wei (2007) and Nakaya et al. (2009). Other techniques such as the hot gas flowing around the droplet were rejected, as a forced convection could change the ignition region from the envelope to the wake of the droplet, changing the ignition mechanism and time.

A source of error as noticed by Bergeron and Hallett (1989b) for mixtures with two different components of very different boiling point, with a very volatile light component, was in

the time between placing the droplet on the fibre and moving the furnace into position. This phenomenon, called “aging”, occurs owing to natural convection (which initially acts down, since fuel vapour is heavier than air): the initial vapour that controls most of the ignition comes from the top of the bead, where evaporation would be increased due to the thin layer of the volatile fuel. This was more dominant in mixtures with a highly volatile component combined with a fuel of a much lower volatility. This had no effect in fuels whose light component was *n*-nonane or a less volatile species, and no effect for the pure compounds. It is unlikely to happen for continuous mixtures with closely spaced components. To minimize the error it was suggested to decrease the time between placing the droplet on the fibre and moving the furnace. Overall the effect was not very significant. Natural convection otherwise has little to no effect on the ignition delay time.

Bergeron and Hallett (1989a, 1989b) had used a suspended droplet / moving furnace technique which is summarized as follows: an electric furnace was used, which was moved by a compressed gas cylinder and guided by rails. The furnace had a small slit for the droplet and its support to enter the furnace and the movement of the furnace over the droplet did not appear to affect the ignition delay time as long as the ignition delay time was significantly longer than the traverse time of the furnace (about 0.2 s). The effect of the fibre being present and adding to heat addition by conduction was found to have very little effect, especially since the ignition was observed to occur on the farthest side of the droplet from the fibre. The experimental setup used by Bergeron and Hallett (1989a, 1989b) was almost identical to the setup used for this thesis, which is described in detail in the following section.

3.2 Experimental setup

The schematic and diagram of the experimental setup can be seen below in Figure 3-1. The furnace design was based on available heaters which created an oval volume around the droplet when installed, providing perhaps more evenly distributed heat than the earlier rectangular design of Bergeron. As illustrated in Figure 3-1c) the heating elements are two 125 mm diameter half-cylindrical electric heaters separated by a 50 mm space for the windows and the sides; top and bottom are insulated with 50 mm thick insulating board. The droplet is suspended from a quartz fibre of approximately 0.2 mm in diameter with a 0.6 mm diameter bead at the tip to hold the droplet (Figure 3-2 a)). The measurements of the quartz rod, bead and fuel droplet were done with the aid of a picture similar to Figure 3-2 which included a millimetre scale held in the plane of the fibre. The measurements were determined by counting the number of pixels in 1 mm and the pixels in the measurements of the quartz fibre, bead and fuel droplet. The fibre is suspended from a steel arm that is static and connected to the base of the supporting table. The furnace is moved by a compressed air cylinder with a valve to control the direction of travel either towards or away from the droplet. The pressure of air required to move the furnace the distance from its initial position to its final position, surrounding the droplet, is approximately 55 psig. The furnace moves on Thomson Roundway linear ball bearings. The furnace has two small circular quartz windows at the sides of the furnace perpendicular to the direction of travel. These windows allow for visual inspection, photography and ignition detection. There is a slit in the furnace at the front, in the direction of travel, through which the droplet and fibre enter. This is normally blocked by a pivoting shutter whose purpose is to prevent fresh air from entering the furnace for as long as possible while the furnace is in motion.

The shutter is opened by a cam-follower system just before it reaches the suspended droplet; it should be noted there is a possibility of a small amount of cool (room temperature) air entering the furnace when the pivoting shutter opens to let the droplet enter the furnace. The shutter then remains open until the furnace is retracted away from the droplet.

Underneath the furnace a microswitch is actuated at the instant when the droplet enters the furnace. When the furnace is in the retracted position, farthest from the droplet, a small hole at the back of the furnace relative to the direction of travel allows for a K-type thermocouple probe and a small tube to protrude into the centre of the furnace. The thermocouple is used to determine the temperature of the furnace directly before moving it towards the droplet, and is set so that it occupies the same position in the furnace that the droplet will take up after the furnace has moved. The precision of the K-type thermocouple used is +/-2^{o}C. The tube is used to admit purging air from a compressed air tank to expel the products of the previous ignition out of the furnace prior to an experiment. The purging time and flow rate were determined based on calculations shown in Section 3.4, and the air flow rate entering the furnace was monitored by a flow meter. The final positioning of the furnace after it moves is critical to ensure that the droplet ends up opposite the windows. To ensure this positioning, a pin drops into a hole at the end of the track at that specific position.

An array of photodiodes was used to detect ignition, ignition being defined by the first emission of visible light. These diodes were shielded from other light by being placed at the back of a black cylinder with the opposite side open and facing towards the furnace window and in the line of sight of the droplet when the furnace was in the forward position. The cylinder interior was painted black to reduce noise in the form of reflected light from the surroundings. The photodiodes were connected together in parallel and joined into a circuit with the oscilloscope

and a resistor as shown in Figure 3-3. The photodiodes become electrically conducting when exposed to light, allowing current to flow and producing a voltage drop over the resistor which is measured by the oscilloscope. The oscilloscope's time base is triggered by the microswitch when the droplet enters the furnace, and recording begins from that moment. The oscilloscope used was a Tektronix TDS1001B digital storage unit.

An optical system was used in order to concentrate the light on the photodiodes and reduce the effects of extraneous light. At higher furnace temperatures the light emitted from the furnace walls increased, which added more noise to the signal on the oscilloscope and diminished the ability to distinguish the point of ignition. This effect was reduced by adding a shielding disc at the opening of the cylinder. The disc had a much smaller opening, just big enough to allow the magnified fibre, droplet, and ignition zone to be visible to the diodes, which blocked most surrounding light from the furnace walls. This was necessary at temperatures above 820 degrees Celsius.

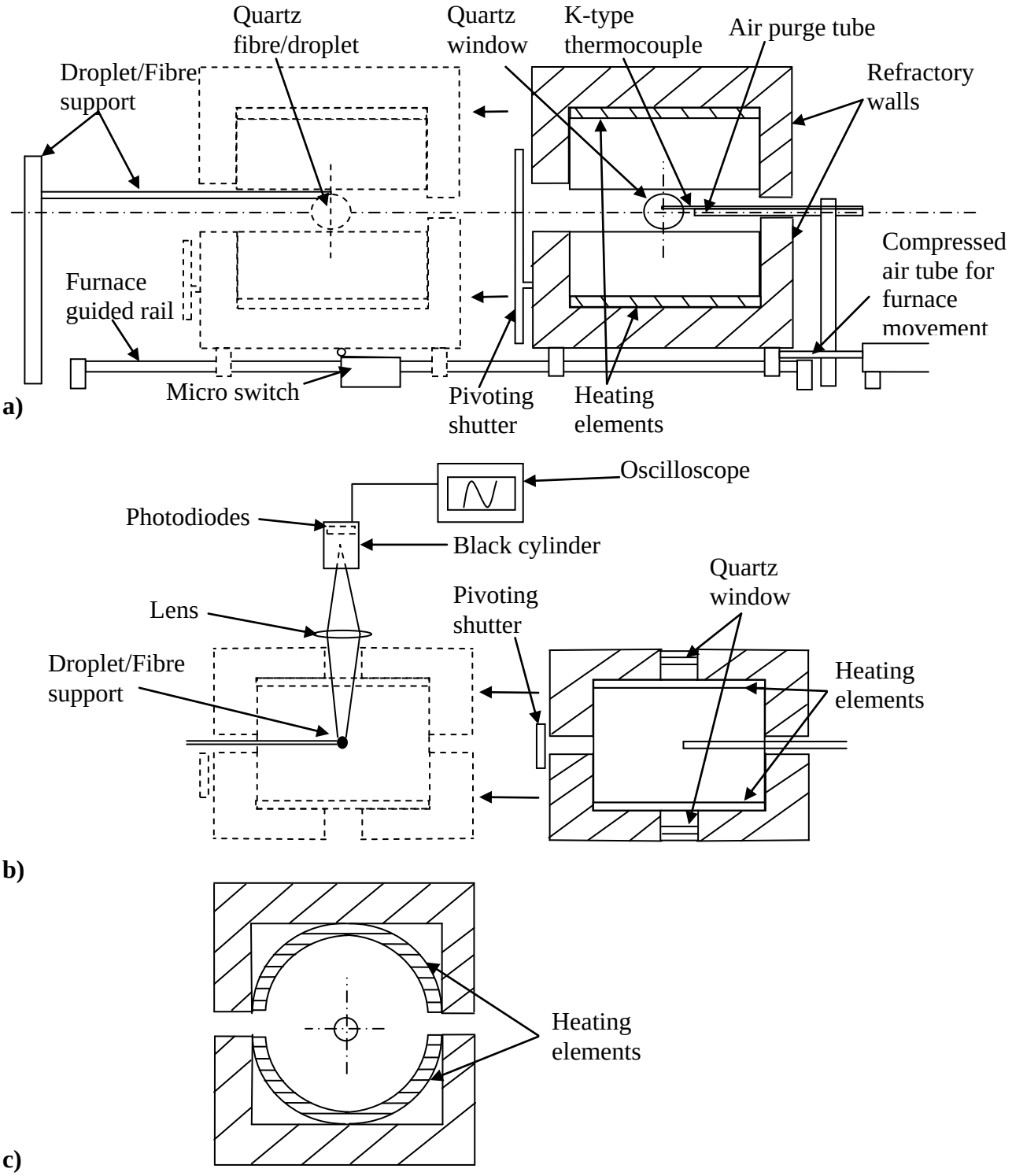

Figure 3-1: Schematic of experimental apparatus [Note: not to scale] a) Side section-view (mid-plane) showing the retracted position in solid lines and forward position with dashed lines b) Top section-view (mid-plane) showing the retracted position in solid lines and forward position with dashed lines c) Front section-view (mid-plane) normal to the direction of travel showing the heating elements

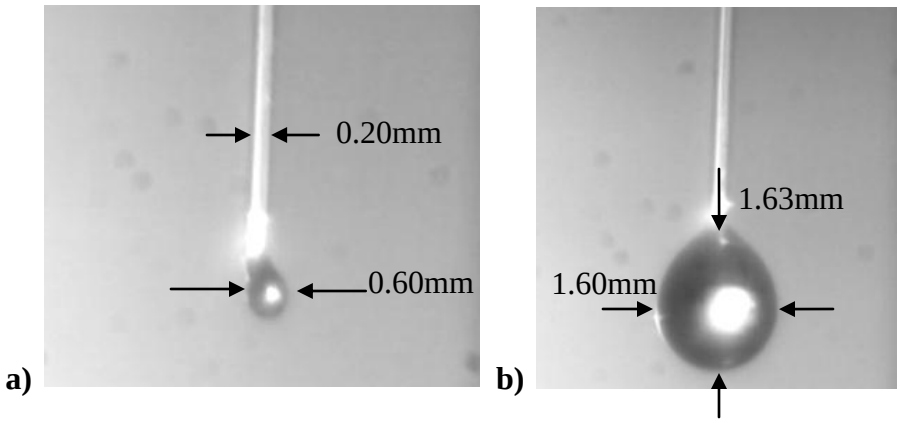

Figure 3-2: a) Dimensions of quartz fibre b) Dimensions of droplet

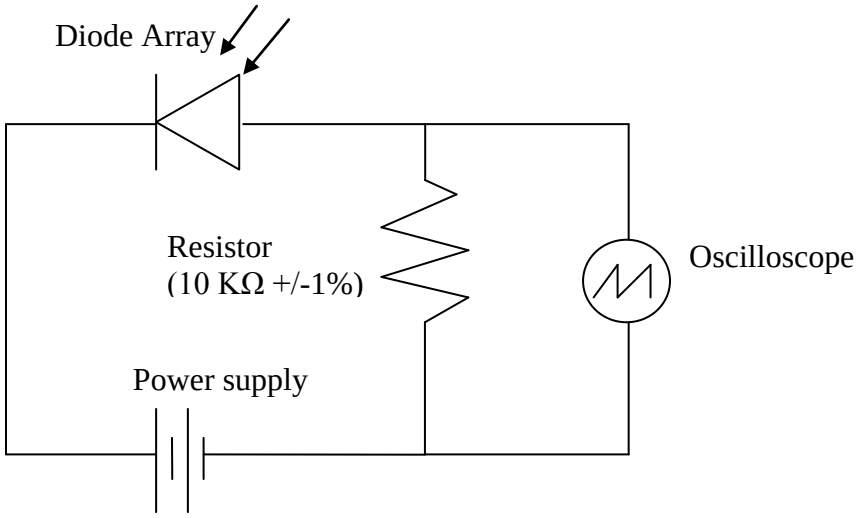

Figure 3-3: Diode connection circuit

3.3 Experimental procedure

A micro-litre syringe, as used by Bergeron and Hallett (1989a, 1989b), was used to generate the droplets and place them on the quartz fibre. For this work, all droplet volumes used were 2μL and each fuel used had a purity greater than or equal to 99%. Both the volume of the fuel and the bead at the end of the quartz fibre contribute to the droplet volume and must be

taken into account to accurately determine the diameter of the fuel droplet. By adding the volume of the fuel to the volume of the quartz fibre bead that had a diameter of 0.6 mm the diameter of the droplet hanging from the quartz fibre was determined to be 1.6 mm; however, the droplet was not actually spherical and a volume-equivalent spherical diameter was used (Figure 3-2 b)). The droplet volume was very precisely reproduced by a stopper on the micro-litre syringe that allowed the same volume of fuel to be drawn for each test. The precision of the micro-litre syringe is ± 0.025 μL and the accuracy of the bead diameter was ± 0.1 mm, providing an overall accuracy to the fuel droplet diameter of ± 0.04 mm.

To begin a droplet ignition after planting a droplet on the fibre, a valve is turned to move the furnace from the retracted position to fully forward to cover the droplet. Just as the droplet enters the furnace the microswitch is triggered, which prompts the oscilloscope to start recording. The oscilloscope is programmed to record the photodiode's signal 5.00 seconds prior to the trigger and 5.00 seconds after the trigger. The furnace continues moving forward until the pin on the furnace falls into position, at which point the droplet is positioned in front of the window and in line with the ignition detection optics. During the ignition process the photodiodes are continuously recording the amount of light from the furnace and display a very distinguishable sharp rise in signal when ignition occurs as shown in Figure 3-4. The data are then saved to a Universal Serial Bus (USB) flash drive in the form of a .CSV file. This file is opened in Excel to determine the time that ignition has occurred. Since the ignition spike rises over 0.01 seconds, this makes the precision of the ignition time measurement +/- 0.005 seconds. After the ignition event, the furnace is returned to its original position and is then purged with fresh air from the compressed air tank for two minutes at a flow rate of 40 L/min. This causes the temperature of the furnace to drop significantly, so that time is required for the temperature to

rise back to the desired level. To ensure that a steady temperature level has been reached, the furnace temperature must be observed to have reached a plateau, roughly defined by more than fifteen seconds being required for the temperature to rise one degree Celsius. This state required about 8-12 minutes to reach after purging.

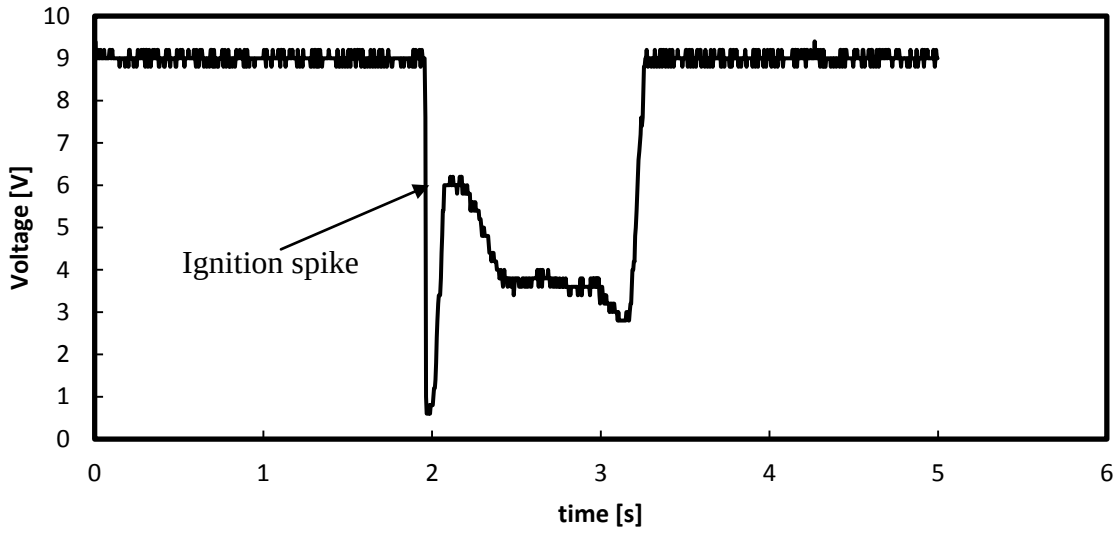

Figure 3-4 Ignition spike signal viewed on the oscilloscope

3.4 Purging requirements for furnace

The following calculations were used for determining the required time to purge the furnace of all combustion products with fresh air.

A mass balance on the gas in the furnace gives:

$$\dot{m}_{AIRIN} = \dot{m}_{GASOUT} \tag{3-1}$$

and a mass balance on the combustion products gives,

$$\dot{m}_{AIRIN} X_{P\infty} = \dot{m}_{GASOUT} X_{POUT} + \frac{d}{dt}(mX_P)_{FURNACE} \tag{3-2}$$

where $X_{P\infty}$ is the mass fraction of the products in the ambient air (= 0). To solve the differential equation two main assumptions are used: a well-mixed reactor, in which the concentration of products exiting the furnace X_{POUT} is equal to the concentration inside the furnace $X_{P\ FURNACE}$; and a constant mass inside the furnace. (In reality, the mass does change slightly due to the temperature drop from purging with air.) The solution of the differential equation is then

$$X_P = X_{P0} \exp\left(-\frac{\dot{m}_{AIR}}{m_{FURNACE}} t\right) \quad \textbf{(3-3)}$$

where X_{P0} is the initial concentration of products in the furnace. The initial concentration of products could be determined from simple combustion stoichiometry calculations for a droplet which is typically 1.6 mm in diameter. Purging was deemed to be sufficient when the concentration of products within the furnace reached less than 0.2% of the original value. Using a mass flow of 40 L/min and a purging time of 2 min provided a more than the required time of 30 seconds to purge down to 0.2% of the original mass of products within the furnace. This was based on the furnace dimensions of roughly 12.7 cm wide x 15.2 cm high x 15.2 cm long. The fuel mixture will be chosen later.

3.5 Designing the experimental mixtures

For the experiments, the objective was to design a mixture that could be accurately represented by a continuous thermodynamics distribution and be tested experimentally. The method used to do this will be outlined in this section. The basis of the method is the use of a numerical simulation of the standard ASTM D-86 distillation test (Annual Book of ASTM Standards, issued annually). An ASTM distillation test in summary is performed by evaporating a mixture and recording the vapour temperature (also known as the bubble point) of the mixture

until all of the mixture has been evaporated. The mixture is composed of lighter and heavier components: as the lighter components evaporate out of the mixture they leave behind heavier components which have higher boiling points and increase the boiling point of the mixture. A continuous thermodynamics model of the distillation test is used to generate the distillation curve for a distribution, while a discrete component model of the same test is used to generate the curve for experimental mixtures composed of multiple *n*-paraffin fuels. The continuous thermodynamics ASTM model was used to provide the distribution parameters of the mixture and the ASTM discrete component mixture model was used to aid in physically designing the mixture by applying known mass fractions of each pure fuel.

Initially a trial mixture of discrete components was selected, specifying the mass fraction of each pure component. Next an ASTM distillation curve for this discrete component mixture was simulated by an existing model developed by Hallett and Ricard (1991); it required inputs of the mass fraction of each fuel component in the mixture. (A real distillation test on the experimental mixtures was not carried out owing to the cost of chemicals for the substantial volume of liquid needed for a test according to ASTM specifications.) Following this, an ASTM distillation curve model for continuous mixtures, given by Hallett and Beauchamp-Kiss (2010), with input parameters θ, σ, and γ, was used, and its inputs were iterated to produce a distillation curve that closely fitted the distillation curve for the discrete component mixture. The parameter γ is the distribution origin, which here was set to 0, while θ and σ are the mean and standard deviation respectively. Both models gave the boiling temperature of the mixture versus the volume percent evaporated. If a close match could not be achieved (for example, if the discrete distribution produced a distillation curve with “bumps” in it that could not be matched by the smooth continuous distribution), the components of the discrete mixture were adjusted until a match was

achieved. When a match was achieved the physical mixture was created with the assistance of a balance and with very reasonable accuracy to the theoretical mass fractions, since the accuracy of the balance was +/- 0.0001 grams.

Chapter 4 Model

4.1 Theory

Continuous thermodynamics is a method of representing a multicomponent mixture using a probability density function *f*(I) with as few as three distribution parameters instead of discrete components. The number of parameters is independent of the number of components in the mixture, making this a very practical method for droplet evaporation, for example. As concluded in the literature sections, continuous thermodynamics is a useful mixture modelling technique for complex multi-component mixtures and has been applied successfully to droplet evaporation, but has not been combined with chemical reaction to simulate droplet ignition or combustion. This chapter will illustrate the method of developing such a model and then testing it.

4.1.1 Mathematical Model - Evaporating Droplet

The equations used to solve the continuous thermodynamics problem of an evaporating droplet were developed by Tamim (1996). This model was based on assumptions that are standard in most droplet models: transport properties vary in space and time in the vapour phase; the liquid droplet is well-mixed, which assumes a uniform temperature and concentration within the droplet (however, both of these vary with time); and spherical symmetry is assumed for the droplet and the surroundings, making the problem one-dimensional in the radial direction.

However, to extend the model to multi-component mixtures the following modifications were required: development of transport equations for a continuous mixture , selection of an appropriate distribution function to represent the fuel mixture, selection of appropriate characterizing variables for the distribution, and development of correlation equations for the transport properties in terms of the distribution characterizing variable (Tamim and Hallett, 1995). Abdel-Qader and Hallett (2004) mentioned that some internal circulation is present in most real droplets; however, the extreme case of diffusion-limited droplets may only be important in two-component mixtures with widely differing boiling points. The well-mixed case for droplet mixtures with boiling points that vary relatively little from neighbouring components with similar molecular weight is a reliable assumption (Aggarwal (1988); Bergeron and Hallett (1989b); Abdel-Qader and Hallett (2004)). These equations were derived from first principles for a continuous mixture and they did not include chemical reaction.

This thesis is an extension of Tamim (1996) and solves five governing differential equations for the vapour phase (overall continuity, energy, and diffusion of the fuel mixture as a whole and of the distribution mean and standard deviation), shown below,

$$\frac{\partial c}{\partial t} + \nabla \cdot cv^* = 0 \tag{4-1}$$

$$\overline{C}_P \frac{\partial}{\partial t}(cT) + \overline{C}_P \nabla \cdot (cv^* \cdot T) = \nabla \cdot \lambda \nabla T - \sum_{i=1}^{n} J_i^* \cdot \nabla \overline{h}_i + S \tag{4-2}$$

$$\frac{\partial}{\partial t}(cy_i) + \nabla \cdot (cv^* \cdot y_i) = \nabla \cdot \left(cD_{im} \nabla y_i \right) \tag{4-3}$$

$$\frac{\partial}{\partial t}(cy_i\theta) + \nabla \cdot (cv^* \cdot y_i\theta) = \nabla \cdot \left(cD_{im} \nabla \left(y_i\theta \right) \right) \tag{4-4}$$

$$\frac{\partial}{\partial t}(cy_i\psi) + \nabla \cdot (cv^* \cdot y_i\psi) = \nabla \cdot \left(cD_{im} \nabla \left(y_i\psi \right) \right) \quad \textbf{(4-5)}$$

where ψ is defined in equation (4-13). The energy equation contains a source term *S* for the heat released by chemical reaction, but no such term appears in the other equations for reasons that will be explained in the next section. The other elements of the model are an energy balance on the droplet to describe droplet heating, mol balances on the droplet to describe how the liquid composition changes in time, and appropriate properties relationships.

4.1.2 Single Distribution Function

A continuous thermodynamics model was developed by Tamim (1996) to model the evaporation of a single droplet mixture, but did not include chemical reaction. A one-step oxidation reaction of the form developed by Westbrook and Dryer (1981) and also used by Bergeron and Hallett (1989a, 1989b) to model the ignition time of a single droplet will be used for this thesis with the addition of applying continuous thermodynamics to it. One key assumption made was that no reactants were consumed prior to reaction. This simplifies the problem, as no reaction source term is required in the conservation equations for individual species (fuel and oxygen) and there are no requirements to track the products. There is of course a reaction source term in the energy equation (term *S* in equation 4-2 above), which calculates the heat released by the reaction – an essential part of any thermal ignition model – and a suitable expression for this must now be devised. The following steps are taken to develop a usable

continuous thermodynamics formulation to model the reaction of a mixture comprising many components.

The chemical reaction rate equation developed by Westbrook and Dryer (1981) as used by Bergeron and Hallett (1989a) is

$$W_F = M_F K \rho^{(m+n)} \left(\frac{X_F}{M_F}\right)^m \left(\frac{X_O}{M_O}\right)^n \exp\left(-\frac{E}{\bar{R}T}\right) \quad \textbf{(4-6)}$$

where W_F is the consumption of fuel in kg fuel/m^{3}s, M_F and M_O are the molecular mass of the fuel and oxygen in kg/kmol, K is the pre-exponential coefficient, X_F and X_O are the mass fractions of fuel and oxygen, E is the activation energy in kJ/gmol, R is the universal gas constant and T is the temperature in Kelvin. For this equation to be used in the existing continuous thermodynamics droplet model it must be converted to use mol fractions rather than mass fractions:

$$W_{Fi} = M_{F_i} K_i c^{(m_i+n_i)} \left(Y_{F_i}\right)^{m_i} (Y_O)^{n_i} \exp\left(-\frac{E_i}{\bar{R}T}\right) \quad \textbf{(4-7)}$$

Despite the use of mol fraction, W_{Fi} is still in kg/m^3 s because it will later be multiplied by the enthalpy of reaction in kJ/kg for insertion into the energy equation. This form was then required to be converted to a continuous thermodynamics form. This was done by equating the fuel molecular mass M_{Fi} to the distribution variable I. The fuel mol fraction Y_{Fi} then becomes $Y_F f(I) dI$, where Y_F is the total fuel vapour mol fraction, and $f(I)$ is the distribution function, which will be discussed in the next section. The rate parameters K and E will be represented as functions of I which will be derived from data for pure fuels; these expressions will be introduced later.

The chemical reaction rate equation then becomes, for a single component

$$W(I) = IK(I) c^{m+n} \left[Y_F f(I) dI\right]^m \left[Y_O\right]^n \exp\left(\frac{-E(I)}{\bar{R}T}\right) \quad \textbf{(4-8)}$$

Since dI is a differential quantity, $W(I)$ is effectively a differential reaction rate.

The reaction rate multiplied by the enthalpy of reaction must be inserted into the energy equation. Tamim and Hallett (1995) give the energy equation for the vapour phase of an evaporating droplet in continuous mixture form; it is derived by writing it for a single component and then integrating over the distribution function from zero to infinity. The same operation now needs to be performed for the reaction rate. The values for the exponents *m* and *n* used by Bergeron and Hallett (1989a) were 0.25 and 1.5 respectively, and were taken directly from Westbrook and Dryer (1981), who recommended them as optimal values. A differential to a non-integer power is not defined, so that *m* must be taken as 1 from now on and the rate parameters for pure fuels will be different from those of Bergeron and Hallett (1989a). The use of unity concentration exponents *m* and *n* will be justified later by showing that they represent the ignition process well for pure fuels. The rate equation (4-8) then becomes

$$W = \int_0^\infty IK(I)c^{1+n}Y_F\left[Y_O\right]^n \exp\left(\frac{-E(I)}{\bar{R}T}\right) f(I)dI \qquad \textbf{(4-9)}$$

Three different models for the variation of *K* and *E* with *I* were tested, with a view to computational simplicity without giving up much accuracy. The first was the special case of the activation energy *E* being constant for all components, while *K* was allowed to vary linearly with *I*:

$$K(I) = a_K + b_K I \qquad \textbf{(4-10)}$$

The values of a_K and b_K were fitted using the numerical model developed here to best match ignition data for pure fuels generated by Bergeron and Hallett (1989a) and in the present work. The value of *E* then becomes an average activation energy for all components. The chemical rate equation then simplifies to,

$$W = \int_0^\infty \left(a_K I + b_K I^2\right) c^{(1+n)} Y_F \left(Y_O\right)^n \exp\left(\frac{-E_{avg}}{\bar{R}T}\right) f(I)dI \qquad \textbf{(4-11)}$$

which can be integrated analytically to

$$W = \left(a_K \theta + b_K \psi^2\right) c^{(1+n)} Y_F \left(Y_O\right)^n \exp\left(\frac{-E_{avg}}{\bar{R}T}\right) \quad \textbf{(4-12)}$$

where θ is the mean molecular weight and Ψ is the second central moment of the distribution function, equal to

$$\psi = \theta^2 + \sigma^2 \quad \textbf{(4-13)}$$

As will be shown later, for the *n*-paraffin mixtures which are the subject of the present experiments, the activation energy varies substantially with I. The second formulation tested therefore used a linear formula for both the values of activation energy *E* and pre-exponential coefficient *K*. The equation for *K* is shown above in Equation (4-10), while the linear equation used for *E* is

$$E(I) = a_E + b_E I \quad \textbf{(4-14)}$$

The values of a_E and b_E were fitted to best match data for pure fuels from Bergeron and Hallett (1989a) and from the present work. This model is similar but not identical to the conclusion of Bergeron and Hallett (1989b) that a reaction for a two component mixture could be modelled well by combining component values of *K* and *E* by mol fraction. The rate equation then becomes

$$W = \int_0^\infty \left(a_K I + b_K I^2\right) c^{(1+n)} Y_F \left(Y_O\right)^n \exp\left(-\frac{a_E + b_E I}{\bar{R}T}\right) f(I) dI \quad \textbf{(4-15)}$$

This formulation can no longer be integrated analytically.

Again, as will be shown later, for *n*-paraffins a linear variation of *K* with *I* was found to show relatively large deviations from the experimental results. A much better approximation was found with an exponential dependence of *K* on molecular mass for the fuels used. The following correlation was used:

$$K(I) = \exp(a_K + b_K I) \tag{4-16}$$

The activation energy relationship was kept linear since it is in fact nearly linear with varying molecular mass, as will be shown later. The rate equation then becomes

$$W = \int_0^\infty \left(\exp\left(a_K I + b_K I^2\right)\right) c^{(1+n)} Y_F \left(Y_O\right)^n \exp\left(-\frac{a_E + b_E I}{\bar{R}T}\right) f(I) dI \tag{4-17}$$

Since these equations cannot be integrated analytically, either Simpson's rule or the trapezoid rule would be required to complete the integration. For the case of this work, the trapezoid rule was used; it is defined as

$$\int_a^b f(x)dx \cong \frac{b-a}{2N}[f(x_0) + 2f(x_1) + 2f(x_2) + \cdots + 2f(x_{N-2}) + 2f(x_{N-1}) + f(x_N)] \tag{4-18}$$

which can also be written as

$$\int_a^b f(x)dx \cong \frac{b-a}{N}\left[\frac{f(a)-f(b)}{2} + \sum_{k=1}^{N-1} f\left(a + k\frac{(b-a)}{N}\right)\right] \tag{4-19}$$

Applying the trapezoidal rule to the chemical rate equation it becomes

$$\int_a^b W(I)dI \cong \frac{b-a}{N}\left[\frac{W(a)-W(b)}{2} + \sum_{k=1}^{N-1} W\left(a + k\frac{(b-a)}{N}\right)\right] \tag{4-20}$$

The range of integration was chosen to be from I = 0 to 400 kg/kmol, and the size of integration step N was chosen to be 1 kg/kmol. The integration limits were varied to see the effect on the results as were the step size. The step size had the largest impact on the model's speed, but it had little to no effect on the results up to a certain step size, as will be discussed later in the Section 4.2.3.

4.1.3 Distribution function

For this work, the distribution function $f(I)$ was chosen as a gamma distribution, defined as

$$f(I) = \frac{(I-\gamma)^{\alpha-1}}{\beta^{\alpha}\Gamma(\alpha)} \exp\left[-\left(\frac{I-\gamma}{\beta}\right)\right] \quad \textbf{(4-21)}$$

where $\Gamma(\alpha)$ is the gamma function, and α, β and γ are distribution parameters which are related to the distribution moments by

$$\theta = \alpha\beta + \gamma \quad \textbf{(4-22)}$$

$$\sigma^2 = \alpha\beta^2 \quad \textbf{(4-23)}$$

where θ is the mean molecular weight of the mixture and σ^2 is the variance. For the work done for this thesis γ was equated to zero.

For numerical calculations, the gamma function $\Gamma(z)$ can be represented by Stirling's Formula (Abramowitz and Stegun (1965)):

$$\Gamma(z) \cong e^{-z} z^{z-\frac{1}{2}} (2\pi)^{\frac{1}{2}} \left[1 + \frac{1}{12z} + \frac{1}{188z^2} - \frac{139}{51840z^3} - \frac{571}{2488320z^4} + \cdots\right] \quad \textbf{(4-24)}$$

which holds for $(z \to \infty \; in \; |\arg z| < \pi)$.

The distribution variable *I* can be one of many different parameters that distinguish differences between compounds, including carbon number, boiling point and molecular chain length. In this thesis work, as in other continuous mixture droplet work, the distribution variable is molecular weight.

Pure fuels were also represented with this approach. This was done by setting the mean to the molecular weight of the pure compound and setting the standard deviation to a small value, ideally σ = 1 kg/kmol (this is outlined in more detail in Section 5.1.2).

4.1.4 Multi-distribution ignition

The approach of continuous thermodynamics evaporation was first used to model mixtures using a single distribution function; however, it has been further developed to model mixtures with multiple distributions by Abdel-Qader and Hallett (2004). This approach introduces the use of *J* different mixtures, each with a distribution function $f_j(I)$, represented by its mean mixture molecular weight θ_j and distribution variance σ_j^2 for the mixture *j*. The values of θ_j and σ_j^2 must be known for the individual mixtures *j* prior to combining them into a multi-mixture blend, and the mass and mole fraction must be known for each mixture *j* after combining the mixtures. The distribution functions are again chosen to be gamma distributions, defined as

$$f_j(I) = \frac{(I-\gamma_j)^{\alpha_j - 1}}{\beta_j^{\alpha_j}\Gamma(\alpha_j)} \exp\left[-\left(\frac{I-\gamma_j}{\beta_j}\right)\right] \quad \textbf{(4-25)}$$

where $\Gamma(\alpha_j)$ is the gamma function, and α_j, β_j and γ_j are distribution parameters of mixture *j* and can be characterized by

$$\theta_j = \alpha_j \beta_j + \gamma_j \quad \textbf{(4-26)}$$

$$\sigma_j^{\,2} = \alpha_j \beta_j^{\,2} \quad \textbf{(4-27)}$$

Again, for the work done for this thesis γ was equated to zero.

The multi-distribution model did not require any additional manipulation or additional equations to calculate the reaction rates; however, the multi-mixture model had to be coded to include chemical reaction in similar fashion to the single mixture model, as it had not been done previously to this thesis work. The difference for the reaction rate equation to be used in the multi-distribution model is the addition of the subscript *j* to represent mixture *j*:

$$W = \sum_{j=1}^{J} \int_{0}^{\infty} IK_j(I) c_j^{1+n} x_{Fj} \left[x_{Oj}\right]^n \exp\left(\frac{-E_j(I)}{\bar{R}T}\right) f(I)\, dI \quad \textbf{(4-28)}$$

The expressions for pre-exponential coefficient $K_j(I)$ and activation energy $E_j(I)$ will be the same as for a single distribution function and after a proper relationship is determined the same integration techniques will be applied here. The exponents m and n are set to one for the same reason as described earlier.

Additionally the continuous thermodynamics model uses the Clausius-Clapeyron equation in continuous mixture form to describe phase equilibrium at the droplet surface. For more information on the details of the continuous thermodynamics model the reader is referred to Tamim (1996).

4.2 Numerical Model

Equations (4-1) - (4-5) are solved using finite volume techniques following the method of Patankar (1980). This method discretizes the droplet and surrounding atmosphere into a number of nodes. In this situation the implicit finite difference technique was used to advance to the next time step. Ignition occurs when the temperature at any node reaches 2000 K. The following will outline the techniques used. Only the solution of the energy (temperature) equation will be presented, as the others are identical to Tamim's work.

4.2.1 Finite Volume Solution

Prior to setting up and solving the numerical solution, the governing equations in the vapour phase had to go through a transformation of coordinates in the radial direction. This was

required to keep the first node point at the surface of the droplet, since the droplet surface recedes as it evaporates and produces vapour. This is accomplished by using the following relationships,

$$\xi = \frac{r}{R} \tag{4-29}$$

where r is the distance in the radial direction and R is the radius of the liquid droplet. Additionally, a new velocity relative to the new coordinates was defined as

$$w = v - \xi \dot{R} \tag{4-30}$$

where

$$\dot{R} = \frac{dR}{dt} \tag{4-31}$$

which defines the rate at which the droplet surface is receding.

The equations for temperature (energy), for the vapour phase mol fraction and for the mean and standard deviation of the distribution equations were solved using finite volume techniques outlined by Patankar (1980). The equations were discretized and had the general form of

$$a_p T_p = a_E \left[f T_E + (1-f) T_E^o \right] + a_W \left[f T_W + (1-f) T_W^o \right] + \left[a_P^o - (1-f) a_E - (1-f) a_W \right] T_P^o + b \tag{4-32}$$

where $f = 1$ for the fully implicit scheme as developed by Patanakar (1980), for which this reduces to

$$a_p T_p = a_E T_E + a_W T_W + a_P^o T_P^o + b \tag{4-33}$$

where the coefficients "a" with different subscripts are determined by integrating the differential equations over the control volume and over time from zero to $t + \Delta t$. The subscripts E, W and P refer to the neighbouring nodes east and west and the point P being analyzed as illustrated in

Figure 4-1, and the variable *b* refers to the source term, which for the energy equation includes the reaction rate expression. The superscript ^{o} refers to the value at the previous time step (Patankar, 1980).

The power-law scheme developed by Patankar (1980) and used by Tamim (1996) is a way of combining the convection and diffusion terms in calculating the coefficients a_P, a_E and a_W by the following

$$a_E = D_e A(P_e) + \|-F_e, 0\| \quad \textbf{(4-34)}$$

$$a_W = D_w A(P_w) + \|-F_w, 0\| \quad \textbf{(4-35)}$$

$$a_E = -a_E - a_W - F_e + F_w \quad \textbf{(4-36)}$$

where *D* and *F* represent diffusion and convection respectively and will be defined later when solving the energy equation. The subscripts *e* and *w* refer to the faces of the control volume for east and west respectively (Figure 4-1). The variable *P* is the Peclet number and is defined as

$$P = \frac{F}{D} \quad \textbf{(4-37)}$$

and the function *A(P)* is given by

$$A(P) = \left\| 0, \left(1 - 0.1|P|\right)^5 \right\| \quad \textbf{(4-38)}$$

where the brackets ||...|| mean "the greater of".

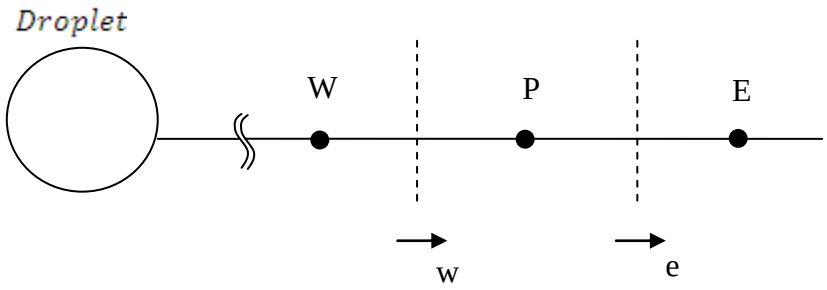

Figure 4-1 Diagram of sample grid points in the one dimensional problem for the droplet

The energy equation derived for the vapour phase of an evaporating droplet using continuous thermodynamics by Tamim (1996) is shown below, with, however, the addition of the source term *S* for chemical reaction. This is the same as equation (4-2) with the interdiffusion term expanded as in Tamim and Hallett (1995):

$$\overline{C}_P \frac{\partial}{\partial t}(cT) + \overline{C}_P \nabla \cdot (cv^* T) = \left[(a_c - C_{PA}) c \overline{D} \nabla y_F + b_c \theta c D \nabla y_F \right] \nabla T + \nabla \cdot \lambda \nabla T + S \tag{4-39}$$

where a_C and b_C are coefficients of a linear expression for the variation of fuel vapour specific heat with molecular mass, and include the effect of temperature, as given by Tamim (1996) and defined by

$$C_P(I) = a_C + b_C I \tag{4-40}$$

With the change of coordinates defined in Equations (4-29), (4-30) and (4-31), Equation (4-39) becomes

$$\begin{aligned} \xi^2 \overline{C}_P \frac{\partial}{\partial t}(cT) + \overline{C}_P cT \frac{\dot{R}}{R} \frac{\partial \xi^3}{\partial \xi} + \frac{\overline{C}_P}{R} \frac{\partial}{\partial \xi}\left(\xi^2 T w c\right) &= \frac{1}{R^2} \frac{\partial}{\partial \xi}\left(\xi^2 \lambda \frac{\partial T}{\partial \xi} \right) \\ &+ \frac{\xi^2}{R^2}\left[(a_c - C_{PA}) c \overline{D} \frac{\partial y_F}{\partial \xi} + b_c c D \frac{\partial y_F \theta}{\partial \xi} \right] \frac{\partial T}{\partial \xi} + \xi^2 S \end{aligned} \tag{4-41}$$

Dividing by the specific heat and integrating over the control volume, it becomes

$$\begin{aligned} \int_w^e \int_t^{t+\Delta t} \xi^2 \frac{\partial}{\partial t}(cT) dt d\xi + \int_t^{t+\Delta t} \int_w^e cT \frac{\dot{R}}{R} \frac{\partial \xi^3}{\partial \xi} d\xi dt &= -\int_t^{t+\Delta t} \int_w^e \frac{1}{R} \frac{\partial}{\partial \xi}\left(\xi^2 c w T\right) d\xi dt \\ &+ \int_t^{t+\Delta t} \int_w^e \frac{1}{R^2 \overline{C}_P} \frac{\partial}{\partial \xi}\left(\xi^2 \lambda \frac{\partial T}{\partial \xi} \right) d\xi dt \\ &+ \int_t^{t+\Delta t} \int_w^e \frac{\xi^2}{R^2 \overline{C}_P}\left[(a_c - C_{PA}) c \overline{D} \frac{\partial y_F}{\partial \xi} + b_c c D \frac{\partial y_F \theta}{\partial \xi} \right] \frac{\partial T}{\partial \xi} d\xi dt \\ &+ \int_t^{t+\Delta t} \int_w^e \frac{S}{\overline{C}_P} \xi^2 d\xi dt \end{aligned} \tag{4-42}$$

The left hand side integrates to

$$\int_w^e \int_t^{t+\Delta t} \xi^2 \frac{\partial}{\partial t}(cT)dtd\xi + \int_t^{t+\Delta t} \int_w^e cT \frac{\dot{R}}{R} \frac{\partial \xi^3}{\partial \xi} d\xi dt = \frac{1}{3}\left(\xi_e^3 - \xi_w^3\right)\left(c_P T_P - c_P^o T_P^o\right) + c_P T_P \frac{\dot{R}\Delta t}{R}\left(\xi_e^3 - \xi_w^3\right) \quad \textbf{(4-43)}$$

For the second last term on the right hand side in Equation (4-42), if the term between the square brackets can be represented by

$$Z = \left[(a_c - C_{PA}) c\overline{D} \frac{\partial y_F}{\partial \xi} + b_c c D \frac{\partial y_F \theta}{\partial \xi} \right] \quad \textbf{(4-44)}$$

and the second last term on the right hand side in Equation (4-42) can be expressed as

$$\frac{\xi^2}{R^2 \overline{C}_P}\left[(a_c - C_{PA}) c\overline{D} \frac{\partial y_F}{\partial \xi} + b_c c D \frac{\partial y_F \theta}{\partial \xi} \right] \frac{\partial T}{\partial \xi} = \frac{1}{R^2 \overline{C}_P}\left[\frac{\partial}{\partial \xi}\left(\xi^2 ZT\right) - T \frac{\partial}{\partial \xi}\left(\xi^2 Z\right) \right] \quad \textbf{(4-45)}$$

The first term on the right hand side in Equation (4-42) is combined with the first term on the right hand side of Equation (4-45) and integrated using the power-law hybrid scheme to give the convection term as

$$F_e = \frac{\left(\xi^2 cw\right)_e \Delta t}{R} - \frac{\xi_e^2 \Delta t}{c_P R^2 \left(\xi_E - \xi_P\right)}\left[c\overline{D}\left((y_F)_E - (y_F)_P\right)\left(a_{CP} - C_{PA}\right) + b_{CP} c D\left((y_F\theta)_E - (y_F\theta)_P\right) \right] \quad \textbf{(4-46)}$$

The second term on the right hand side of Equation (4-42) is integrated to become

$$D_e = \frac{\lambda}{c_P R^2} \frac{\xi_e^2 \Delta t}{\left(\xi_E - \xi_P\right)} \quad \textbf{(4-47)}$$

The second term on the right hand side in Equation (4-45) can be integrated to

$$\int_t^{t+\Delta t} \int_w^e -T \frac{\partial}{\partial \xi}(\xi^2 Z) = -T_P \frac{\xi_e^2 Z_e - \xi_w^2 Z_w}{\xi_e - \xi_w} \quad \textbf{(4-48)}$$

The last term in Equation (4-42) integrates to

$$\int_{t}^{t+\Delta t}\int_{w}^{e}\frac{S}{\overline{C_P}}\xi^2 d\xi dt = \frac{S}{\overline{C_P}}\left(\xi_e^3 - \xi_w^3\right)\frac{\Delta t}{3} \tag{4-49}$$

where S is the reaction rate W_F as defined in Equation (4-7) multiplied by the enthalpy of reaction (*i.e.* the heating value) in kJ/kg fuel. S is defined as

$$S = W_F \Delta h_F \tag{4-50}$$

The expression just derived is the one added to the program to include reaction. The term $\frac{S}{\overline{C_P}}$ is equated to the variable b in the discretized equation which represents the source term.

The equations developed by Tamim (1996) were solved iteratively at each time step together with mass and energy balances on the liquid phase and relations for properties. As in the previous work of Bergeron and Hallett (1989b), Hallett and Ricard (1991) and Tamim and Hallett (1995), an average temperature and concentration were defined at each time step for properties in the vapour phase, since in this work, all properties are assumed uniform in space but time varying (except diffusivity and density, which are allowed to vary both in space and time). A mean state ($\bar{T}, \bar{X}$), is taken for the evaluation of properties in the gas phase, where

$$\overline{T} = \frac{2}{3}T_R + \frac{1}{3}T_\infty \tag{4-51}$$

$$\overline{X_i} = \frac{2}{3}X_{iR} + \frac{1}{3}X_{i\infty} \tag{4-52}$$

where R denotes the droplet surface, ∞ a distance far from the droplet, and X_i the mass fraction of i at time t.

The details of the calculations required for the reaction rate are provided in Section 4.1.2 and these calculations were added to both the single-distribution and multi-distribution model with the use of two subroutines. The first subroutine, titled “WF0TRP”, calculates the reaction rate by carrying out the integration using the trapezoidal rule, and the second, titled

"XGAMMA", calculates $\Gamma(z)$ using Stirling's Formula; this is used in the first subroutine function while calculating the distribution function *f*(I).

The reaction rate term for the multi-distribution model is essentially the same. The only difference is that the variables passed to the first subroutine function are those representing each separate distribution. The rest of the code contains the necessary diffusion equations to produce these values.

4.2.2 Computational Grid and Time Step

The same calculation grid was used as in Bergeron and Hallett (1989a), Bergeron and Hallett (1989b), Hallett and Ricard (1991) and Tamim (1996). The grid point spacing was exponential, so there were more grid points placed near the surface of the droplet where most of the changes occur and the gradients are much higher relative to further from the droplet surface. This is defined by

$$\xi(i) = exp\left[\frac{ln\xi(N)}{N-1}(i-1)\right] \quad \textbf{(4-53)}$$

where *i* is the grid point index and *N* is the total number of grid points, shown in Figure 4-2. Similar to Tamim (1996), 40 grid points were used, with the boundary grid point being 500 radii from the droplet surface. The selection for the number of grid points will be justified later in this section.

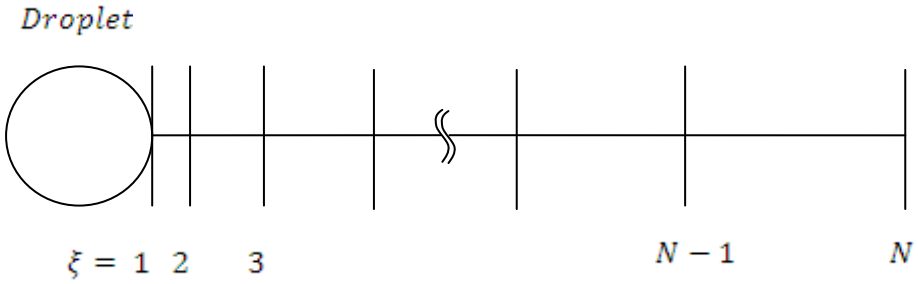

Figure 4-2 Exponential grid

Tamim (1996) used a time step of 0.2% of the lifetime of an evaporating droplet; however, the time step used for this thesis was 0.001 seconds, which was less than 0.1% of the droplet lifetime. The selection of the time step will be justified later in this section. The droplet size Tamim (1996) used was 1.5mm in diameter. The time step should be scaled according to the size of the droplet, noting that droplet lifetimes are roughly proportional to the square of the droplet diameter. Tamim (1996) experienced convergence issues when the mass of the droplet became about 1 - 2% of its original mass. This was corrected in the model by reducing the time step to 1/5th the original value when the mass of the droplet fell below 10% of its original value. This is used for the code in this work; however, it may not be required for temperatures greater than the ignitable limit, as the droplet will usually ignite long before reaching 10% of its original mass.

The time step size (Δt) greatly affected the computational time, next to the integration step size. The effect of step size on ignition time can be seen in Table 4-1; the time step used for this thesis is 0.001 seconds as it provides an ignition time accurate to the limits of the experiments and a smaller step size increased the computational effort.

The computational grid was tested for convergence by Tamim and Hallett (1995); however, it was re-tested to ensure the solution has converged for the updated model. The number of grid points were varied from 20 to 40 and the use of 40 grid points allows for the solution to converge illustrated in Table 4-2.

Table 4-1 Effect of time step on ignition time

	Fuel					
	***n*-Octane**			***n*-Dodecane**		
	Time Step [s]			**Time Step [s]**		
	0.01	0.001	0.0005	0.01	0.001	0.0005
Temperature [K]	**Ignition time [s]**					
1073	0.90000	0.87699	0.87601	1.01000	0.97899	0.97652

Table 4-2 Effect of the number of grid points on ignition time

	Mixture 1			
	n-Octane			
	Number of grid points			
	20	30	35	40
Temperature [K]	**Ignition time [s]**			
1073	0.86899	0.87599	0.87699	0.87699

4.2.3 Reviewing the selection of integration step sizes

As mention in Section 4.1.2, the integration limits for the reaction rate term were varied to see the effect on the results. The ignition time was not affected unless the limits were within the distribution function curve ("limits" being defined as $f(I)$ being larger than 1% of the peak value). Since the molecular weight of the fuels used in the experiments ranged from 114 to 283 kg/kmol, a range of I = 0 to 400 kg/kmol was selected. A narrower range of I = 80 to 320 kg/kmol had a negligible effect on computational time, but affected the results by decreasing the accuracy as shown in

Table 4-3 for mixture 1, since the limits of the latter range gave values of f(I) greater than 1% of the peak values of the distribution curve. The integration limits used in this thesis for the reaction rate term are adequate, as they allow for a wider range of molecular weights to be tested without manipulating the model inputs and have a negligible effect on computational speed. An overflow was encountered during the summation of the trapezoidal rule at the tail end of the distribution shape, where the values of $f(I)$ were smaller than the source program (model) could store (*i.e.*: $f(I) \leq 1.0E^{-300}$). This issue was corrected by stopping the summation at the tail end of the distribution shape when the values became excessively small (*i.e.*: $f(I) \leq 1.0E^{-100}$) ; the

addition of this change did not affect the results of the program. The largest effect on computational time was the choice for the size of the integration step *N* and this is shown in Table 4-4. An integration step size of *N* = 1 kg/kmol was chosen for all the models, as it guaranteed the best accuracy for the results with a reasonable computation time. It is recommended to increase the step size slightly when running repeated calculations, as it could prove to be more efficient for the user to significantly decrease the computational time. If this is done, the outputs should be periodically checked to ensure that the results are the same as for a step size of *N* = 1 kg/kmol.

Table 4-3 Effect of integration limits on ignition time

	Mixture 1		
	Integration limits		
	I = 0 to 400 [kg/kmol]	I = 80 to 320 [kg/kmol]	I = 100 to 300 [kg/kmol]
Temperature [K]	**Ignition time [s]**		
1073	0.94499	0.94599	0.96399

Table 4-4 Effect of integration step size N on ignition time and computational time

	***n*-Octane**			
	Integration step size N			
	0.5	1	5	10
Temperature [K]	**Ignition time [s]**			
1073	0.87699	0.87699	0.87699	1.126

Chapter 5 Results and Discussion

In this chapter, sample calculations and experimental results for an igniting fuel droplet will be presented in order to demonstrate the capabilities of the theory just developed and to show how the distribution functions were chosen to represent the mixtures using the ASTM distillation curve simulations.

5.1 Pure Fuels

5.1.1 Experimental results for pure fuels

The droplet ignition model was first tested by performing experiments with pure fuels and comparing the results with calculations. These data were additionally used to fit rate constants for pure fuels for later use in mixture modelling. Bergeron and Hallett (1989a) give ignition data and rate parameters for some but not all of the pure components used here. The experimental setup was also tested by comparing these measurements to the results of Bergeron and Hallett (1989a), and the very close agreement between the present data and Bergeron and Hallett (1989a) as illustrated by the slopes of the fitted curves in Figure 5-1 and Figure 5-2 gave a measure of confidence to the present data. The fuels that were tested included *n*-octane, *n*-decane, *n*-dodedecane, *n*-tetradecane and *n*-hexadecane.

The tests done for pure fuels were used to determine the relationships to represent the pre-exponential coefficient and the activation energy as a function of molecular mass. The pure fuel data points for this thesis are given as individual points for each experimental trial and not

combined statistically into mean ignition time and standard deviation as they were in Bergeron and Hallett (1989a). Figure 5-1 and Figure 5-2 show the comparison between *n*-dodecane and *n*-hexadecane from the tests performed for this thesis and Bergeron and Hallett (1989a). The latter used droplet diameters of approximately 1.5 mm and 1.4 mm for *n*-decane and *n*-dodecane respectively, and their results may be compared with the pure fuel data in this thesis, which used a droplet diameter of 1.6 mm. A smaller droplet diameter produces a slight decrease in ignition time, which is consistent with what Figure 5-1 and Figure 5-2 show. The curves in Figure 5-1 and Figure 5-2 were fitted to the data. The results for the other pure fuels will be shown in Section 5.1.3 while generating the relationships for rate constants.

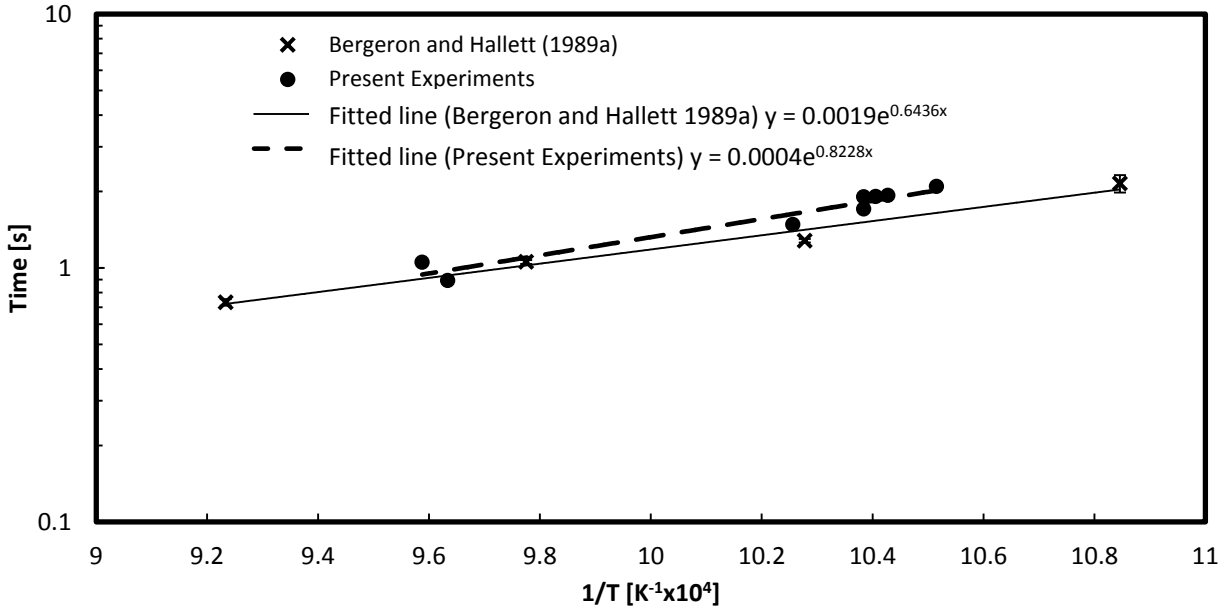

Figure 5-1 Comparison of ignition test results for *n*-dodecane from Bergeron and Hallett (1989a) and results from this thesis

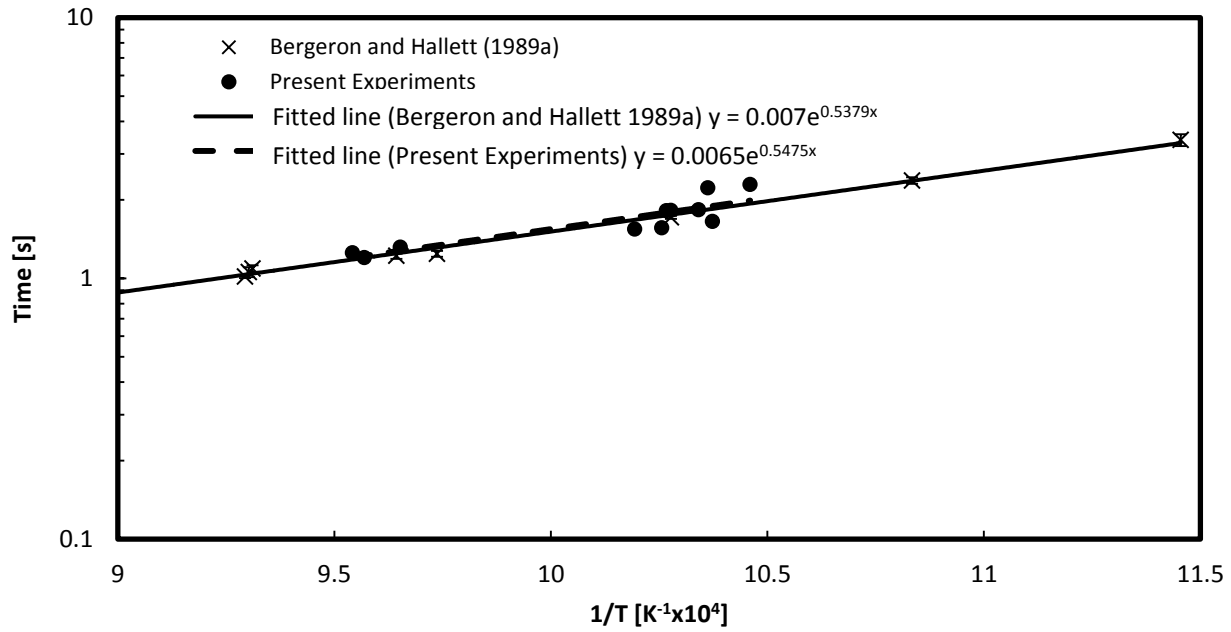

Figure 5-2 Comparison of ignition test results for *n*-hexadecane from Bergeron and Hallett (1989a) and results from this thesis

5.1.2 Modelling of pure fuels

To represent pure fuels using continuous thermodynamics, the mean of the distribution θ_L is set to the molecular weight of the pure component and the standard deviation should be as small as possible (ideally σ = 1 kg/kmol). However, it was found necessary to use standard deviations ranging from 3 kg/kmol (for *n*-octane) to 7 kg/kmol (for *n*-eicosane) for the fuels ranging from low to high molecular mass respectively, as the model either would not converge or produced an overflow error for smaller values. However, the choice of σ had a negligible effect on the ignition time, as is shown by Table 5-1. The values for the distribution parameters α and β were then calculated using Equation (4-22) and (4-23), with the distribution origin γ set to 0. Pure *n*-paraffins ranging from *n*-octane to *n*-eicosane were selected for later use in forming mixtures, and the calculated values of α and β can be seen in Table 5-2. The droplet ignition

model was used to fit rate parameters *K* and *E* for best agreement with the experimental data, and the results of this were compared to the work of Bergeron and Hallett (1989a). The fitting of the rate parameters was made relatively easy by the fact that the activation energy essentially controlled the slope of ignition time variation with temperature and the pre-exponential controlled the y-intercept. The values of rate parameters are quite different from Bergeron and Hallett (1989b) because this thesis has been forced to use unity reaction orders. However, the model predictions behave in almost exactly the same way in spite of this difference, giving the same linear behaviour on a semi-log plot, and they can be made identical by choosing K and E appropriately. The simulation was done for a 1.6mm diameter droplet initially at room temperature (25^{o}C) with ambient temperatures ranging from 600^{o}C to 850^{o}C.

Table 5-1 Effect of distribution function standard deviation on predicted ignition time

	Fuel					
	n-Octane			*n*-Dodecane		
	Standard deviation "σ" [kg/kmol]			Standard deviation "σ" [kg/kmol]		
	2	3	8	3	5	10
Temperature [K]	Ignition time [s]					
1073	0.87699	0.87699	0.87999	0.97899	0.97899	0.97799

Table 5-2 Distribution parameters for pure fuels

Fuel	Mean molecular weight "θ" [kg/kmol]	Standard deviation "σ" [kg/kmol]	α	β
n-Octane	114.2	3	1449.7	0.0788
n-Decane	142.3	4	1265.2	0.1125
n-Dodecane	170.3	5	1160.5	0.1468
n-Tetradecane	198.4	5	1574.2	0.1260
n-Hexadecane	226.4	5	2050.9	0.1104
n-Octadecane	254.5	6	1799.2	0.1415
n-Eicosane	282.6	7	1629.9	0.1734

5.1.3 Fitting rate parameters

The following will illustrate and discuss the results of the experimental data for the pure fuels *n*-octane, *n*-decane, *n*-dodecane, *n*-tetradecane and *n*-hexadecane based on the expressions used for the pre-exponential coefficient and activation energy. The fuels *n*-octadecane and *n*-eicosane were not tested experimentally as pure fuels, since at room temperature both are solids and cannot be easily made into droplets. Bergeron and Hallett's (1989a, b) values for the activation energies and pre-exponential coefficient for pure fuels were used as an initial guideline for the relationships developed for the rate parameters for this thesis, but were subsequently modified to accommodate the different values of *m* and *n* in the present work, and further checked by new measurements on pure fuels. The modified values for the pre-exponential coefficient *K* and the activation energy *E* derived using $m = n = 1$ in the rate equation are shown in Figure 5-3 and Figure 5-4; these values are also shown in Table A - 23 and Table A - 24.

As mentioned earlier in Section 4.1.2, the first relationship tried for the rate parameters was constant activation energy and a linear relationship between the pre-exponential and the molecular mass. The activation energy was taken to be an average of the values derived using $m = n = 1$, as a starting point, for the fuels ranging from *n*-octane to *n*-hexadecane, which was 83.3 kJ/gmol; the values for the individual fuels are shown in Table A - 24 and also in Figure 5-3.

The pre-exponential coefficients vary with molecular weight as did those determined by Bergeron and Hallett (1989a, b) and are shown in Table A - 23 as well as in Figure 5-4. Since the values for the pre-exponential derived using $m = n = 1$ illustrate a linear trend on a log scale graph, as shown in Figure 5-4, the difficulty was finding suitable parameters for a linear relationship as a suitable starting point. It was determined that the correlation would either fit the light range of fuels, the heavier fuels, or the fuels ranging in the middle based on molecular

mass, but that a linear relationship would not be able to fit the entire range with great accuracy. These three cases of the linear relationship for the pre-exponential coefficient used are

$$K1 = -5.5x10^{-7} + 5x10^{5} \cdot I \text{ for } 110 < I < 150$$

$$K2 = 0 + 5x10^{4} \cdot I \qquad \text{for } 150 < I < 200$$

$$K3 = -1x10^{-8} + 1x10^{6} \cdot I \text{ for } 200 < I < 240$$

where *K1* fitted the mid range of fuels, *K2* fitted the light fuels, and i fitted the heavy fuels. The three linear equations for *K* are shown in Figure 5-4.

The continuous thermodynamics ignition model, although intended for mixtures, was first applied to pure fuels to test the rate parameter expressions and fit their constants. The following Figure 5-5 to 5-9 compare the experimental results for pure fuels with the models using the different rate parameter expressions for the linear relationships for *K* and constant activation energy.

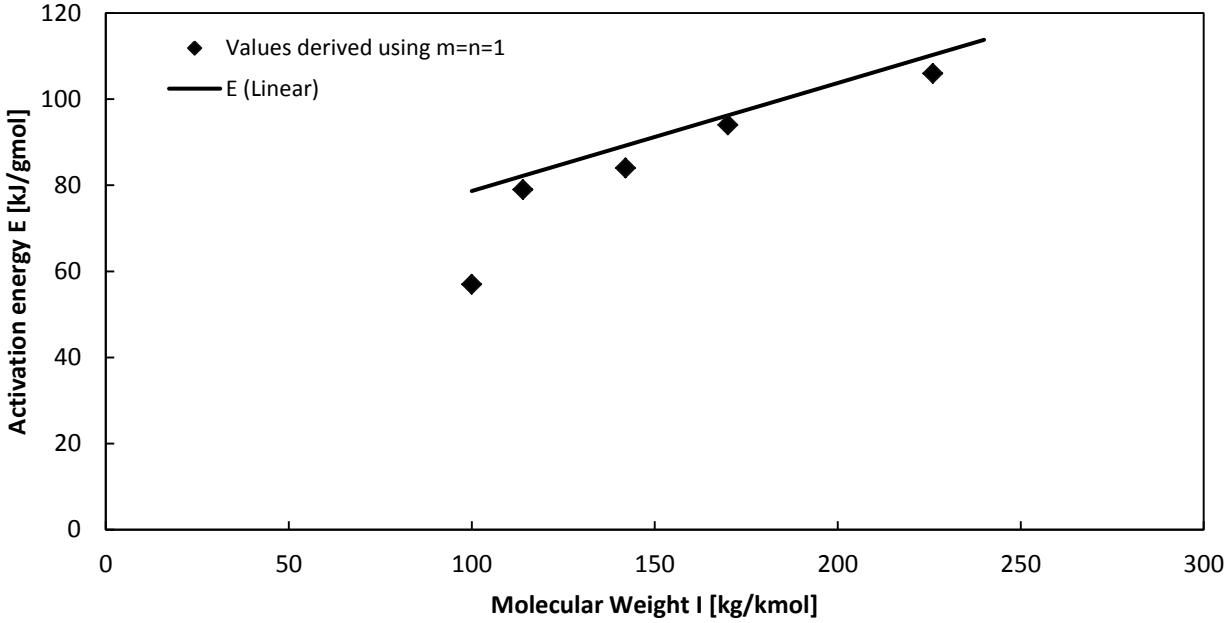

Figure 5-3 Comparison between the relationship used for activation energy E(I) and values derived from experimental data.

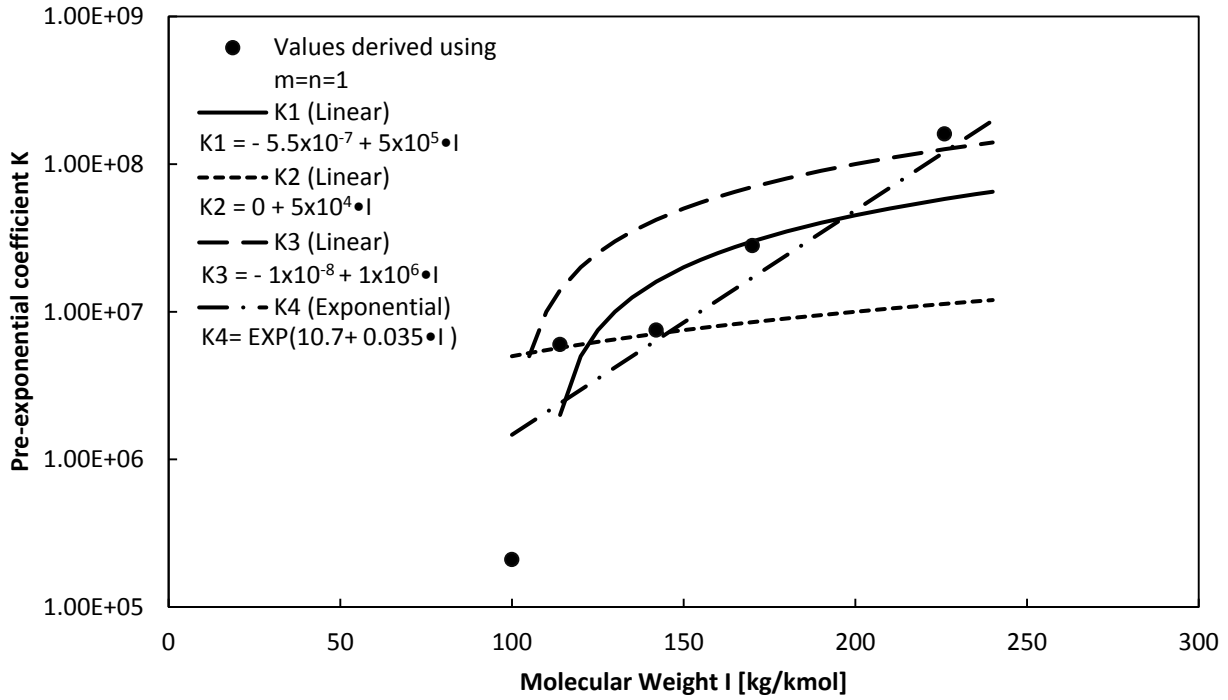

Figure 5-4 Comparison between the relationships used for pre-exponential coefficient K(I) and values derived from experimental data

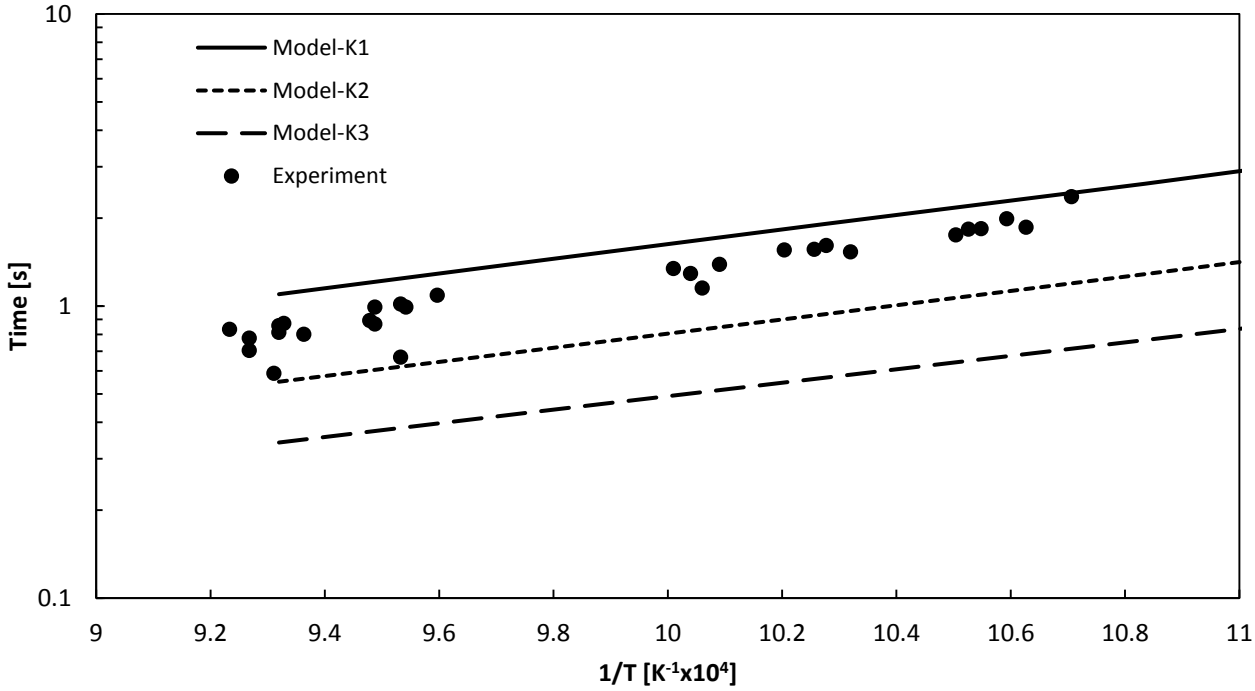

Figure 5-5 Ignition results for *n*-octane from both the experiments and the model using three different linear relationships for K and a constant value for E

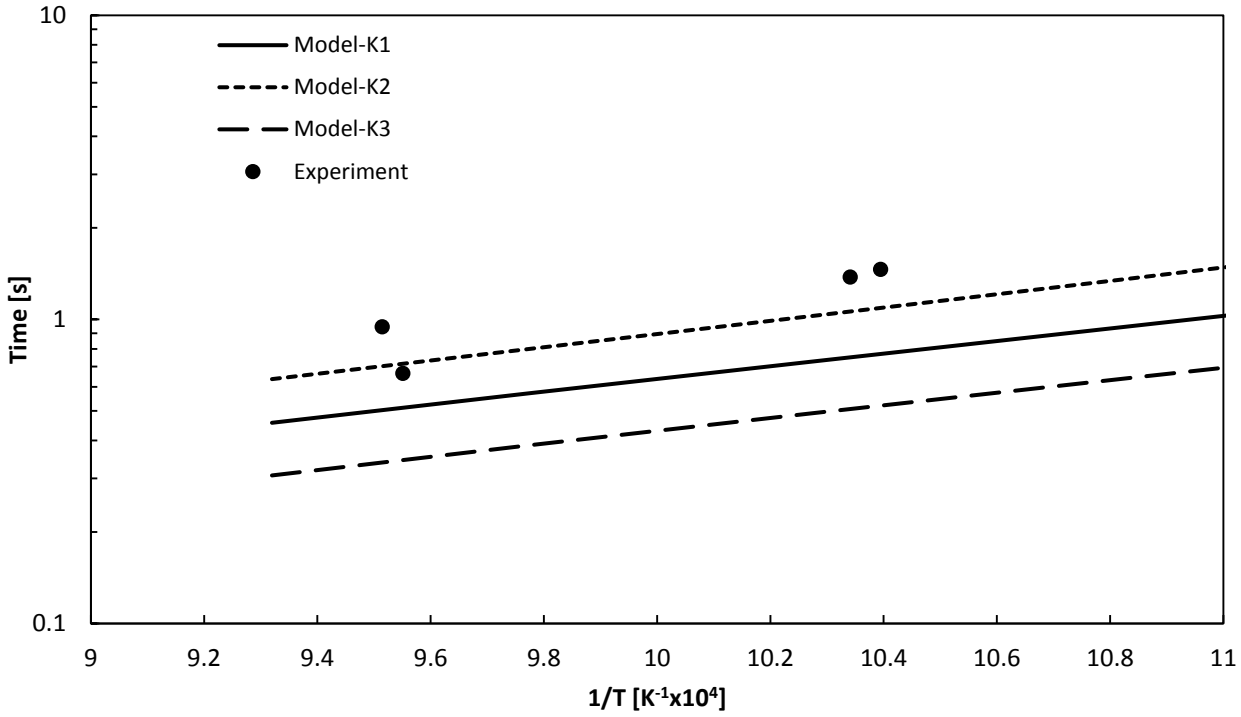

Figure 5-6 Ignition results for *n*-decane from both the experiments and the model using three different linear relationships for K and a constant value for E

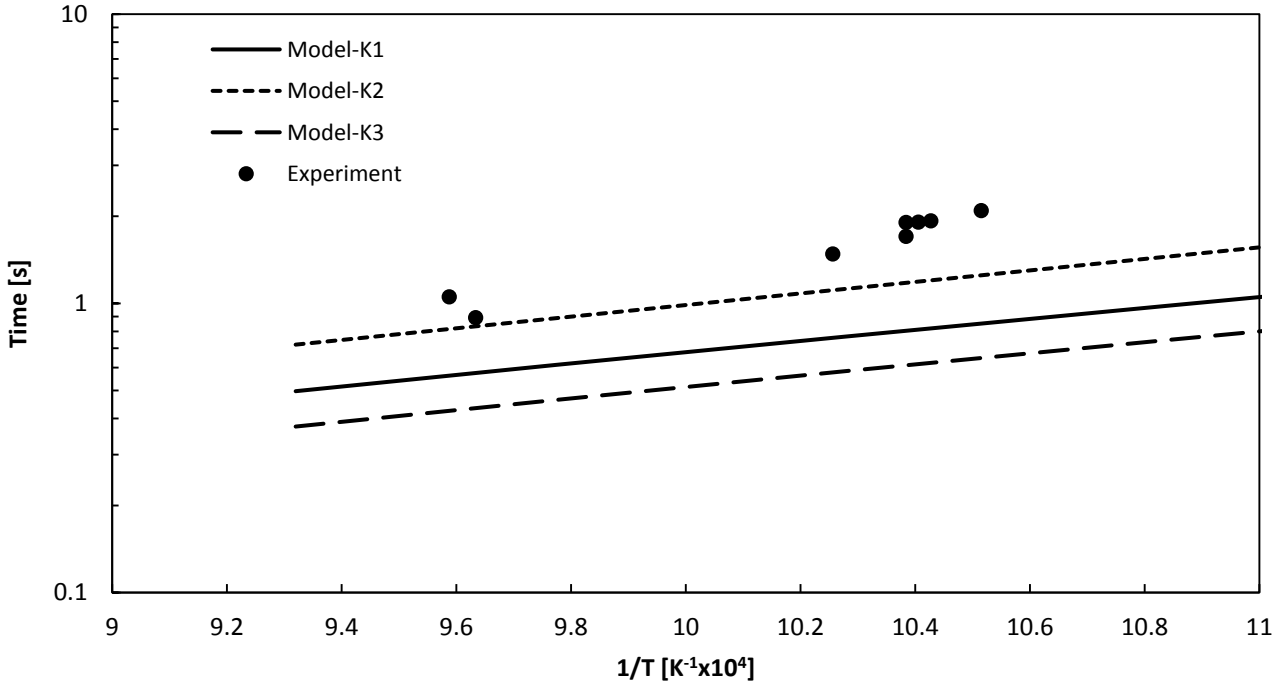

Figure 5-7 Ignition results for *n*-dodecane from both the experiments and the model using three different linear relationships for K and a constant value for E

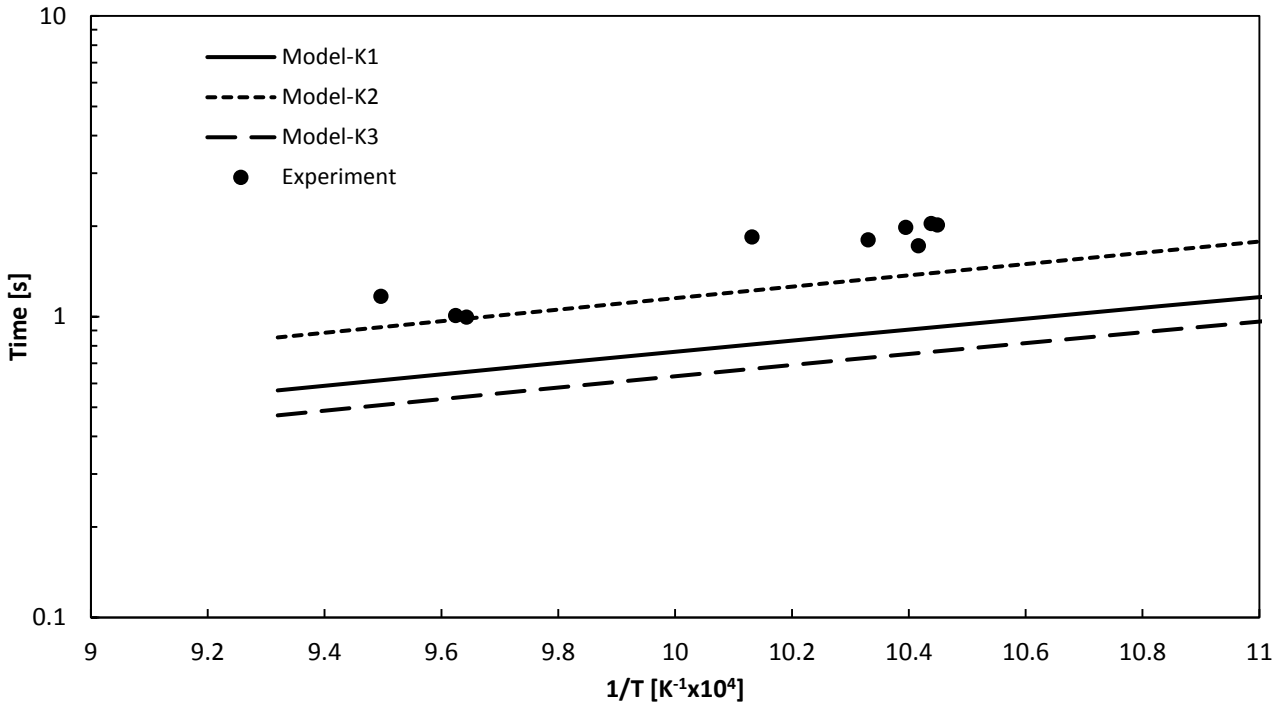

Figure 5-8 Ignition results for *n*-tetradecane from both the experiments and the model using three different linear relationships for K and a constant value for E

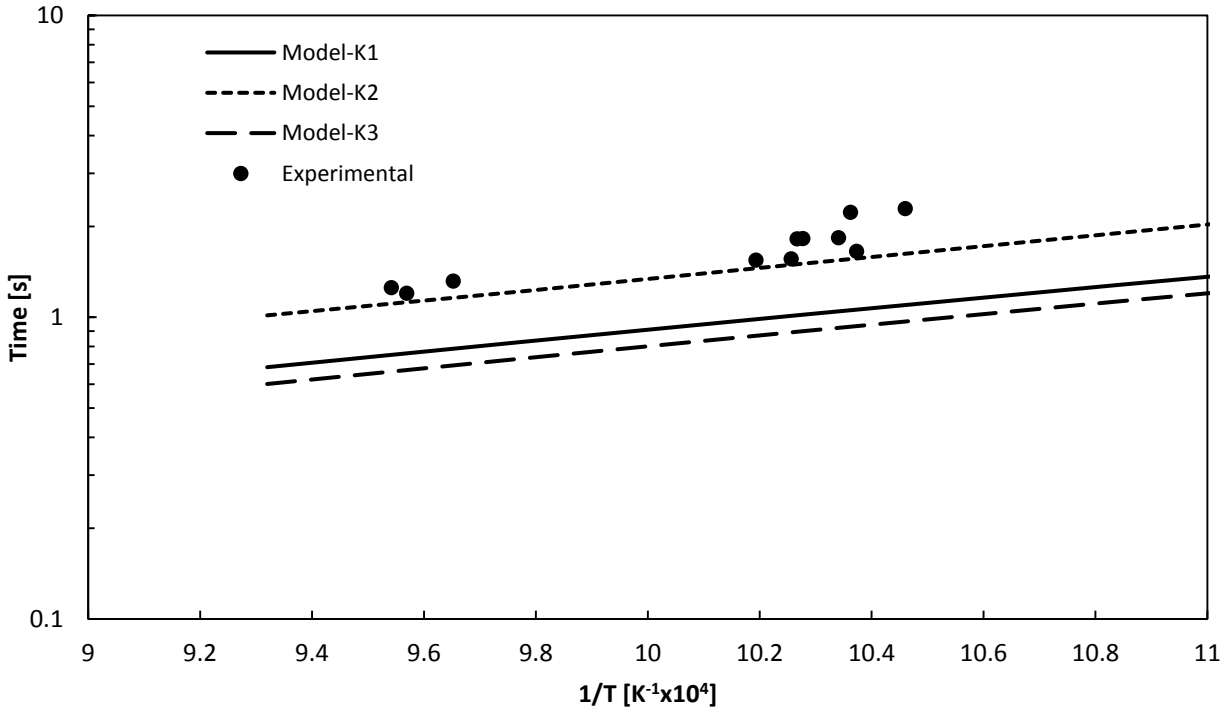

Figure 5-9 Ignition results for *n*-hexadecane from both the experiments and the model using three different linear relationships for K and a constant value for E

The relationships used for the previous approach did not require numerical integration of the rate expression over the distribution variable - it could be integrated analytically; however, as shown above in Figure 5-5 to 5-9, the model results were quite different from the ignition tests. It is known that the pre-exponential coefficient controls the y-intercept and the activation energy controls the slope, and it is noticeable that the y-intercept and the slopes did not fit the range of pure fuels tested and the equations used to describe the variables *K* and *E* required modification.

After reviewing the results for the constant activation energy and linear relationship for the pre-exponential coefficient, the second model was tried, with the activation energy represented by a linear relationship along with the linear relationship for the pre-exponential coefficient using the same three equations/cases used previously. The linear formula for activation energy gave a much better fit, since the activation energies for *n*-paraffins of molecular mass greater than *n*-heptane really do vary roughly linearly with molecular mass, as shown in Figure 5-3 and Table A - 24. The following Figure 5-10 to 5-14 compare the experimental ignition times for pure fuels with the model using linear relationships for both the pre-exponential coefficient and the activation energy, where $a_E = 53.6$ and $b_E = 0.25$ and Equation (4-14) becomes

$$E = 53.6 + 0.25I \quad \textbf{(5-1)}$$

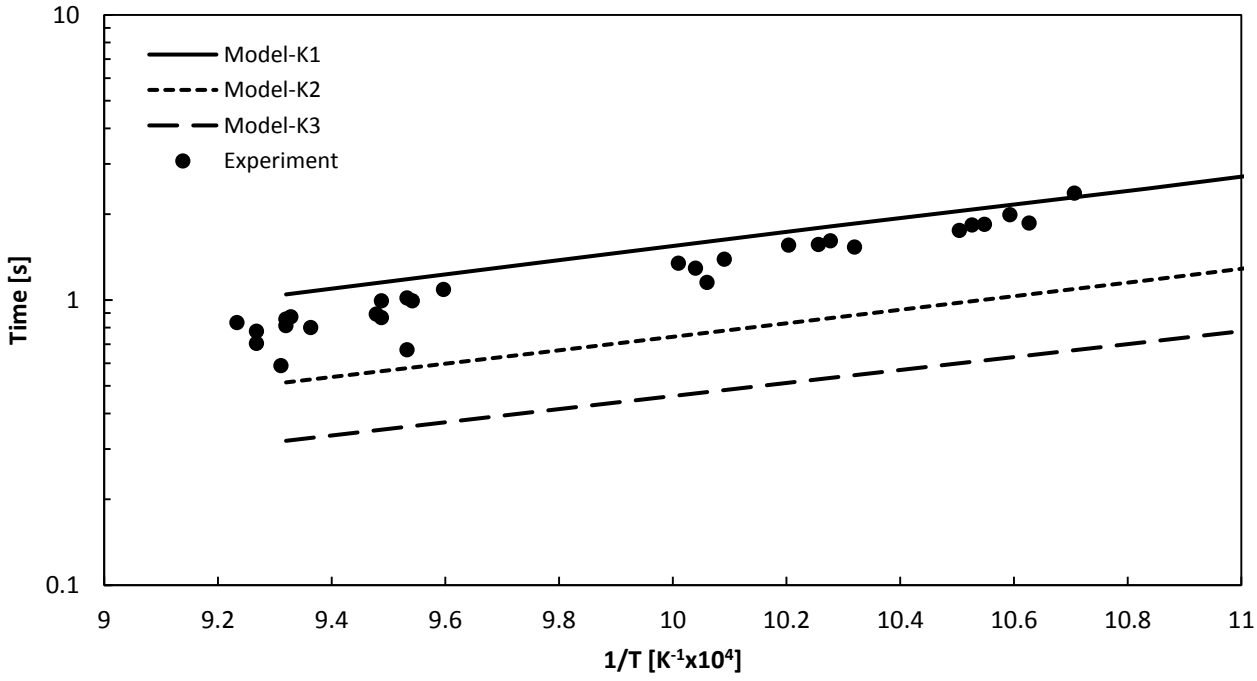

Figure 5-10 Ignition results for *n*-octane from both the experiments and the model using three different linear relationships for K and a linear relationship for E

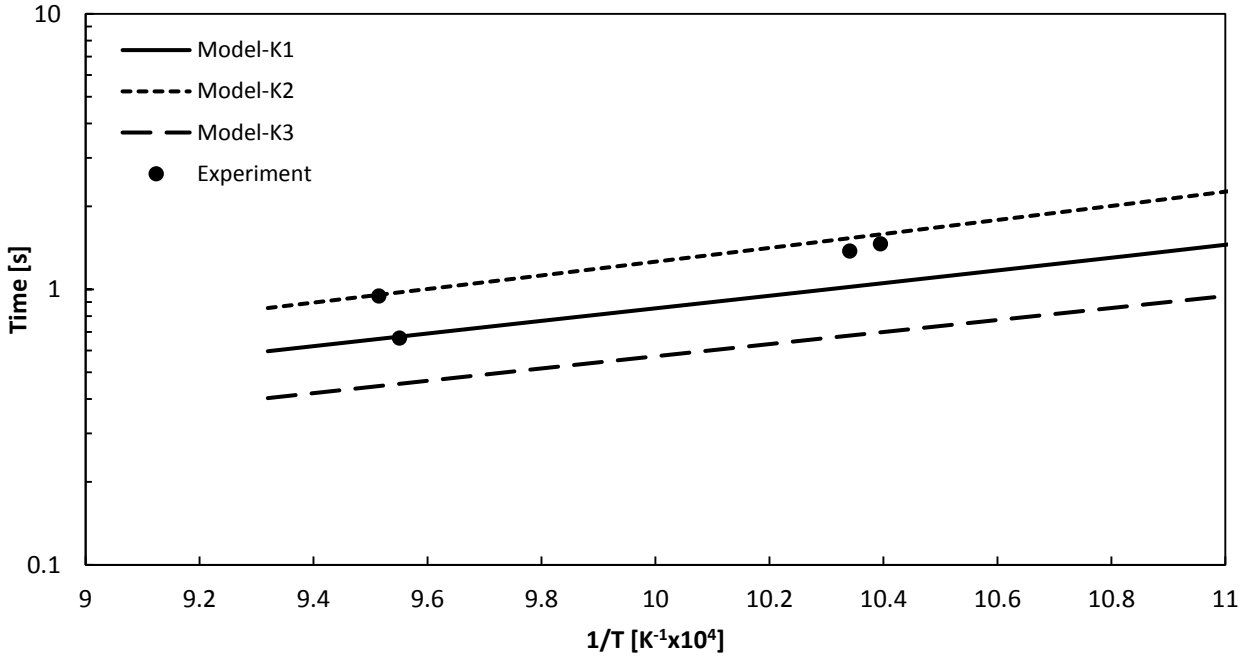

Figure 5-11 Ignition results for *n*-decane from both the experiments and the model using three different linear relationships for K and a linear relationship for E

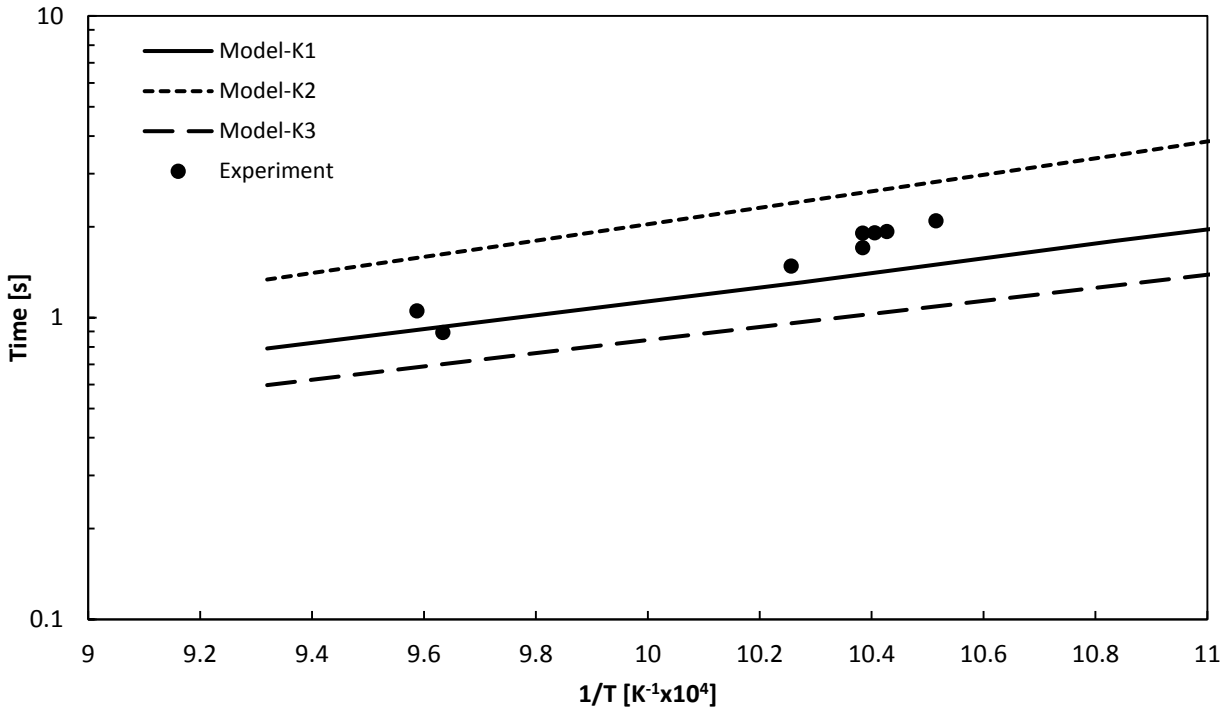

Figure 5-12 Ignition results for *n*-dodecane from both the experiments and the model using three different linear relationships for K and a linear relationship for E

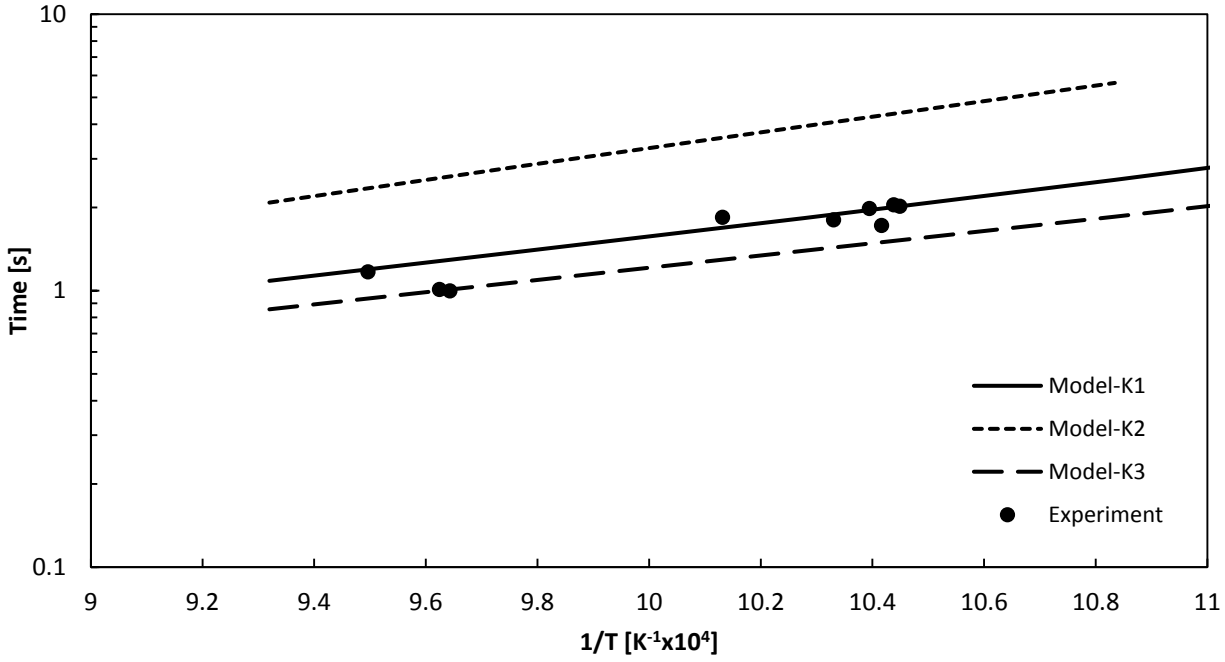

Figure 5-13 Ignition results for *n*-tetradecane from both the experiments and the model using three different linear relationships for K and a linear relationship for E

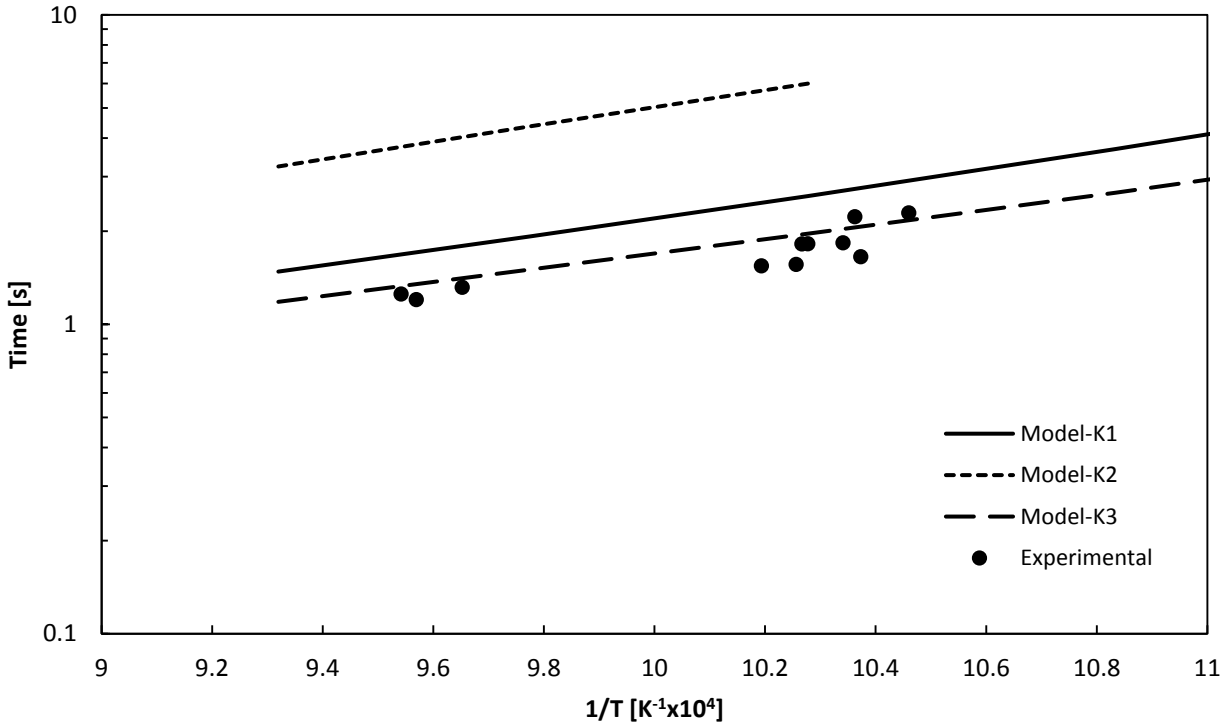

Figure 5-14 Ignition results for *n*-hexadecane from both the experiments and the model using three different linear relationships for K and a linear relationship for E

The second relationship tried required numerical integration of the rate equation and therefore much more computational time; however, this was necessary since the previous relationship was inadequate. This relationship provided more accuracy than the initial relationship when comparing it to the experimental results as each equation *K1*, *K2* and *K3* satisfied a small range of fuels; however, it still produced quite different results to the ignition tests and required a new relationship. As mentioned in Section 5.1.2, since the pre-exponential coefficient controlled the y-intercept and the activation energy controlled the slope, it is noticeable that the y-intercept seemed to create the most error, while the slopes seemed to fit the slope of the experimental data. The three equations developed for *K* as mentioned earlier could not reproduce the data derived using $m=n=1$ for the full range of fuels; they could only fit a small range, either the fuels with lower molecular mass, mid-range molecular mass or high molecular

mass relative to the range of fuels. Further comparing the results in Figure 5-10 to 5-14, it is evident that the ignition time is under-predicted for the lighter and heavier fuels using *K1*, as *K1* is fitted to the mid range of fuels; the ignition time is under-predicted for the mid- to heavier fuels using *K2*, as *K2* is fitted to the lighter range of fuels; and the ignition time is over-predicted for the lighter to mid range fuels using *K3*, as *K3* is fitted to the heavier range of fuels. Based on these results it was evident that the values for *K* should increase exponentially with molecular mass, as the values in Figure 5-4 show this trend and the values from Bergeron and Hallett (1989a, b) showed a similar trend.

After reviewing the results using linear relationships for both activation energy and the pre-exponential coefficient, the expression for the pre-exponential coefficient was changed to use an exponential of a linear function, Equation (4-16), where $a_K = 10.7$ and $b_K = 0.035$:

$$K = \exp(10.7 + 0.035I) \quad \textbf{(5-2)}$$

This fitted the values for each individual component over the range of fuels used well, since the individual values do increase roughly exponentially with increasing molecular mass. The comparison of the exponential expression developed for the pre-exponential coefficient and the rate parameters for the individual components are shown in Figure 5-4. The following Figure 5-15 to 5-19 compare the experimental results of pure fuels with the models using the different rate parameters expressions for the exponential relationship for the pre-exponential coefficient and a linear relationship for the activation energy.

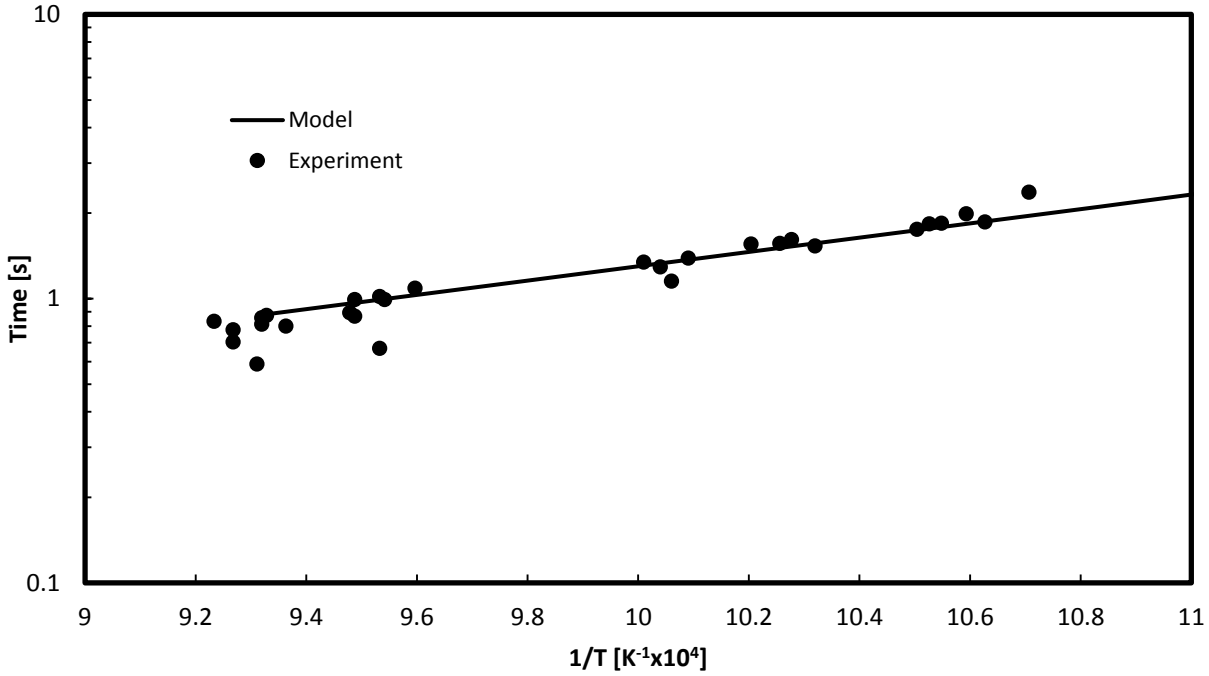

Figure 5-15 Ignition results for *n*-octane from both the experiments and the model using an exponential relationship for K and a linear relationship for E

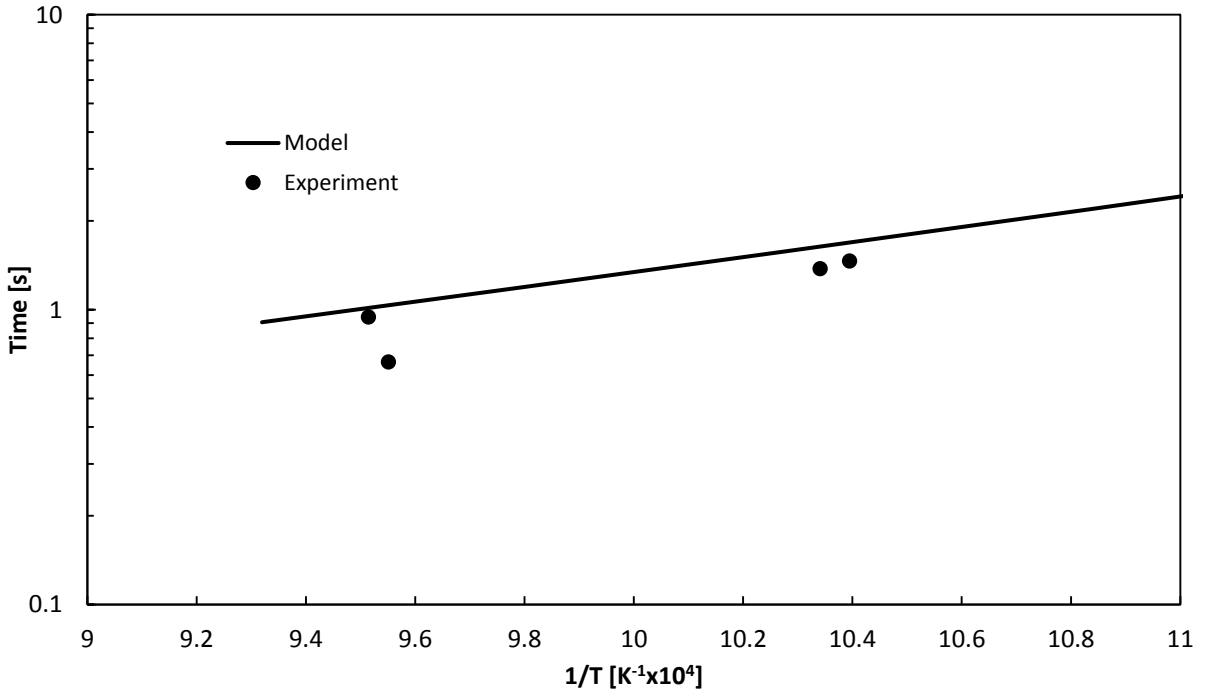

Figure 5-16 Ignition results for *n*-decane from both the experiments and the model using an exponential relationship for K and a linear relationship for E

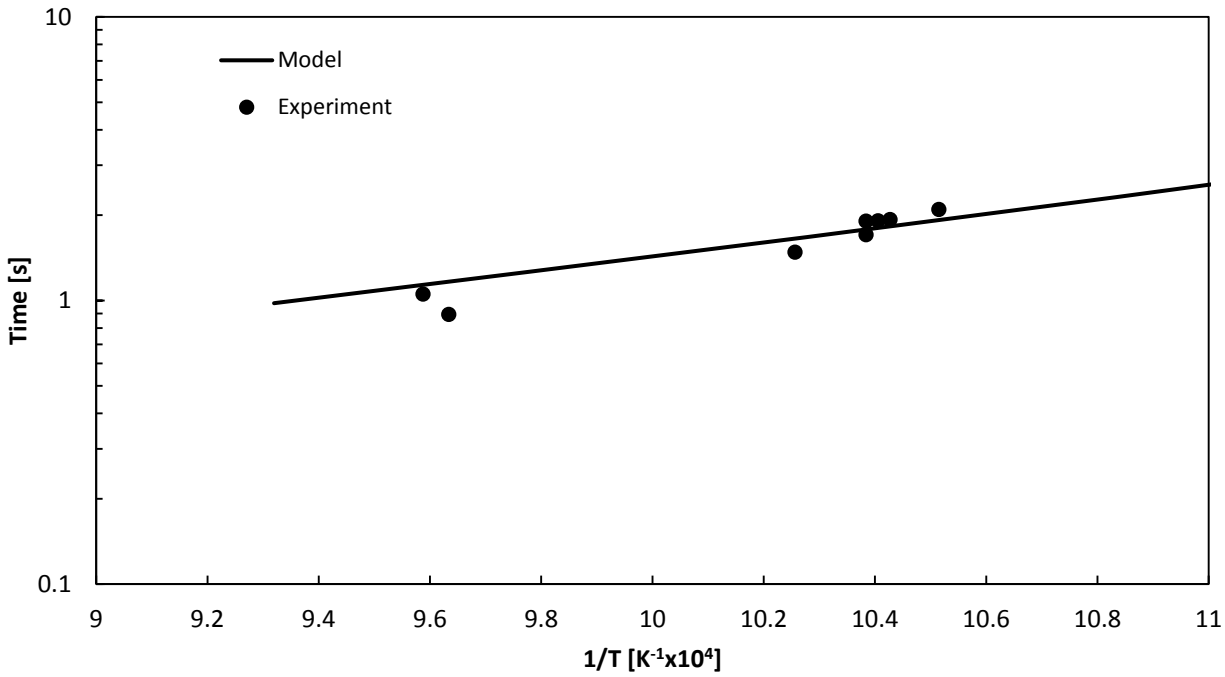

Figure 5-17 Ignition results for *n*-dodecane from both the experiments and the model using an exponential relationship for K and a linear relationship for E

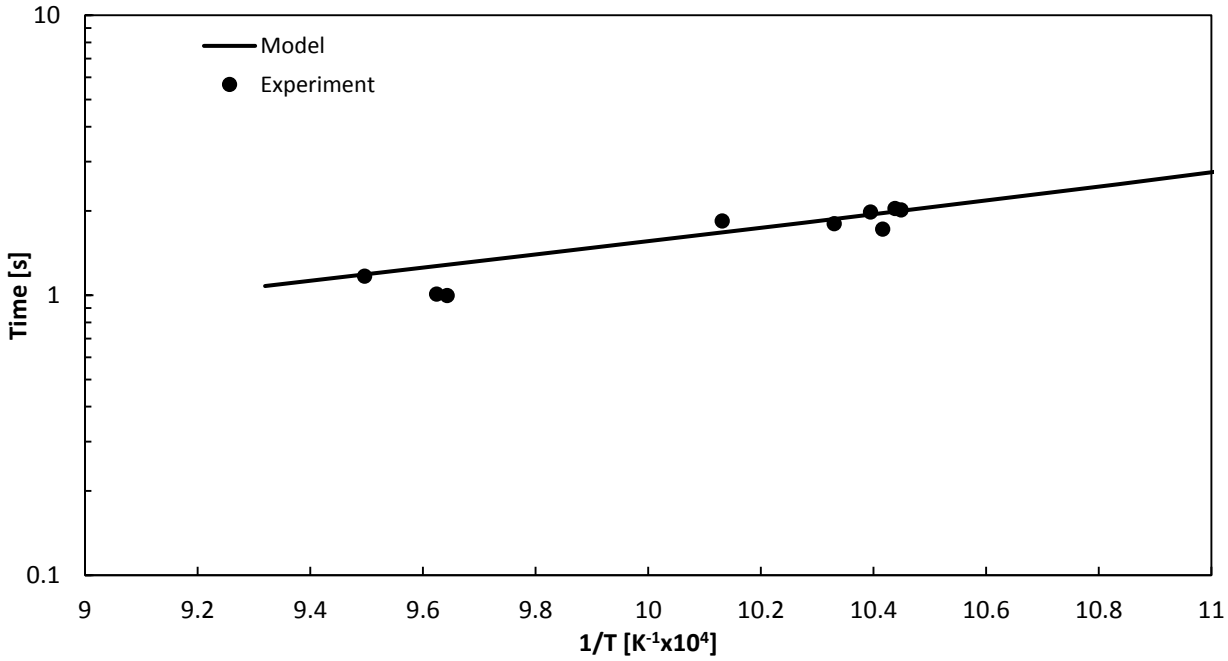

Figure 5-18 Ignition results for *n*-tetradecane from both the experiments and the model using an exponential relationship for K and a linear relationship for E

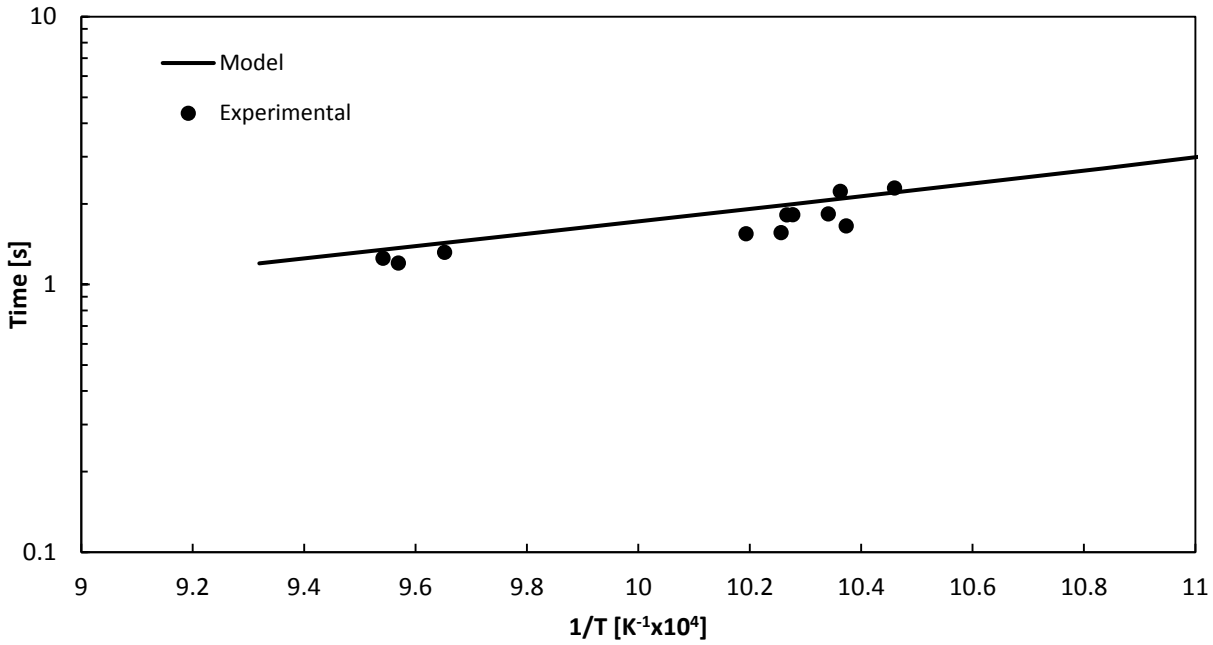

Figure 5-19 Ignition results for *n*-hexadecane from both the experiments and the model using an exponential relationship for K and a linear relationship for E

This third, exponential, relationship is solved with the same numerical integration approach as the previous case and therefore does not require the solution approach to become more difficult. As illustrated in Figure 5-15 to 5-19 the pure fuel experimental results using the third relationship for the pre-exponential coefficient agreed well with the model. This relationship provided great accuracy as the model results "fall" within the experimental data within the entire fuel and temperature range and did not require further modifications. There are some slight discrepancies between the data and the model for *n*-decane; however, this may be due to the small number of tests performed for this fuel. Since the remaining fuels provided good guidance for determining the relationships for *K* and *E*, this discrepancy is not significant. As mentioned, the values of *K* and *E* derived for each fuel component using m=n=1 were quite different from those of Bergeron and Hallett (1989a, b) (for example: K and E for *n*-decane from Bergeron and Hallett (1989b) were 2.80 x 10^4 and 73 kJ/kmol respectively versus 7.5 x 10^6 and

84 kJ/kmol respectively for the present work), the modifications being required since the concentration exponents *m* and *n* were set to 1.0 for this thesis and 0.25 and 1.5 respectively for Bergeron and Hallett (1989a). In Westbrook and Dryer's (1981) work with laminar flame propagation modelling, the exponents *m* and *n* affected the results significantly; however, based on the results for this thesis compared to the results of Bergeron and Hallett (1989a, b) the concentration exponents have very little effect on ignition time, and the agreement of the model with experimental data is equally good with either set of exponents.

As the ambient temperature decreased the ignition time increased exponentially as shown in the experimental results illustrated in this section. This was the same result shown by Faeth and Olson (1968), Aggarwal (1984), Bergeron and Hallett (1989a, b) and Stauch and Maas (2007). The times are slightly higher than those of Bergeron and Hallett (1989a) due to the use of a slightly larger droplet diameter. Another minor source of discrepancy between the present model and Bergeron's is that the earlier model used the more accurate Antoine equation for vapour-liquid equilibrium, while Tamim (1996) and subsequent continuous thermodynamics models (including this one) use the Clausius-Clapeyron equation. The continuous model developed by Tamim (1996) therefore predicts slightly lower liquid temperatures compared to Bergeron and Hallett (1989a); however, the difference is negligible for the first half of the droplet lifetime and less than a 5^{o}C difference for the remaining time. Since the model used for this thesis is an extension of Tamim (1996), this explains the slightly slower ignition times.

5.2 Mixtures

5.2.1 Selection of distribution function parameters to design the mixtures

Following the successful fitting of rate parameters for pure fuels, multi-component mixtures were designed to test the continuous thermodynamics ignition model for multi-component mixtures using *n*-paraffin fuels. This model uses the reaction rate expressions fitted from the pure fuel results. Three mixtures were designed and tested with the model. The first two mixtures were developed to produce a continuous distribution of molecular mass; the third mixture will be discussed in Section 5.2.3. The first of these was intended to be a lighter mixture and ranged in molecular mass from *n*-octane to *n*-hexadecane, while the second was a heavier one ranging from *n*-dodecane to *n*-eicosane. Both mixtures were designed using a comparison of the computed ASTM distillation curves for both discrete and continuous mixtures.

As mentioned in the previous section, for pure fuels the mean of the distribution θ_L was set to the molecular weight of the pure component and σ to a small value, giving a narrow distribution. For mixtures the main objective is to generate *n*-paraffin mixtures of a number of discrete components that can be accurately simulated using continuous thermodynamics. To do this, simulations of the ASTM distillation test were used as outlined in Section 3.5. The following Figure 5-20 and Figure 5-21 shows the comparison between the two simulated ASTM tests for discrete and continuous mixtures for mixture 1 and 2. The fitted distribution parameters

and the details of the individual components fractions for the mixtures used can be seen in Table 5-3 and Table 5-4 respectively.

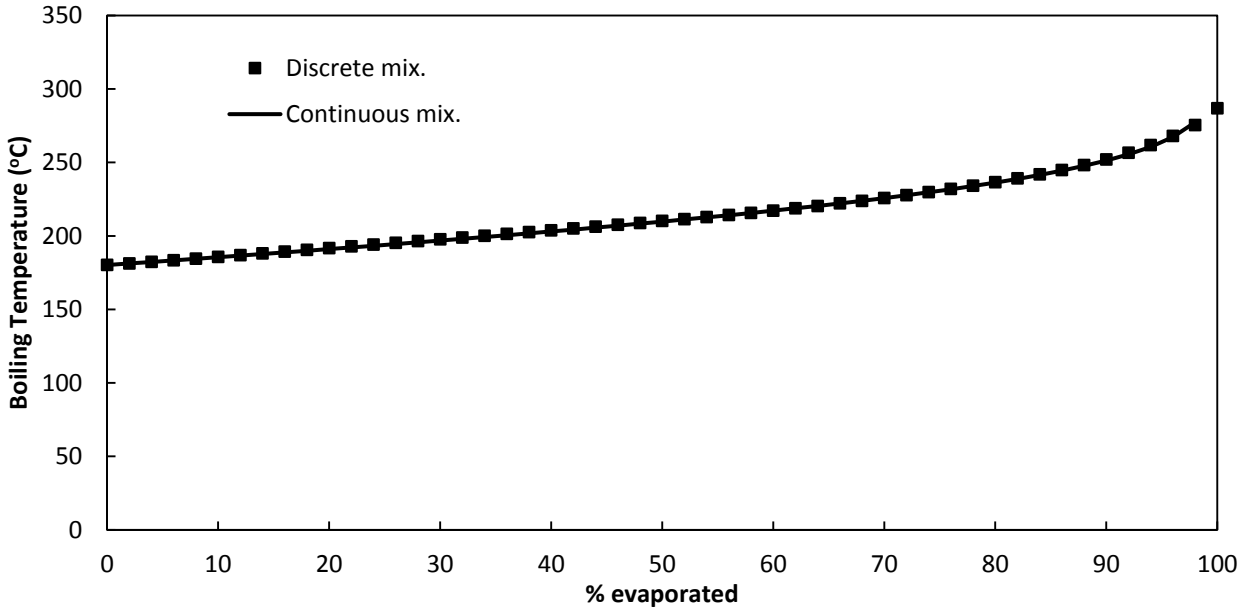

Figure 5-20 Comparison of the ASTM model results for both the discrete mixture and continuous mixture for mixture 1

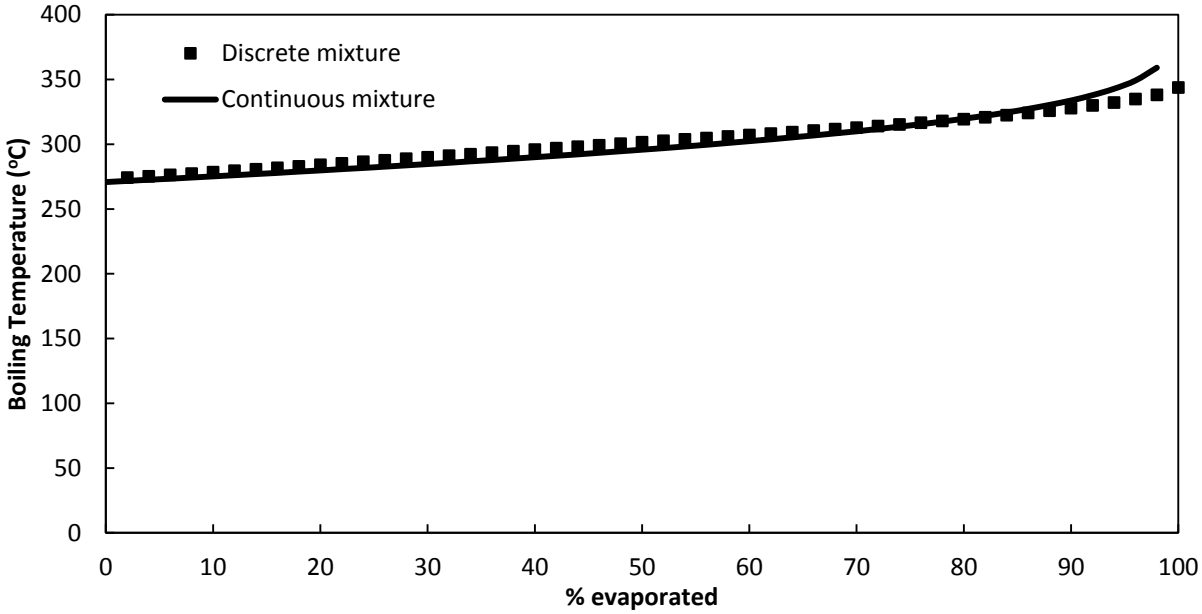

Figure 5-21 Comparison of the ASTM model results for both the discrete mixture and continuous mixture for mixture 2

Table 5-3 Distribution parameters for mixtures 1 and 2 and the composition used for mixture 3

					Mixture 3	
	θ	σ	α	β	% Mass Fraction	% Mole Fraction
Mixture 1	159.20	29.40	29.32	5.43	50.08	59.12
Mixture 2	220.00	29.40	56.00	3.93	49.92	40.88

Table 5-4 Details of the three mixture composition

Mixture	Fuel	Molecular weight (l) [kg/kmol]	Mass Fraction	Mole Fraction	Molecular mass of sample [kg/kmol]
Mixture 1	*n*-Octane	114.22	0.079	0.1106	
	n-Decane	142.28	0.340	0.3813	
	n-Dodecane	170.33	0.359	0.3369	
	n-Tetradecane	198.38	0.145	0.1168	
	n-Hexadecane	226.432	0.077	0.0544	159.76
Mixture 2	*n*-Dodecane	170.3	0.085	0.1149	
	n-Tetradecane	198.4	0.135	0.1566	
	n-Hexadecane	226.4	0.333	0.3391	
	n-Octadecane	254.5	0.280	0.2537	
	n-Eicosane	282.6	0.166	0.1357	230.32
Mixture 3	*n*-Octane	114.22	0.040	0.0654	
	n-Decane	142.28	0.170	0.2254	
	n-Dodecane	170.3	0.222	0.2462	
	n-Tetradecane	198.4	0.140	0.1331	
	n-Hexadecane	226.4	0.205	0.1708	
	n-Octadecane	254.5	0.140	0.1037	
	n-Eicosane	282.6	0.083	0.0554	188.59

5.2.2 Results: single distribution mixtures

The approach described in the previous section provided both the exact mass fraction of each species of fuel to physically produce the mixture and the continuous distribution parameters

for the model. The selected mixtures can be seen in Table 5-4. The purpose of creating these two mixtures was to test the complete model using mixtures of well-defined composition that were accurately represented by the chosen continuous distributions. The second mixture was designed to have an analogous distribution shape to mixture 1 as illustrated in Figure 5-22 and Figure 5-23. As mentioned previously, the rate parameters were fitted to the fuels ranging from *n*-octane to *n*-hexadecane, while for the fuels *n*-eicosane and *n*-octadecane it was assumed that the fitted expressions used continued to be valid, although as mentioned in Section 5.1.3 this was not tested experimentally. This relationship was then further tested with mixture 2. The model for both mixtures agreed well with the experimental results as shown in Figure 5-24 and Figure 5-25. The ability of the model to fit the experimental results for both mixtures one and two illustrate that the relationships for the pre-exponential coefficient and the activation energy used are good fits for fuels ranging from *n*-octane to *n*-eicosane. This also tends to support the assumption of a well-mixed liquid phase for a continuous mixture, following the arguments of Bergeron and Hallett (1989b) and Tamim and Hallett (1995) and the computations of Abdel-Qader and Hallett (2004). Comparing the experimental results for the two mixtures, it was noticed that the first mixture with *n*-octane created some scatter, which increased as the ambient temperature was reduced, while the second mixture, which contained *n*-dodecane as the most volatile component, had very repeatable ignition times (little scatter) for all ranges of temperature. The standard deviation for both mixture 1 and 2 is overall small, less than +/-13% and +/-7% of the ignition time respectively, as shown in Table A - 27 and Table A - 29 and illustrated in Figure 5-24 and Figure 5-25. Comparing the model results for mixture 1 and 2 to the results for pure fuels, shown in Figure 5-26 and Figure 5-27, it appears that mixture 1 behaves similarly to *n*-dodecane and mixture 2 behaves similarly to *n*-tetradecane or *n*-

hexadecane; demonstrating that generally a continuous mixture will behave similarly to the "average" component of the mixture. This is different than what was concluded by Bergeron and Hallett (1989b), who said that in a two-component mixture the most volatile component controls ignition time. This further illustrates that a mixture that contains a number of components that vary closely in molecular weight will behave in a continuous fashion. These results have provided a model to determine the ignition time of *n*-paraffin fuel mixtures as single droplets using continuous thermodynamics for a single-distribution mixture that allows for a good comparison to experimental results.

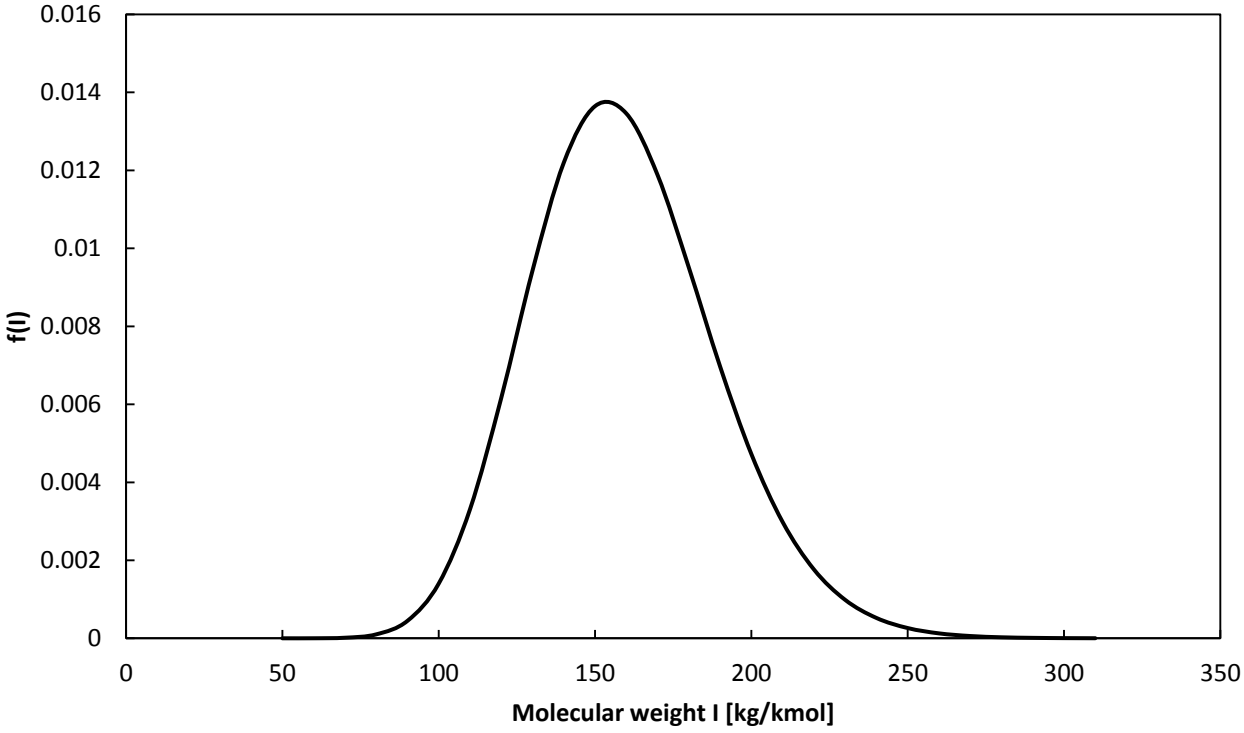

Figure 5-22 The distribution function for mixture 1

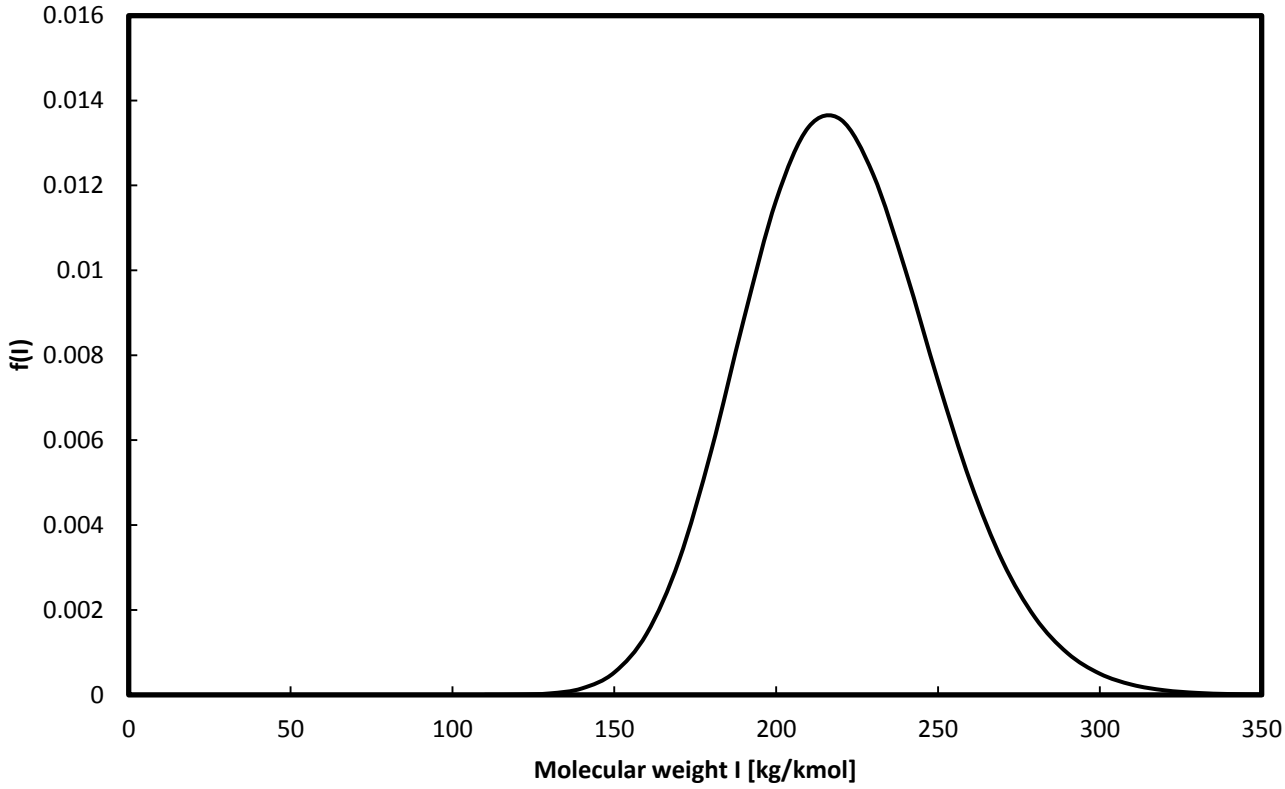

Figure 5-23 The distribution function for mixture 2

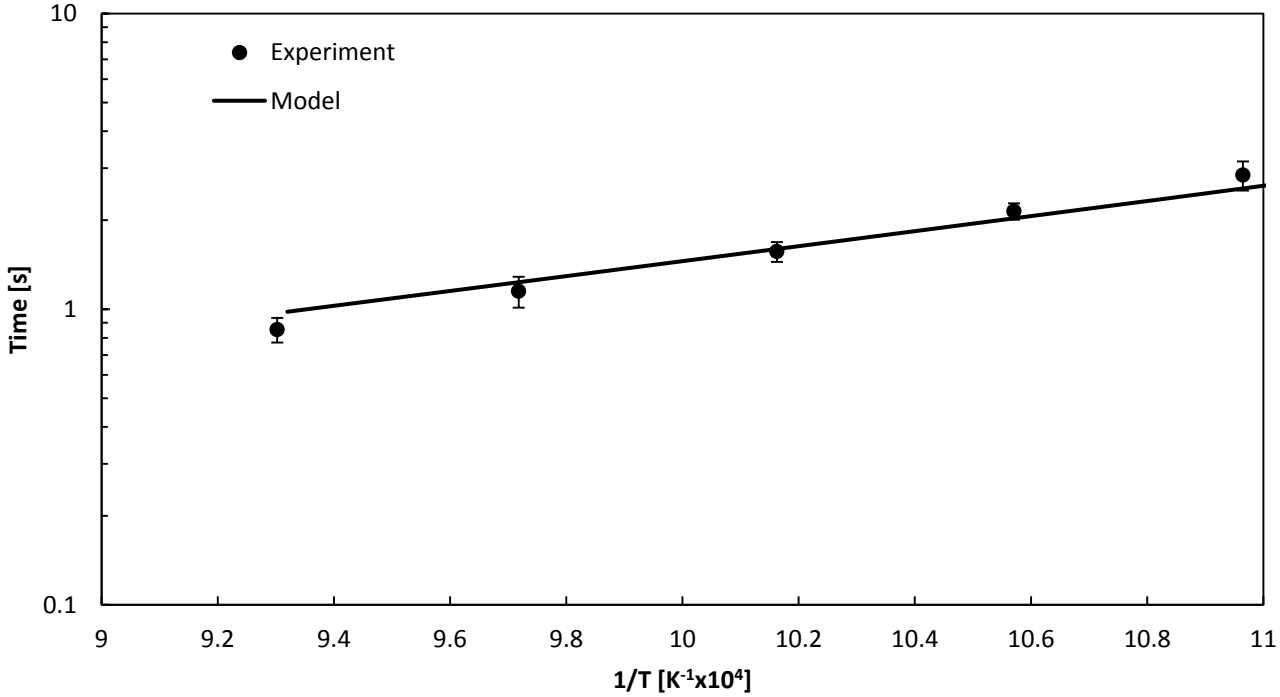

Figure 5-24 Ignition results for mixture 1 from both the experiments and the model and the bars gives +/- one standard deviation

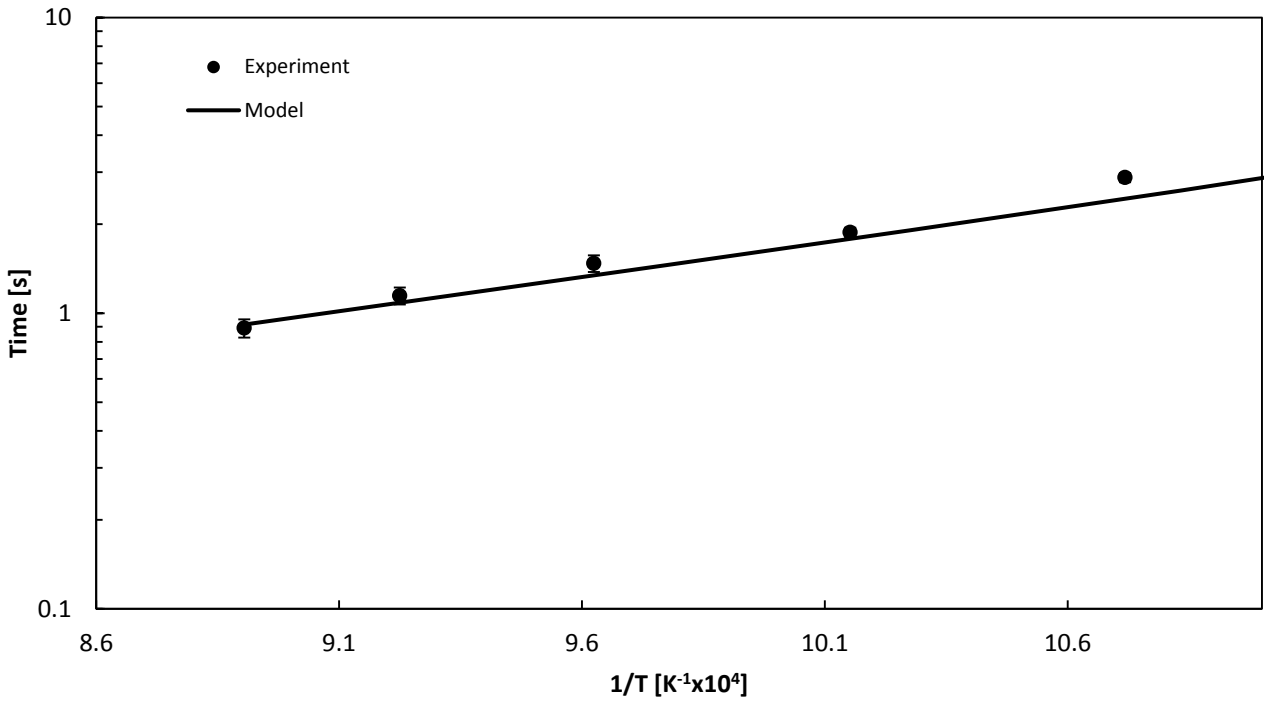

Figure 5-25 Ignition results for mixture 2 from both the experiments and the model and the bars gives +/- one standard deviation

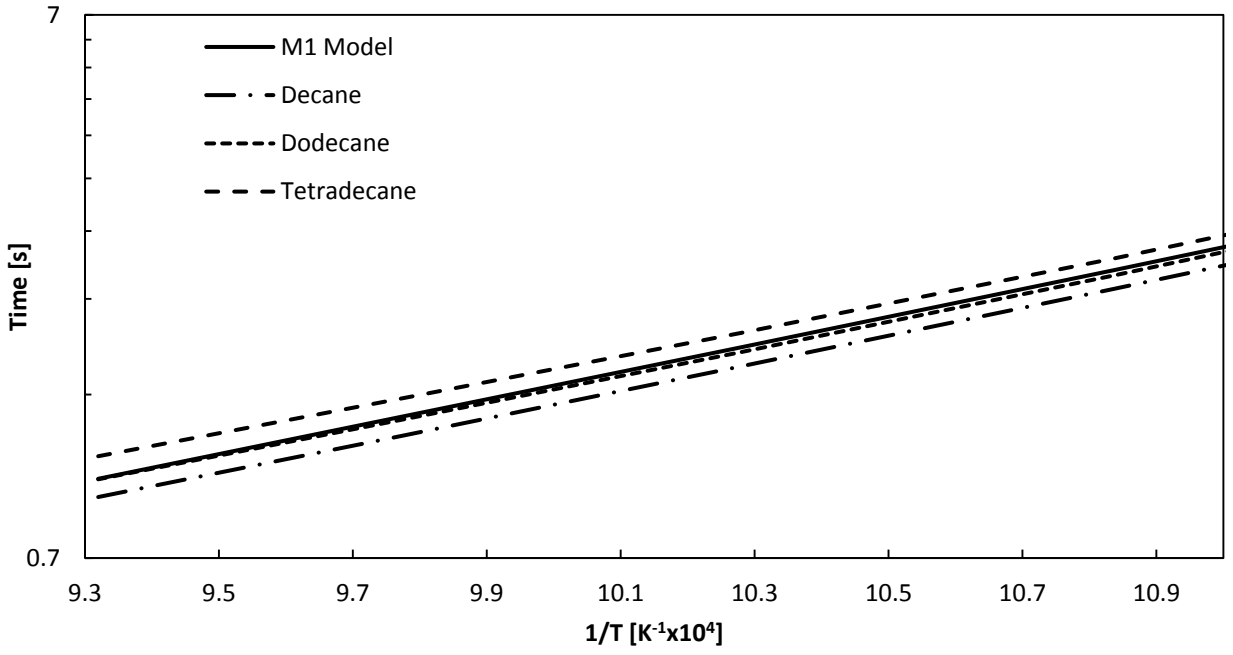

Figure 5-26 Comparing the model results for mixture 1 to various pure fuels to illustrate that a continuous mixture behaves similarly to its average component

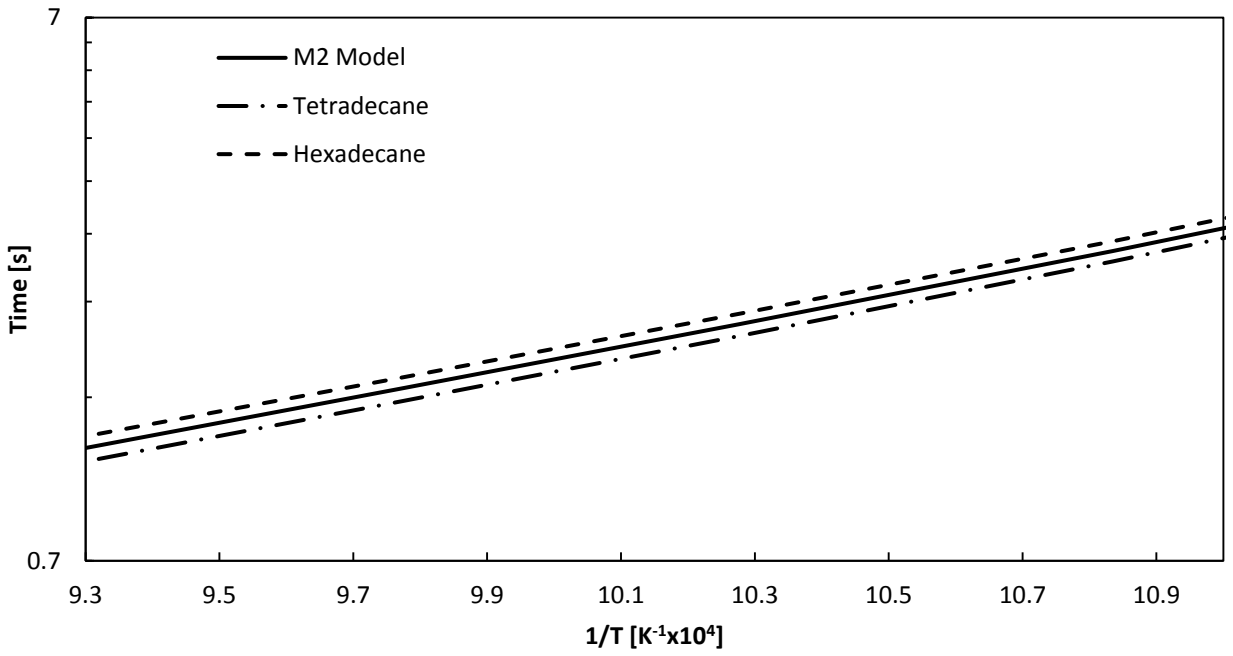

Figure 5-27 Comparing the model results for mixture 2 to the pure fuels to illustrate that a continuous mixture behaves similar to its average component

5.2.3 Results: two-distribution mixture

The additional purpose of creating the second mixture that contained fuels with higher molecular mass was to test and simulate a third "dumbbell" mixture – *i.e.* a mixture with two different fractions of quite different mean molecular mass. This mixture provides a test of the multi-distribution model. This "multi-mixture" was produced by mixing mixture 1 and mixture 2 in the proportion 49.9%/50.1% by mass. These values can be seen in Table 5-5 along with the resulting distribution in Figure 5-28. The results of the third mixture can be seen in Figure 5-29. The model again fits the experimental results fairly well, but this mixture shows larger discrepancies than the other two at lower ambient temperatures. This could be due to the small amount of *n*-octane in the mixture: as stated by Bergeron and Hallett (1989b), a mixture with a

small concentration of a fuel with a higher volatility than *n*-nonane could create a problem with the suspended droplet technique; however, since this did not create any problems with mixture 1 there could be other reasons for the discrepancy. The work on liquid mixing by Abdel-Qader and Hallett (2004) also concludes that when two distribution functions are combined to create a "dumbbell" mixture, the well-mixed liquid assumption may become less accurate. However, as illustrated in Figure 5-28 the distribution is not very “dumbbell”, as the mixture has a wide overlap between the two component distributions, but nevertheless the mixture has a much wider distribution than mixtures one or two. The third mixture, which contained a smaller amount of *n*-octane than Mixture 1, showed scatter at different temperatures with no general trend, illustrated by the error bars in Figure 5-29, unlike the first two mixtures. The standard deviation for the third mixture is overall small, less than +/-12% of the ignition time, as shown in Table A - 31 and illustrated in Figure 5-29, but increases substantially at high temperatures. There is a small difference between model and experimental results for the third mixture, and it is apparent that the measured ignition times for Mixture 3 tend to increase (above the model) and behave more like mixture 2 at low ambient temperatures, as shown in Figure 5-30. This could possibly be due to “aging” of the droplet prior to the test, as discussed in Section 3.1, due to the small amount of *n*-octane in the mixture. Due to “aging” the amount of *n*-octane could have been reduced to the point of not providing enough vapour to control ignition at lower ambient temperatures, making the mixture based on much less volatile fuels and therefore requiring more time for vapour to be produced. The possibility of “aging” is also suggested from the amount of scatter in the results, as discussed earlier: mixture 1, which contained *n*-octane, had a noticeable amount of scatter, while mixture 2, which did not have *n*-octane in the mixture, had a very small amount of scatter. This suggests that “aging” affected the results only slightly for the third mixture at lower ambient

temperatures, as there was noticeable scatter in the results only at high ambient temperatures, illustrating that shorter ignition times reduce the opportunity for "aging".

Overall, it was concluded that the discrepancy between the experimental results and the model was more likely due to internal mixing processes than to "aging". This was concluded because there is less *n*-octane and less *n*-decane in this mixture and these two compounds are rapidly vaporized and deplete from the surface layer. The model assumes a well-mixed droplet, so that the concentrations of *n*-octane and *n*-decane must be supplied from within the droplet. This rate of supply is restricted by diffusion, hence the surface concentration of these two compounds is less than predicted and the droplet behaves more like mixture 2. The support of this conclusion is from the fact that deviations increase as temperature decreases and longer ignition times give more time for *n*-octane and *n*-decane to be depleted in the surface layer. This also agrees with the conclusion of Abdel-Qader and Hallett (2004) that the well-mixed assumption could become less reliable for two-component or "dumbbell" mixtures with widely-spaced component boiling points.

These results have provided a model to determine the ignition time of *n*-paraffin fuel mixtures as single droplets using continuous thermodynamics for a two-distribution mixture that allows for a good comparison to experimental results, achieving the goal of this thesis successfully.

As a final note, Lasheras et al (1979) researched the burning of binary *n*-paraffin mixtures where internal boiling of the droplets causes explosions; however, this was not experienced prior to ignition for any of the pure fuels or mixtures used in this thesis.

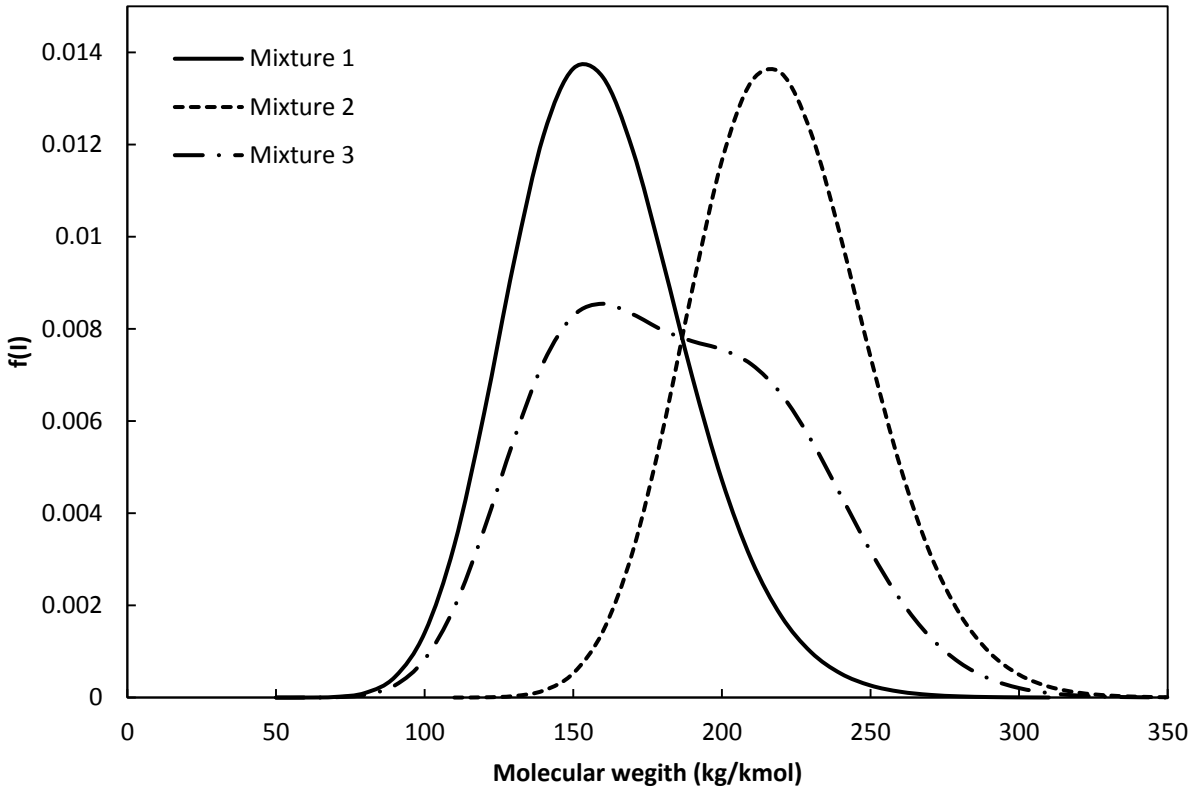

Figure 5-28 Distribution shape of mixture 3 ("Dumbbell" mixture)

Table 5-5 Mixture 3 composition

	% Mass Fraction	% Mole Fraction
Mixture 1	50.08	59.12
Mixture 2	49.92	40.88

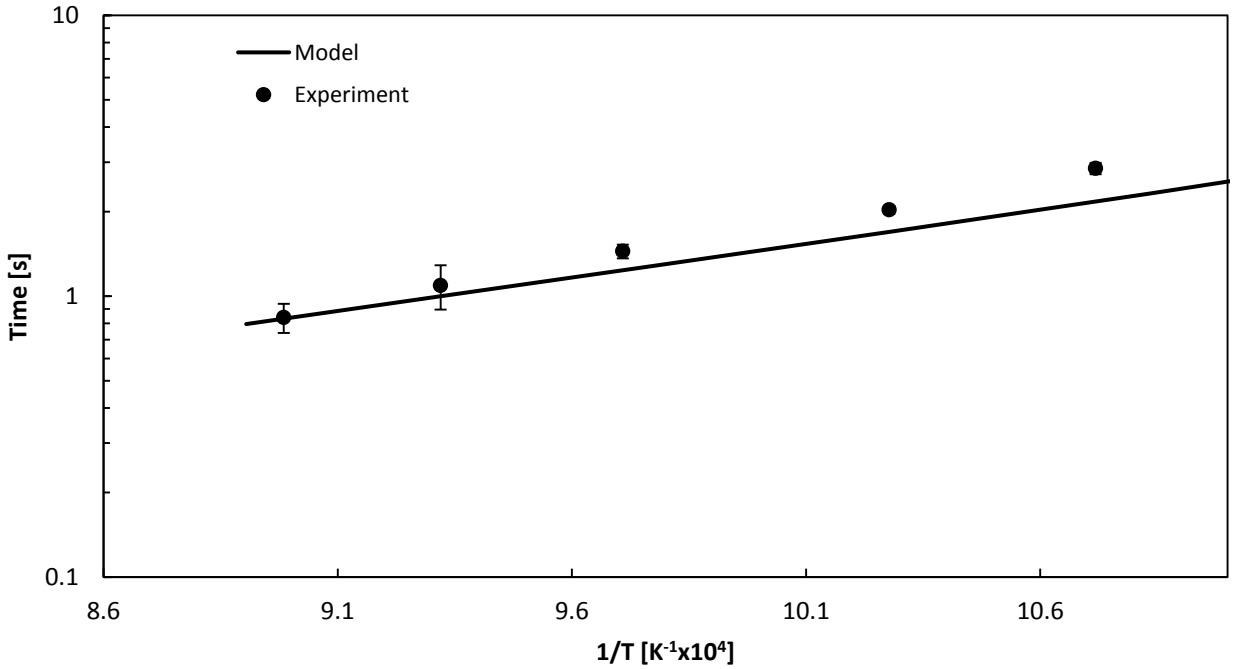

Figure 5-29 Ignition results for mixture 3 from both the experiments and the model and the bars gives +/- one standard deviation

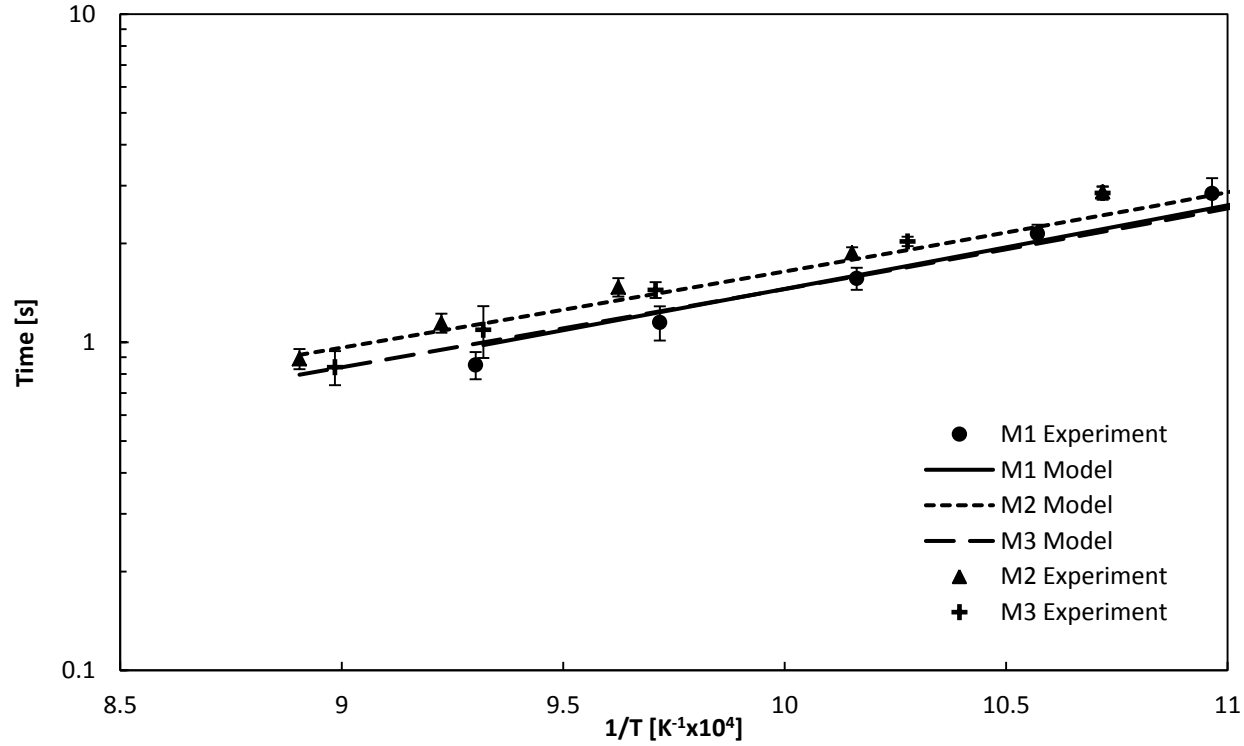

Figure 5-30 Comparison of the ignition results for all three mixtures from both the experiments and the model (M1=Mixture 1, M2=Mixture 2, M3= Mixture 3), the bars gives +/- one standard deviation

Chapter 6 Conclusions and Recommendations

6.1 Conclusions

The results illustrated and discussed above showed that adding chemical reaction/ignition to a continuous thermodynamics evaporation model provides an accurate model for the ignition delay times of *n*-paraffin fuel mixtures as single droplets. The following can be concluded:

1. The model can successfully reproduce ignition times for pure *n*-paraffin fuels. However, it has not been tested for other types of chemical compounds, since the rate parameters used were fitted to experimentally measured ignition times for pure *n*-paraffins.
2. In deriving the continuous thermodynamics ignition model, it was necessary to assume unity reaction order for fuel in the one-step Arrhenius rate equation used. However, the results show that the ignition behaviour is essentially the same as with the more commonly used fuel exponent of 0.25. For pure fuels, the model will give the same results for either reaction order if appropriate values of K and E are chosen. The concentration exponents m and n therefore do not greatly affect ignition calculations.
3. The expressions used for the rate parameters *K(I)* and *E(I)* as functions of species molecular mass were successfully matched to pure fuels from *n*-octane to *n*-hexadecane

by using an exponential of a linear function for *K* and a linear function for *E*. These expressions for *K(I)* and *E(I)* were also assumed to hold for *n*-octadecane and *n*-eicosane, although these two pure fuels were not individually tested experimentally.

4. The model successfully predicts the measured ignition times for *n*-paraffin mixtures described by a single distribution function.
5. The model successfully predicts the ignition times for mixtures described by two overlapping distribution functions, although the agreement is not as good as in the case of a single distribution.
6. The use of discrete and continuous ASTM distillation test computational models is a useful tool for designing experimental mixtures which can be accurately represented by a continuous distribution function.
7. The well-mixed model appears to work well, although departures from perfect mixing may play a role in the deviations of the two-distribution mixture from the model.
8. "Aging" – two- or three-dimensional convection phenomena causing the measured ignition time to change slightly with different delay times between forming the droplet and its entrance into the furnace - could affect a mixture with a small amount of fuel that has a higher volatility than *n*-nonane.

6.2 Future work

The following points would provide more rigorous testing of the model and help support the conclusions made:

1. The work should be extended to different types of fuels other than *n*-paraffins, which are the "best behaved" chemical family in terms of being able to correlate structure and

properties to molecular mass. Other chemical groups of interest include aromatics, branched paraffins, olefins, and cycloparaffins,which are not so simple.

2. Other types of fuels should be used to create mixtures with more components (a wider distribution function), since the fuels used provide ignition times that are not too different from each other.
3. Experiments should be performed with more mixtures that are composed of multiple distributions, and also “dumbbell” mixtures with distributions that are further separated in molecular mass, and the results compared with the model generated in this thesis.
4. Computations should be carried out to test the well-mixed versus the diffusion-limited models of the liquid.
5. The model should be extended to use a more realistic multi-step reaction model rather than a one-step reaction model.

References

American Society for Testing and Materials, ASTM Test D-86: Distillation of Liquid Fuels, Annual Book of ASTM Standards, issued annually

Abramowitz, M., Stegun, I. A., (1965), "Handbook of Mathematical Functions", Dover, New York, page 257

Abdel-Qader, Z. and Hallett, W.L.H., (2004), "The role of liquid mixing in evaporation of complex multicomponent mixtures: modelling using continuous thermodynamics", Chemical Engineering Science, 60: 1629-1640

Aggarwal, S. K., (1988), "Futher results on evaporating bicomponent fuel sprays", Int. J. Heat Mass Transfer. 31: 2593-2597

Aggarwal, S., (1984), "Effects of internal heat transfer models on the ignition of fuel droplets", Combust. Sci. and Tech., 42: 325-334

Aris, R., and Gavalas, G. R., (1966), "Theory of reactions in continuous mixtures", Philosophical Transactions of the Royal Society of London. Series A, Mathematical and Physical Sciences, 260: 351-393

Arias-Zugasti, M., and Rosner, D. E., (2003), "Multicomponent fuel droplet vaporization and combustion using spectral theory for a continuous mixture", Combustion and Flame, 135: 271-284

Astarita, G., and Ocone, R., (1992), "Chemical reaction engineering of complex mixtures", Chemical Engineering Science, 47: 2135-2147

Bardon, M. F., Gauthier, J. E. D. and Rao, V. K., (1990), “Flame propagation through sprays of multicomponent fuel”, J. Inst. Energy, 63: 53-60

Bergeron, C. A., and Hallett, W. L. H., (1989a), “Ignition Characteristics of Liquid Hydrocarbon Fuels as Single Droplets”, Canadian Journal of Chemical Engineering, 67: 142-149

Bergeron, C. A., and Hallett, W. L. H., (1989b), “Autoignition of Signle Droplets of Two-Component Liquid Fuels”, Combust. Sci. and Tech., 65: 181-194

Braide, K. M., Isles, G. L., Jordan, J. B., and Williams, A., (1979), "The combustion of single droplets of some fuel oils and alternative liquid fuel combinations" Journal of the Institute of Energy 52, 115.

Chou, M. Y., and Ho, T. C., (1989), "Lumping coupled nonlinear reactions in continuous mixtures", AIChE Journal 35: 533-538

Chou, M. Y., and Ho, T. C., (1988), "Continuum theory for lumping nonlinear reactions", AIChE Journal 34: 1519-1527

Cotterman, R. L., Bender, R., and Prausnitz, J. M., (1984),"Phase equilibria for mixtures containing very many components, development and application of continuous thermodynamics for chemical process design", Ind. Eng. Chem. Process Des. Dev., 24: 194-203

Faeth, G. M., and Olson, D. R., (1968), "The ignition of hydrocarbon fuel droplets in air", SAE Paper 680465, 1793-1802

Ghassemi, H., Baek, S. W., and Khan, Q. S., (2006), "Experimental study on evaporation of kerosene droplets at elevated pressures and temperatures", Combust. Sci. and Tech., 178: 1669-1684

Hallett, W.L.H., (2009), "Combustion in diffusion systems", pg 3.2-15

Hallett, W. L. H., and Ricard, M. A., (1991), “Calculations of the auto-ignition of liquid hydrocarbon mixtures as single droplets”, Fuel,. 71: 225-229

Hallett, W. L. H., (2000), “A Simple Model for the Vaporization of Droplets with Large Numbers of Components”, Combustion and Flame, 121: 334-344

Hallett, W.L.H., and Beauchamp-Kiss, S., (2010), "Evaporation of single droplets of ethanol-fuel oil mixtures", Fuel 89: 2496-2504

Hallett, W.L.H., (2011), Legault, N.V., Modelling biodiesel droplet evaporation using continuous thermodynamics, Fuel 90, 1221-1228

Harstad, K., and Bellan, J., (2004), "Modelling evaporation of Jet A, JP-7, and RP-1 drops at 1 to 15 bars", Combustion and Flame, 137: 163-177

Hottel, H. C., Williams, G. C., and Simpson, H. C., (1955), “Combustion of Fuel Droplets in Air”, SAE Paper 680465

Lasheras, J. C., Fernandez-Pello, A. C., and Dryer, F. L., (1979), "Experimental observations on the disruptive combustion of free droplets of multicomponent fuels", Combustion Science and Technology,. 22: 195-209

Law, C. K., Prakash, S., and Sirignano, W. A., (1976), "Theory of convective, transient, multicomponent droplet vaporization", 16. Symp. (Int.) on Combustion: 605-617

Nakaya, S., Tsue, M., Imamura, O., Nishida, S., Yamashita, K., Segawa, D., and Kono, M., (2009), "Effects of fuel vapour in ambience on spontaneous ignition of isolated fuel droplet", Combust. Sci. Tech., 181: 1464-1479

Patankar, S. V., (1980), "Numerical Heat Transfer and Fluid Flow", Hemisphere Publishing Corporation, Washington, New York, London

Rah, S.-C., Sarofim, A. F., and Beér, J. M., (1986), "Ignition and combustion of liquid droplets. Part II. Ignition Studies", Combust. Sci. Technol., 49: 169-184

Ratzsch, M. T., Kehlen, H., and Schumann, J., (1988), "Flash calculations for a crude oil by continuous thermodynamics", Chem. Eng. Comm, 71: 113-125

Rivard, E., and Bruggemann, D., (2010), "Numerical investigation of semi-continuous mixture droplet vaporization at low temperature", Chemical Engineering Science, 65: 5137-5145

Saitoh, T., Ishiguro, S., and Niioka, T., (1982), "An experimental study of droplet ignition characteristics new the ignitable limit", Combustion and Flame 48: 27-32

Shaw, B. D., and Wei, J. B., (2007), "Propanol droplet flammability and combustion in air-diluent environments under normal and reduced gravity", Combust. Sci. and Tech., 179: 1205-1223

Stauch, R., and Maas, U., (2007), "The auto-ignition of single *n*-heptane/*iso*-octane droplets", International Journal of Heat and Mass Transfer 50: 3047-3053

Talley D. G., and Yao, S. C., (1986), "A semi-empirical approach to thermal and composition transients inside vaporizing fuel droplets", Twenty-first Symposium (International) on Combustion/ The Combustion Institute: 609-616

Tamim, J., (1996), "A Continuous Thermodynamics Model for Multicomponent Droplet Vaporization", MASc thesis, Chemical Engineering, University of Ottawa

Tamim, J., and Hallett, W. L. H., (1995), "A Continuous Thermodynamics Model for Multicomponent Droplet Vaporization", Chemical Engineering Science, 50, 18: 2933-2942

Tong, A. Y., and Sirignano, W. A., (1986), "Multicomponent droplet vaporization in a high temperature gas", Combustion and Flame 66: 221-235

Westbrook, C. K., and Dryer, F. L., (1981), "Simplified reaction mechanisms for the oxidation of hydrocarbon fuels in flames", Combustion Science and Technology, 27: 31-43

Willman, B., and Teja, A. S., (1987), "Prediction of dew points of semicontinuous natural gas petroleum mixtures. 1. Characterization by use of an effective carbon number and ideal solution predictions", Ind. Eng. Chem. Res., 26: 948-952

Li, X., and Renksizbulut, M., (1990), "Droplet ignition with variable properties and distinct bindary diffusion coefficients", AIAA Journal, 27: 1131-1135

Zhang, L., and Kong, S-C., (2009), "Modeling of multi-component fuel vaporization and combustion for gasoline and diesel spray", Chemical Engineering Science, 64: 3688-3669

Appendix A

A.1 Pure Fuel Data

A.1.1 Experimental Data

Table A - 1 Experimental ignition time data for *n*-Octane for a 1.6mm diameter droplet

Temp [K]	Temp [C]	1/T [K^{-1} x 10^4]	Time [s]
1068	795	9.36329588	0.8
1049	776	9.532888465	1.016
1042	769	9.596928983	1.088
1049	776	9.532888465	0.668
1054	781	9.487666034	0.867
1055	782	9.478672986	0.892
1054	781	9.487666034	0.992
1048	775	9.541984733	0.992
941	668	10.62699256	1.86
948	675	10.54852321	1.84
934	661	10.70663812	2.368
944	671	10.59322034	1.988
952	679	10.50420168	1.752
950	677	10.52631579	1.832
980	707	10.20408163	1.556
999	726	10.01001001	1.344
991	718	10.09081736	1.388
994	721	10.06036217	1.152
996	723	10.04016064	1.292
975	702	10.25641026	1.564
973	700	10.27749229	1.612

969	696	10.31991744	1.532
1074	801	9.310986965	0.588
1072	799	9.328358209	0.872
1083	810	9.233610342	0.832
1079	806	9.267840593	0.776
1079	806	9.267840593	0.704
1073	800	9.319664492	0.856
1073	800	9.319664492	0.812

Table A - 2 Experimental ignition time data for *n*-Decane for a 1.6mm diameter droplet

Temp [K]	Temp [C]	1/T [K^{-1} x 10^4]	Time [s]
1051	778	9.514747859	0.944
1047	774	9.551098376	0.664
967	694	10.34126163	1.376
962	689	10.3950104	1.46

Table A - 3 Experimental ignition time data for *n*-Dodecane for a 1.6mm diameter droplet

Temp [K]	Temp [C]	1/T [K^{-1} x 10^4]	Time [s]
1038	765	9.633911368	0.892
1043	770	9.587727709	1.052
975	702	10.25641026	1.48
961	688	10.40582726	1.908
963	690	10.38421599	1.704
959	686	10.42752868	1.928
963	690	10.38421599	1.904
951	678	10.51524711	2.092

Table A - 4 Experimental ignition time data for *n*-Tetradecane for a 1.6mm diameter droplet

Temp [K]	Temp [C]	1/T [K^{-1} x 10^4]	Time [s]
1053	780	9.496676163	1.168
1039	766	9.624639076	1.008
1037	764	9.643201543	0.996

958	685	10.43841336	2.04
968	695	10.33057851	1.8
987	714	10.13171226	1.84
960	687	10.41666667	1.72
962	689	10.3950104	1.98
957	684	10.44932079	2.016

Table A - 5 Experimental ignition time data for *n*-Hexadecane for a 1.6mm diameter droplet

Temp [K]	Temp [C]	1/T [K^{-1} x 10^4]	Time [s]
974	701	10.26694045	1.816
981	708	10.19367992	1.544
975	702	10.25641026	1.56
973	700	10.27749229	1.82
1036	763	9.652509653	1.316
1045	772	9.56937799	1.2
1048	775	9.541984733	1.252
964	691	10.37344398	1.652
965	692	10.3626943	2.224
967	694	10.34126163	1.832
956	683	10.46025105	2.288

Table A - 6 Experimental ignition time data for *n*-Dodecane from Bergeron and Hallett (1989a)

Temperature		Diameter [mm]		Ignition time [s]	
°C	1/T [K^{-1}x10^4]	mm	+/-	s	+/-
649	10.845987	1.436	0.017	2.15	0.17
700	10.2774923	1.433	0.016	1.28	0.021
750	9.77517107	1.443	0.024	1.056	0.018
810	9.23361034	1.458	0.01	0.732	0.022

Table A - 7 Experimental ignition time data for *n*-Hexadecane from Bergeron and Hallett (1989a)

Temperature		Diameter [mm]		Ignition time [s]	
°C	1/T [K^{-1}x10^4]	mm	+/-	s	+/-
600	11.4547537	1.53	0.011	3.394	0.178

650	10.8342362	1.532	0.007	2.373	0.068
700	10.2774923	1.536	0.006	1.714	0.024
754	9.73709834	1.506	0.014	1.242	0.033
764	9.64320154	1.506	0.005	1.22	0.033
801	9.31098696	1.536	0.005	1.091	0.032
802	9.30232558	1.524	0.024	1.057	0.046
803	9.2936803	1.51	0.03	1.016	0.014
851	8.89679715	1.535	0.005	0.854	0.038

A.1.2 Model Predictions

Table A - 8 Model ignition time predictions for *n*-octane using a constant activation energy and the three linear equations for the pre-exponential coefficient (using a 1.6mm droplet). K1, K2 and K3 are defined in Section 5.1.3 on page 59

			Time [s]		
Temp [K]	Temp [C]	1/T [K^{-1} x 10^4]	K1	K2	K3
1073	800	9.319664492	1.098	0.551	0.341
1023	750	9.775171065	1.43101	0.70999	0.436
973	700	10.27749229	1.91203	0.93899	0.569
923	650	10.83423619	2.62099	1.286	0.76499
873	600	11.45475372	3.80391	1.83703	1.06499
823	550	12.15066829	6.20573	2.77298	1.55302

Table A - 9 Model ignition time predictions for *n*-decane using a constant activation energy and the three linear equations for the pre-exponential coefficient (using a 1.6mm droplet). K1, K2 and K3 are defined in Section 5.1.3 on page 59

			Time [s]		
Temp [K]	Temp [C]	1/T [K^{-1} x 10^4]	K1	K2	K3
1073	800	9.319664492	0.457	0.636	0.307
1023	750	9.775171065	0.572	0.79999	0.386
973	700	10.27749229	0.72799	1.02799	0.492
923	650	10.83423619	0.94899	1.36101	0.642

873	600	11.45475372	1.275	1.87003	0.85699
823	550	12.15066829	1.78103	2.69799	1.18

Table A - 10 Model ignition time predictions for *n*-dodecane using a constant activation energy and the three linear equations for the pre-exponential coefficient (using a 1.6mm droplet). K1, K2 and K3 are defined in Section 5.1.3 on page 59

			Time [s]		
Temp [K]	Temp [C]	1/T [K^{-1} x 10^4]	K1	K2	K3
1073	800	9.319664492	0.497	0.71999	0.375
1023	750	9.775171065	0.613	0.88999	0.464
973	700	10.27749229	0.76699	1.122	0.583
923	650	10.83423619	0.97899	1.44701	0.74499
873	600	11.45475372	1.279	1.92403	0.97299
823	550	12.15066829	1.72102	2.66699	1.304

Table A - 11 Model ignition time predictions for *n*-tetradecane using a constant activation energy and the three linear equations for the pre-exponential coefficient (using a 1.6mm droplet). K1, K2 and K3 are defined in Section 5.1.3 on page 59

			Time [s]		
Temp [K]	Temp [C]	1/T [K^{-1} x 10^4]	K1	K2	K3
1073	800	9.319664492	0.569	0.85299	0.47
1023	750	9.775171065	0.69499	1.04499	0.575
973	700	10.27749229	0.86099	1.302	0.71399
923	650	10.83423619	1.08599	1.65502	0.90099
873	600	11.45475372	1.39601	2.16103	1.159
823	550	12.15066829	1.84203	2.92397	1.52602

Table A - 12 Model ignition time predictions for *n*-hexadecane using a constant activation energy and the three linear equations for the pre-exponential coefficient (using a 1.6mm droplet). K1, K2 and K3 are defined in Section 5.1.3 on page 59

			Time [s]		
Temp [K]	Temp [C]	1/T [K^{-1} x 10^4]	K1	K2	K3
1073	800	9.319664492	0.68299	1.01499	0.601
1023	750	9.775171065	0.82899	1.218	0.72999
973	700	10.27749229	1.01999	1.50601	0.89899
923	650	10.83423619	1.276	1.89703	1.125
873	600	11.45475372	1.62502	2.44701	1.43201
823	550	12.15066829	2.12003	3.25895	1.86503

Table A - 13 Model ignition time predictions for *n*-octane using a linear relationship for activation energy and the three linear equations for the pre-exponential coefficient (using a 1.6mm droplet). K1, K2 and K3 are defined in Section 5.1.3 on page 59

			Time [s]		
Temp [K]	Temp [C]	1/T [K^{-1} x 10^4]	K1	K2	K3
1073	800	9.319664492	1.04599	0.514	0.321
1023	750	9.775171065	1.36101	0.657	0.409
973	700	10.27749229	1.81303	0.86399	0.533
923	650	10.83423619	2.457	1.173	0.71299
873	600	11.45475372	3.52893	1.66102	0.98599
823	550	12.15066829	5.90175	2.481	1.42601

Table A - 14 Model ignition time predictions for *n*-decane using a linear relationship for activation energy and the three linear equations for the pre-exponential coefficient (using a 1.6mm droplet). K1, K2 and K3 are defined in Section 5.1.3 on page 59

			Time [s]		
Temp [K]	Temp [C]	1/T [K^{-1} x 10^4]	K1	K2	K3
1073	800	9.319664492	0.596	0.85599	0.403
1023	750	9.775171065	0.75799	1.107	0.51
973	700	10.27749229	0.98699	1.47901	0.658
923	650	10.83423619	1.32601	2.04803	0.86999
873	600	11.45475372	1.85903	2.97297	1.187
823	550	12.15066829	2.75298	4.57185	1.68602

Table A - 15 Model ignition time predictions for *n*-dodecane using a linear relationship for activation energy and the three linear equations for the pre-exponential coefficient (using a 1.6mm droplet). K1, K2 and K3 are defined in Section 5.1.3 on page 59

			Time [s]		
Temp [K]	Temp [C]	1/T [K^{-1} x 10^4]	K1	K2	K3
1073	800	9.319664492	0.79099	1.33801	0.598
1023	750	9.775171065	1.00499	1.77303	0.75399
973	700	10.27749229	1.31001	2.42901	0.96799
923	650	10.83423619	1.79703	3.44893	1.277
873	600	11.45475372	2.496	5.15481	1.74203
823	550	12.15066829	3.75891	N/A	2.496

Table A - 16 Model ignition time predictions for *n*-tetradecane using a linear relationship for activation energy and the three linear equations for the pre-exponential coefficient (using a 1.6mm droplet). K1, K2 and K3 are defined in Section 5.1.3 on page 59

			Time [s]		
Temp [K]	Temp [C]	1/T [K^{-1} x 10^4]	K1	K2	K3
1073	800	9.319664492	1.08499	2.08203	0.85599
1023	750	9.775171065	1.38901	2.82798	1.07999
973	700	10.27749229	1.83103	3.9319	1.39401
923	650	10.83423619	2.516	5.64177	1.85303
873	600	11.45475372	3.65592	N/A	2.571
823	550	12.15066829	5.72277	N/A	3.79191

Table A - 17 Model ignition time predictions for *n*-hexadecane using a linear relationship for activation energy and the three linear equations for the pre-exponential coefficient (using a 1.6mm droplet). K1, K2 and K3 are defined in Section 5.1.3 on page 59

			Time [s]		
Temp [K]	Temp [C]	1/T [K^{-1} x 10^4]	K1	K2	K3

1073	800	9.319664492	1.48001	3.23595	1.182
1023	750	9.775171065	1.92403	4.36187	1.50301
973	700	10.27749229	2.59699	5.99475	1.96304
923	650	10.83423619	3.68692	N/A	2.66399
873	600	11.45475372	5.54278	N/A	3.82591

Table A - 18 Model ignition time predictions for *n*-Octane using a linear relationship for activation energy and an exponential relationship for the pre-exponential coefficient (using a 1.6mm droplet)

Temp [K]	Temp [C]	1/T [K^{-1} x 10^4]	Time [s]
1073	800	9.319664492	0.87699
1023	750	9.775171065	1.141
973	700	10.27749229	1.52702
923	650	10.83423619	2.10703
873	600	11.45475372	3.04296
823	550	12.15066829	4.76284

Table A - 19 Model ignition time predictions for *n*-Decane using a linear relationship for activation energy and an exponential relationship for the pre-exponential coefficient (using a 1.6mm droplet)

Temp [K]	Temp [C]	1/T [K^{-1} x 10^4]	Time [s]
1073	800	9.319664492	0.90699
1023	750	9.775171065	1.177
973	700	10.27749229	1.57602
923	650	10.83423619	2.18902
873	600	11.45475372	3.17995
823	550	12.15066829	4.93582

Table A - 20 Model ignition time predictions for *n*-Dodecane using a linear relationship for activation energy and an exponential relationship for the pre-exponential coefficient (using a 1.6mm droplet)

Temp [K]	Temp [C]	1/T [K^{-1} x 10^4]	Time [s]
1073	800	9.319664	0.97799
1023	750	9.775171	1.26

973	700	10.27749	1.67402
923	650	10.83424	2.31701
873	600	11.45475	3.37094
823	550	12.15067	5.2338

Table A - 21 Model ignition time predictions for *n*-Tetradecane using a linear relationship for activation energy and an exponential relationship for the pre-exponential coefficient (using a 1.6mm droplet)

Temp [K]	Temp [C]	1/T [K^{-1} x 10^4]	Time [s]
1073	800	9.319664492	1.07799
1023	750	9.775171065	1.37901
973	700	10.27749229	1.81603
923	650	10.83423619	2.49
873	600	11.45475372	3.60692
823	550	12.15066829	5.60678

Table A - 22 Model ignition time predictions for *n*-Hexadecane using a linear relationship for activation energy and an exponential relationship for the pre-exponential coefficient (using a 1.6mm droplet)

Temp [K]	Temp [C]	1/T [K^{-1} x 10^4]	Time [s]
1073	800	9.319664492	1.199
1023	750	9.775171065	1.52502
973	700	10.27749229	1.99604
923	650	10.83423619	2.71199
873	600	11.45475372	3.8939
823	550	12.15066829	6.04174

Table A - 23 Values of the pre-exponential coefficient "K" fitted to experimental data for pure fuels, together with different correlating equations for K(I)

Molecular Weight I [kg/kmol]	"K"	K1_linear	K2_linear	K3_linear	K_exponential
100	2.10E+05	-5.00E+06	5.00E+06	0.00E+00	1.47E+06

114	6.00E+06	2.00E+06	5.70E+06	1.40E+07	2.40E+06
142	7.50E+06	1.60E+07	7.10E+06	4.20E+07	6.39E+06
170	2.80E+07	3.00E+07	8.50E+06	7.00E+07	1.70E+07
180		3.50E+07	9.00E+06	8.00E+07	2.42E+07
200		4.50E+07	1.00E+07	1.00E+08	4.86E+07
226	1.60E+08	5.80E+07	1.13E+07	1.26E+08	1.21E+08
240		6.50E+07	1.20E+07	1.40E+08	1.97E+08

Table A - 24 Values of the activation energy "E" fitted to experimental data for pure fuels, together with the linear correlation E(I)

Molecular Weight I [kg/kmol]	Activation Energy "E" [kJ/gmol]	E1_linear [kJ/gmol]
100	57	79
114	79	82
142	84	89
170	94	96
180		99
200		104
226	106	110
240		114

Table A - 25 The coefficients used in the relationships to define the pre-exponential coefficient "K" and activation energy "E". The coefficients are referred to Equation (4-10) for K_linear, Equation (4-16) for K_exponential and Equation (4-14) for E.

Coefficient	K1_linear	K2_linear	K3_linear	K_exponential
a_k	-5.50E+07	0	-1.00E+08	10.7
b_k	5.00E+05	5.00E+04	1.00E+06	0.035
Coefficient	**E [kJ/gmol]**			
a_E	53.6			
b_E	0.25			

A.2 Mixture data

A.2.1 Experimental data

Table A - 26 Experimental ignition time data for mixture 1 using a 1.6mm diameter droplet

Temp [K]	Temp [C]	1/T [K^{-1} x 10^4]	Time [s]
912	639	10.96	2.764
912	639	10.96	2.548
912	639	10.96	3.148
912	639	10.96	3.216
912	639	10.96	3.344
912	639	10.96	2.428
912	639	10.96	2.496
912	639	10.96	2.896
912	639	10.96	2.544
912	639	10.96	3.100
913	640	10.95	2.784
946	673	10.57	2.028
946	673	10.57	2.012
946	673	10.57	2.048
946	673	10.57	2.184
946	673	10.57	2.232
946	673	10.57	2.012
946	673	10.57	2.324
946	673	10.57	2.276
946	673	10.57	2.108
946	673	10.57	2.364
946	673	10.57	2.008
983	710	10.17	1.516
984	711	10.16	1.340
984	711	10.16	1.772
984	711	10.16	1.684
984	711	10.16	1.496
984	711	10.16	1.564

984	711	10.16	1.432
984	711	10.16	1.624
984	711	10.16	1.532
984	711	10.16	1.620
986	713	10.14	1.648
1029	756	9.72	1.092
1029	756	9.72	0.928
1029	756	9.72	1.300
1029	756	9.72	1.084
1029	756	9.72	1.252
1029	756	9.72	0.992
1029	756	9.72	1.252
1029	756	9.72	1.300
1029	756	9.72	1.228
1030	757	9.71	0.984
1031	758	9.70	1.232
1075	802	9.30	0.980
1075	802	9.30	0.948
1075	802	9.30	0.764
1075	802	9.30	0.820
1075	802	9.30	0.752
1075	802	9.30	0.896
1075	802	9.30	0.932
1075	802	9.30	0.776
1075	802	9.30	0.860
1075	802	9.30	0.824
1075	802	9.30	0.756
1076	803	9.29	0.824
1077	804	9.29	0.952

Table A - 27 Statistical summary of the experimental ignition time data for mixture 1 using a 1.6mm diameter droplet

Mean Temp [K]	Temp [C]	1/T [K^{-1} x 10^4]	Average Time [s]	Standard Deviation (+/-)
912	639	10.96	2.843	0.321
946	673	10.57	2.145	0.136
984	711	10.16	1.566	0.121
1029	756	9.72	1.149	0.137
1075	802	9.30	0.853	0.081

Table A - 28 Experimental ignition time data for mixture 2 using a 1.6mm diameter droplet

Temp [K]	Temp [C]	1/T [K^{-1} x 10^4]	Time [s]
986	713	10.14	1.896
984	711	10.16	1.964
986	713	10.14	1.788
985	712	10.15	1.764
986	713	10.14	1.940
985	712	10.15	1.836
985	712	10.15	1.712
985	712	10.15	1.984
985	712	10.15	1.952
985	712	10.15	1.932
1039	766	9.62	1.288
1040	767	9.62	1.516
1039	766	9.62	1.604
1039	766	9.62	1.504
1039	766	9.62	1.596
1039	766	9.62	1.480
1039	766	9.62	1.424
1039	766	9.62	1.600
1039	766	9.62	1.392
1039	766	9.62	1.448
1039	766	9.62	1.360
933	660	10.72	2.962
933	660	10.72	2.956
933	660	10.72	2.904
934	661	10.71	2.780
933	660	10.72	2.932
933	660	10.72	2.784
933	660	10.72	2.868
933	660	10.72	2.820
933	660	10.72	2.836
933	660	10.72	2.944
1084	811	9.23	1.080
1084	811	9.23	1.220
1085	812	9.22	1.224
1084	811	9.23	1.212

1084	811	9.23	1.104
1084	811	9.23	1.184
1084	811	9.23	1.016
1084	811	9.23	1.092
1084	811	9.23	1.100
1084	811	9.23	1.228
1123	850	8.90	0.948
1123	850	8.90	0.856
1123	850	8.90	0.852
1123	850	8.90	0.960
1123	850	8.90	0.828
1123	850	8.90	0.808
1123	850	8.90	0.964
1123	850	8.90	0.892
1123	850	8.90	0.848
1123	850	8.90	0.988
1124	851	8.90	0.852

Table A - 29 Statistical summary of the experimental ignition time data for mixture 2 using a 1.6mm diameter droplet

Mean Temp [K]	Temp [C]	1/T [K^{-1} x 10^4]	Average Time [s]	Standard Deviation (+/-)
933	660	10.72	2.879	0.071
985	712	10.15	1.877	0.095
1039	766	9.62	1.474	0.104
1084	811	9.23	1.146	0.076
1123	850	8.90	0.891	0.063

Table A - 30 Experimental ignition time data for mixture 3 using a 1.6mm diameter droplet

Temp [K]	Temp [C]	1/T [K^{-1} x 10^4]	Time [s]
1073	800	9.32	1.156
1073	800	9.32	1.008
1073	800	9.32	1.232
1073	800	9.32	1.076
1073	800	9.32	1.060

1073	800	9.32	1.104
1073	800	9.32	1.048
1073	800	9.32	1.028
1073	800	9.32	1.076
1073	800	9.32	1.132
1030	757	9.71	1.480
1030	757	9.71	1.572
1030	757	9.71	1.324
1030	757	9.71	1.624
1030	757	9.71	1.424
1030	757	9.71	1.592
1030	757	9.71	1.356
1030	757	9.71	1.548
1030	757	9.71	1.280
1030	757	9.71	1.456
1030	757	9.71	1.232
933	660	10.72	2.752
933	660	10.72	2.972
933	660	10.72	2.968
933	660	10.72	2.496
933	660	10.72	3.164
933	660	10.72	2.868
933	660	10.72	2.992
933	660	10.72	2.864
933	660	10.72	2.840
933	660	10.72	2.596
973	700	10.28	2.000
973	700	10.28	2.036
973	700	10.28	2.164
973	700	10.28	2.144
973	700	10.28	2.040
973	700	10.28	1.960
973	700	10.28	1.968
973	700	10.28	1.932
973	700	10.28	1.964
973	700	10.28	2.092
1113	840	8.98	0.942
1113	840	8.98	0.984
1113	840	8.98	0.788
1113	840	8.98	0.744
1113	840	8.98	0.860

1113	840	8.98	0.736
1113	840	8.98	0.972
1113	840	8.98	0.768
1113	840	8.98	0.732
1113	840	8.98	0.872

Table A - 31 Statistical summary of the experimental ignition time data for mixture 3 using a 1.6mm diameter droplet

Mean Temp [K]	Temp [C]	1/T [K^{-1} x 10^4]	Average Time [s]	Standard Deviation (+/-)
933	660	10.72	2.851	0.197
973	700	10.28	2.030	0.081
1030	757	9.71	1.444	0.133
1073	800	9.32	1.092	0.067
1113	840	8.98	0.840	0.100

A.2.2 Model predictions

Table A - 32 Model ignition time predictions for mixture 1 using a 1.6mm diameter droplet

Temp [K]	Temp [C]	1/T [K^{-1} x 10^4]	Time [s]
1073	800	9.319664492	0.97999
1023	750	9.775171065	1.276
973	700	10.27749229	1.70902
923	650	10.83423619	2.36901
873	600	11.45475372	3.42893
823	550	12.15066829	5.2948

Table A - 33 Model ignition time predictions for mixture 2 using a 1.6mm diameter droplet

Temp [K]	Temp [C]	1/T [K^{-1} x 10^4]	Time [s]
1123	850	8.904719501	0.91499
1073	800	9.319664492	1.141
1023	750	9.775171065	1.45601
973	700	10.27749229	1.91003
923	650	10.83423619	2.60199
873	600	11.45475372	3.73791
823	550	12.15066829	5.80676

Table A - 34 Model ignition time predictions for mixture 3 using a 1.6mm diameter droplet

Temp [K]	Temp [C]	1/T [K^{-1} x 10^4]	Time [s]
1123	850	8.90472	0.79599
1073	800	9.319664	0.99899
1023	750	9.775171	1.282
973	700	10.27749	1.69302
923	650	10.83424	2.31901
873	600	11.45475	3.34694
823	550	12.15067	5.2628